ADDIS ABABA UNIVERSITY
SCHOOL OF GRADUATE STUDIES
FACULTY OF TECHNOLOGY
DEPARTMENT OF MECHANICAL ENGINEERING

Modeling, Simulation and Performance Evaluation of Central Receiver System Power Plant with Thermal Storage

A thesis submitted to the School of Graduate Studies of Addis Ababa University in partial fulfillment of the requirements for the Degree of Masters of Science in Mechanical Engineering (Thermal Engineering Stream)

By: Muaz Bedru

Advisor: Dr.-Ing. Abebayehu Assefa

September 2010

ADDIS ABABA UNIVERSITY
SCHOOL OF GRADUATE STUDIES

Modeling, Simulation and Performance Evaluation of Central Receiver System Power Plant with Thermal Storage

By: Muaz Bedru

Faculty of Technology

Approved by Board of Examiners

1. *Dr.-Ing. Edessa Dribssa* _____
   Chairman Dep.'s Graduate Committee *Signature*

2. *Dr.-Ing. Abebayehu Assefa* _____
   Advisor *Signature*

3. *Dr. Tesfaye Dama* _____
   Internal Examiner *Signature*

4. *Dr.-Ing. Demiss Alemu* _____
   External Examiner *Signature*

ABSTRACT

Solar Central Tower systems have a single receiver placed on top of a tower surrounded by hundreds of mirrors (heliostats) which follow the apparent motion of the sun in the sky and which re-direct and focus the sunlight onto the receiver. The key elements of a solar tower system are the heliostats:- provided with a two-axis tracking system, the receiver, the steam generation system and the storage system. A fluid circulates through the receiver, collecting thermal energy at high temperatures, and flows to an insulated storage tank. Steam for the 10 MW turbines is made as needed by pumping the hot fluid to a heat exchanger. The receiver and energy storage fluid is a commercial molten potassium and sodium nitrate mixture. The number of heliostats will vary according to the particular receiver's thermal cycle and the heliostat design.

The power plant analyzed in this paper has a capacity of generating 10MW electric power. The power cycle was modeled using EES to obtain the state point variables such as conductances of the heat exchangers, mass flow rates of steam and HTF, enthalpies, temperatures, pressures etc… at specified state points for steady state operation of the plant. These state point variables are used as reference inputs and/or parameters during system simulation using TRNSYS. The CRS was modeled in TRNSYS simulation studio using existing TRNSYS 16.0 components most of which are from STEC library release 3.0 packages. The CRS financial and economic analysis as well as different system component size and number was optimized using SAM. Without the incorporation of thermal storage, 788 heliostats with 97m^2 area satisfies the power demand specified for this research but the addition of thermal storage increases the number of heliostats to 1200 with significant increase in initial system cost and decrease in levelized energy cost.

A six hour capacity two tank thermal storage is incorporated with the power plant in order to avoid power transient during low and high DNI, to have power when there is no sunlight, to increase the capacity factor and to minimize the levelized cost of energy. The addition of a thermal storage extends the power plant operation to 16 hours with 13 hours of constant 10MW net electrical power output for a clear sunny day. The SAM analysis reveals that the

addition of thermal storage in the system significantly increase the investment cost from $58,072,837.73 to $76,781,394.61 with minimizing effect of LCOE from 33.02 to 26.79 cents/kWh and increasing capacity factor from 17.3 to 30.0%

ACKNOWLEDGMENTS

First and foremost, I would like to thank my advisor, Dr.-Ing. Abebayehu Assefa, for his ideas and technical support during the entire duration of my Masters program generally and during this thesis work specifically. Under his guidance, I have gained a great deal of technical knowledge as well as the completion of this work became true.

I would like to extend my sincere thanks to Mekuanint Mesfin for providing me with all the necessary information and materials that I needed. Not forgetting too are all my friends, who were especially helpful in their invaluable comments.

My special thanks are extended to Kebena Woreda Administration office for their financial and moral support at the expense of their limited budget

Last but not least, I would like to acknowledge my family members for their support. Though far away, my brother Mubarek Bedru and my sister Amria Bedru have always been a great source of encouragement. I would like to express my deepest gratitude to my brother Mubarek Bedru, whose financial support and encouragement has enabled me to continue my graduate study. It is to him that I dedicate this thesis.

Table of Contents

LIST OF FIGURES

LIST OF TABLES

NOMENCLATURES

A	Total heliostat field surface area [m^2]
A_H	Surface azimuth angle [^{o}]
ΔA	Azimuthal distance between heliostats [m]
C_{htf}	Heat transfer fluid specific heat capacity
$\dot{C}_{\min}$	Minimum thermal capacitance rate [W/k]
$\dot{C}_{\max}$	Maximum thermal capacitance rate [W/k]
C_p	Specific heat capacity at constant pressure [kJ/kg-k]
$C_{Operating,n}$	Total operating costs in year n
$C_{Interest,n}$	The loan interest payment in year n
$C_{Principal,n}$	The loan principal payment in year n
$C_{AfterTax,n}$	After tax cash flow in year n
CF	Capacity factor
$DSCR_n$	Debt service coverage ratio in year n
d_{real}	Real discount rate (the discount rate without inflation)
$d_{nominal}$	Nominal discount rate (the discount rate with inflation)
e	Inflation rate expressed as a fraction
$E_{OutputYear1}$	Annual electric generation for first year of operation [kW]
H	Unit vector normal to reflector surface
h	Enthalpy [kJ/kg]
$I_{b,n}$	Beam normal solar irradiance [Wh/m^2]
IRR	Internal rate of return [%]
$\dot{m}_{cw}$	Mass flow rate of cooling water [kg/s]
$\dot{m}_{htf}$	Mass flow rate of heat transfer fluid [kg/s]
$\dot{m}_{steam}$	Mass flow rate of steam [kg/s]
N	Project life in years

n_h	Total number of heliostats in the field
NPV	Net present value of the project over its life [$]
NTU	Number of transfer unit
P_i	Pressure at point i [bar]
$P_{System\,Capacity}$	System's rated capacity [kW]
$\dot{q}_{max}$	Maximum heat flow [W]
$\dot{q}_{boil}$	Heat flow to boiler [W]
$\dot{q}_{ph}$	Heat flow to preheater [W]
$\dot{q}_{sh}$	Heat flow to superheater [W]
$\dot{q}_{hot,tot}$	Total heat flow [W]
$\dot{Q}_{useful}$	Rate of energy addition to the working fluid [kW]
Q_n	Electricity generated by the project in year n [kW]
$\dot{Q}_{inc}$	Total power incident on receiver [W]
R_n	Project revenue from electricity sales in year n
$\boldsymbol{R}$	Aim point unit vector
ΔR	Radial distance between heliostats [m]
$\boldsymbol{S}$	Central sun ray unit vector
s	Entropy [kJ/kg-k]
t	Time [sec.]
T_i	Temperature at point i [^oC]
$T_{H,in}$	Temperature at inlet of hot fluid [^oC]
$T_{C,in}$	Temperature at inlet of cold fluid [^oC]
UA	Conductance of heat exchanger [W/k]
v_{in}	Specific volume at pump inlet [m^3/kg]
$\dot{W}_{cycle}$	Work produced by power cycle [W]
W_p	Pump work [W]
x	Steam quality

ACRONYMS

BCS	Beam Characterization System
CRS	Central Receiver Systems
CSP	Concentrating Solar Power Technology
DNI	Direct Normal Irradiation
DOE	Department of Energy (United States)
ECOSTAR	European Concentrated Solar Thermal Road Mapping
EEPCo	Ethiopian Electric Power Corporation
EES	Engineering Equation Solver
HTF	Heat Transfer Fluid
ICS	Inter Connected System
LCOE	Levelized Cost of Energy
NREL	National Renewable Energy Laboratory
PDCs	Parabolic Dish Collectors
PS	Plataforma Solar de Almerìa
PSA	Plataforma Solar in Almería
PTC	Parabolic Trough Concentrator
PTGen	Power Tower Generation Program
PV	Photovoltaic
SAM	Solar Advisor Model
SCS	Self Contained System
SEGS	Solar Energy Generating Systems
SERI	Solar Energy Research Institute (now NREL)
SGS	Steam Generator System
STE	Solar Thermal Electric
STEC	Solar Thermal Electric Components
TES	Thermal Energy Storage
TRNSYS	Transient Systems Simulation Program

GREEK LETTERS

α	Solar altitude angle [^{o}]
α_H	Suface altitude angle [^{o}]
θ_i	Angle of incidence [^{o}]
θ_z	Zenith angle [^{o}]
$\emptyset$	Altitude angle [^{o}]
δ	Declination angle [^{o}]
ω	Hour angle [^{o}]
ε	Effectiveness
ρ	Density [kg/m^3]
Δ	Difference between two values
θ_L	Altitude angle to the receiver from the heliostat location of interest [^{o}]
τ_a	Atmospheric transmittance
ρ_F	Local field density
η_{col}	Overall energy collection efficiency
η_{field}	Total heliostat field efficiency
$\eta_{receiver}$	Receiver efficiency
η_{cycle}	Rankine cycle efficiency
η_{turb}	Turbine efficiency
η_{pump}	Pump efficiency

CHAPTER ONE

1.1 INTRODUCTION

Solar power towers generate electric power from sunlight by focusing concentrated solar radiation on a tower-mounted heat exchanger (receiver). The system uses hundreds to thousands of sun-tracking mirrors called heliostats to reflect the incident sunlight onto the receiver. These plants are best suited for utility scale applications in the 30 to 400 MWe range. The heliostat field that surrounds the tower is laid out to optimize the annual performance of the plant. The field and the receiver are also sized depending on the needs of the utility. In a typical installation, solar energy collection occurs at a rate that exceeds the maximum required to provide steam to the turbine. Consequently, the thermal storage system can be charged at the same time that the plant is producing power at full capacity. The ratio of the thermal power provided by the collector system (the heliostat field and receiver) to the peak thermal power required by the turbine generator is called the solar multiple. With a solar multiple of approximately 2.7, a molten-salt power tower located in the California Mojave desert can be designed for an annual capacity factor of about 65%, (based on simulations at Sandia National Laboratories with the SOLERGY computer code [Stoddard, M.C., et. al]). Consequently, a power tower could potentially operate for 65% of the year without the need for a back-up fuel source. Without energy storage, solar technologies are limited to annual capacity factors near 25%.

Of all the technologies being developed for Solar Thermal Power Generation, Central Receiver Systems (CRS) are able to work at the highest temperatures and to achieve higher efficiencies in electricity production. The combination of this concept and the choice of molten salts as the heat transfer fluid, both in the receiver and for heat storage, enable solar collection to be decoupled from electricity generation better than water/steam systems, yielding high capacity factors with solar-only or low hybridization ratios.

More recently, a combination of urgent issues including concerns about climate change, Ethiopia's dependence on oil imports, acceptance of the finite nature of fossil-fuel resources, and a tremendous spike in fuel prices has renewed interest in alternative, domestic, and renewable energy technologies like concentrating solar power.

The surge in the renewable energy industry has continued despite the recent drop in the price of oil largely due to the increasingly volatile nature of the market and the remaining balance of energy-related issues. However, the long-term viability of alternative technologies like concentrating solar thermal depends on their ability to obtain subsidies, benefit from carbon emission disincentives, or compete economically with traditional power generation industries like coal, natural gas, and nuclear fission. The purpose of the research and analysis presented in the following work is to advance the knowledge and modeling capability for one particular concentrating solar power (CSP) technology – the solar power tower.

1.2 Background of the Project

Recognizing both the environmental and climatic hazards to be faced in the future and the continued depletion of the world's most valuable fossil energy resources, concentrating Solar Thermal Power can provide critical solutions to global energy problems within a relatively short time frame and is capable of contributing substantially to carbon dioxide reduction efforts. Among all the renewable technologies available for large-scale power production today, Concentrated Solar Power is one with the potential to make major contributions of clean energy because of its relatively conventional technology and ease of scale-up.

Central receiver systems use heliostats to track the sun by two axes mechanisms following the azimuth and elevation angles with the purpose to reflecting the sunlight from many heliostats oriented around a tower and concentrate it towards a central receiver situated at top of the tower. This technology has the advantage of transferring solar energy very efficiently by optical means and of delivering highly concentrated sunlight to one central receiver unit, serving as energy input to the power conversion system.

In spite of the elegant design concept and in spite of the future prospects of high concentration and high efficiencies, the central receiver technology needs still more research and development efforts and demonstration of up-scaled plant operation to come up to commercial use. Its main attraction which consists in the prospect of high process temperatures generated by highly concentrated solar radiation to supply energy to the topping cycle of any power conversion system and to feed effective energy storage systems able to cover the demand of modern power conversion systems.

The solar thermal output of central receiver systems can be converted to electric energy in highly efficient Rankine-cycle/steam turbine generators, in Brayton-cycle/gas turbine generators or in combined cycle (gas turbine with bottoming steam turbine) generators.

Although solar central receivers are less commercially mature than parabolic trough systems, approximately 14 solar central receiver systems have been constructed throughout the world till 2004. Most of these plants are research or proof-of-concept plants of only 1 to 2 MW. Solar One in southern California was planned as a commercial project but at 10 MW, this project was really a pilot demonstration system.

Solar One was built in 1981 and operated from 1982 to 1988. The plant used 1818 heliostats to reflect sunlight onto a central receiver. Water was converted into steam and used to drive a 10 MW turbine. The heat from the solar-heated steam could also be stored in a storage tank filled with rocks and sand using oil as the heat transfer fluid. The stored heat was used to generate power for up to four hours after sunset.

This project proved the technical feasibility of the central receiver concept. The system also had high reliability with 96% availability during sunlight hours. The system did, however, suffer from low annual efficiency (only a 7% heat-to-electricity efficiency) and intermittent turbine operation caused by transient clouds. Solar One was redesigned in the early 1990's to overcome its limitations. The system HTF was converted from water/steam to molten salt. Molten salt is inexpensive and allows for higher storage temperatures ($290^{O}C$). The main disadvantage is that it becomes solid below $220^{O}C$ and therefore must be maintained above this temperature. The receiver and storage tanks were replaced in order to use the new fluid. All pipes that carry the molten salt were heat-traced to avoid freezing the salt.

Solar Two (see Figure 1.1) began operation in 1996 and operated fairly consistently for the next year. Preliminary measurements showed that the plant was operating near design expectations (8% efficiency). Parasitic power required to keep the molten salt from freezing was initially quite high. Changes in operating strategy and modifications in the design reduced parasitic power to acceptable levels. In November 1998, the feeder pipe to the receiver collapsed because of an unforeseen transfer of loads. The system was repaired and

the plant ran until April 1999 – the end of the demonstration phase. Solar Two has successfully demonstrated the concept of molten salt storage. The heliostats have held up well over the almost 20 years that the plant has been in existence.

The Ethiopian Electric Power Corporation (EEPCo), being the sole power producer, maintains two different power supply systems, namely, the Inter- connected system (ICS) and Self - Contained System (SCS). ICS is mainly supplied from hydro - power plants as wells as geothermal (steam) and thermal (diesel) sources. Whereas, SCS consist of mini hydro - power plants and a number of isolated diesel generating units widely spread all over the country.

Demand for electricity in Ethiopia stands at more than 25% by the following fiscal year. At present EEPCo has an installed generating capacity which was 814 MW increased to a level of 1534MW. Currently the hydropower plants installed in the country are experiencing challenges to operate at their design capacity due to shortage of water in dams. The main reasons for these difficulties are the increased power demand and delayed rainfall. Hence, studying central receiver system as an option for power production is very essential.

Figure 1-1: Solar Two Central Receiver Power Plant

1.3 CSP Technology

1.3.1 Parabolic Trough Collector Systems

Parabolic trough power plants are line-focusing STE (solar thermal electric) power plants. Trough systems use the mirrored surface of a linear parabolic concentrator to focus direct solar radiation on an absorber pipe running along the focal line of the parabola. The HTF (heat transfer fluid) inside the absorber pipe is heated and pumped to the steam generator, which, in turn, is connected to a steam turbine. A natural gas burner is normally used to produce steam at times of insufficient insolation. The collectors rotate about horizontal north–south axes, an arrangement which results in slightly less energy incident on them over the year but favors summertime operation when peak power is needed.

The major components in the system are collectors, fluid transfer pumps, power generation system and the controls. This power generation system usually consists of a conventional

Rankine cycle reheat turbine with feedwater heaters deaerators, etc. and the condenser cooling water is cooled in forced draft cooling towers. These types of power plants can have energy storage system comprising these collectors usually have the energy storage facilities. Instead they are coupled to natural gas fired back up systems. A typical configuration of such systems is shown in Figure 1.2.

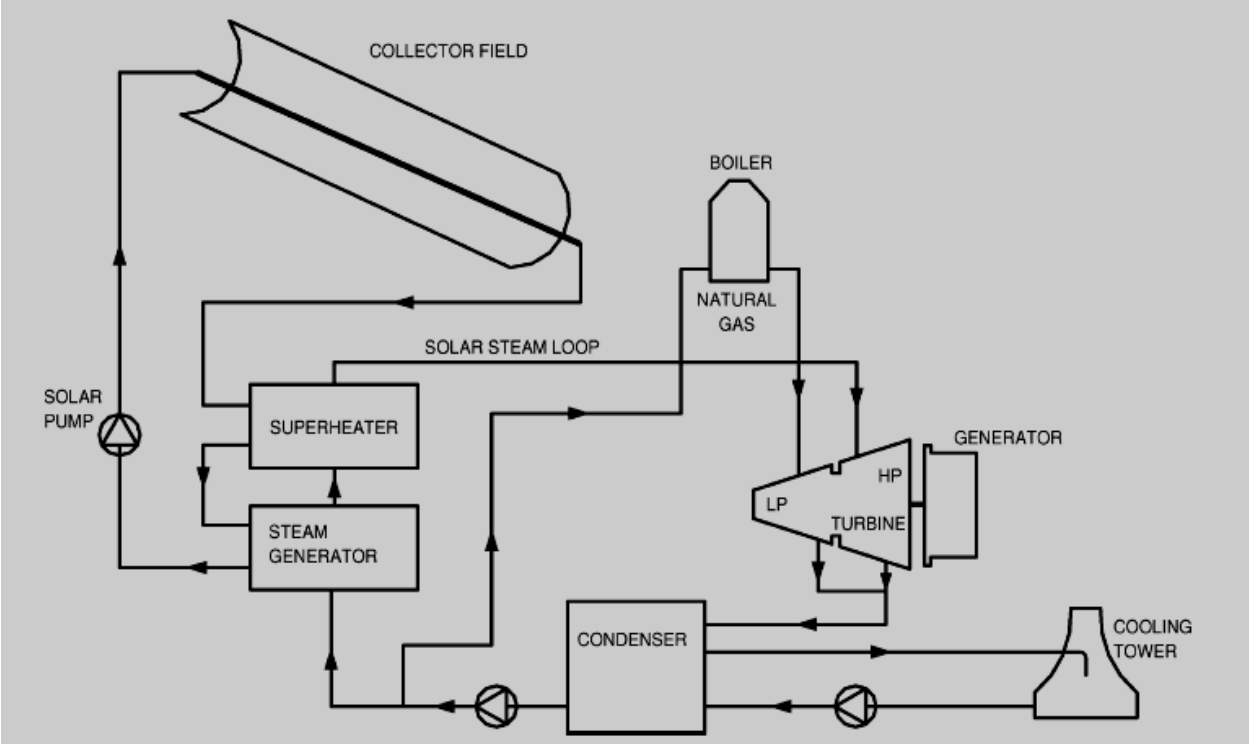

Figure 1-2: Configuration of PTC Solar Thermal Power Plant

Trough plants that incorporate storage capacities often have a separate cycle that utilizes molten salts as the storage medium. This indirect thermal storage further increases the total plant investment costs because of the additional heat exchangers. Therefore, research to identify and develop molten-salt mixtures with sufficiently low freezing points that can be directly pumped into the storage tanks after being heated in the receiver elements is ongoing. The ability to store thermal energy is important to better match the production of electricity with demands for electricity that occur during periods when solar radiation is not available. Storage units that provide up to 16 hours of electricity generation will establish these large-scale CSP systems as competitors for base-load electricity generation. Due to a high deployment capacity compared to the other solar-thermal power systems, the industry has

gained a substantial amount of experience with the parabolic trough systems and therefore the risks are relatively small.

1.3.2 Central Receiver Systems

Solar tower power plants are in the class of central receiver systems that employ an elevated solar receiver that becomes the focal point of a field of mirrors (heliostats) that concentrate the radiation onto the heat absorbing surfaces of the receiver as shown in Figure 1.3. The receiver surface is usually constructed with welded absorber tubes that absorb the concentrated solar radiation from the heliostat field and transfer the absorbed thermal energy to a coolant that is pumped through the tubing system. The high temperature heat transfer fluid can then be used to drive a conventional power cycle or stored in tanks for later use. Successful operation has been shown for receivers and storage systems that operate with molten salts or steam as the working fluid. Molten salt is liquid across the typical operating temperature ranges of 290-560^{O}C. Therefore, it requires less volume capacity and capital costs to store the same amount of energy as for a pressurized steam storage system. Because of the relatively low freeze point temperature, careful operation is required to make sure that the salt does not solidify in the receiver when the solar flux levels become too low. Parabolic trough systems like the Andasol 1-3 plants in Spain [Solar Millennium, 2008] use synthetic oil as the heat carrier in the mirror field and either transfer the heat directly to the boiler of the power cycle to produce steam, or the heat is stored in molten salt storage tanks for later use. This requires an additional heat exchanger to thermally connect the oil and the salt cycle. In contrast, power towers usually operate under higher fluid temperature ranges that simplify the application for available molten salt mixtures in the receiver. The heated molten salt is directly pumped into the storage tank, which saves the additional heat exchanger and reduces the investment costs compared to the trough technology with indirect thermal storage.

The tower technology has the potential for higher overall thermal collection efficiencies compared to the previously mentioned technologies because a large solar flux from the heliostat field is concentrated on the comparatively small surface area of the central receiver. Since the losses of the receiver depend on its geometry and the receiver surface temperatures, the losses are not proportionally affected by the solar flux levels. Due to the highly concentrated solar radiation, it is also possible to achieve higher temperatures of the working

fluid, which increases the efficiency of the power conversion cycle. However, higher temperatures of the working fluid lead to higher surface temperatures and therefore to higher thermal losses of the receiver. This tradeoff must be optimized. These considerations are currently limited by the maximum bearable solar flux levels (1.2 MW/m^2 for Solar Tres [Lata, Rodriguez, & Lara, 2006] of the materials used for the receiver and also the metallurgical restraints for maximum temperature in steam turbines. Research on approaches that will allow increasing the receiver flux limits as well as the development of high efficiency supercritical steam turbines for the solar power tower plants that operate with steam temperatures up to $650^{O}C$ [Sargent & Lundy LLC Consulting Group, 2003] is ongoing.

Figure 1-3: Solar Two-MOJAVE DESERT, CALIFORNIA

1.3.3 Linear Fresnel Systems

Similar to the parabolic trough system, the linear Fresnel collector heats a linear receiver element that carries a liquid or gaseous heat transfer medium (usually water/steam). Instead of parabolic concentrators, the solar radiation is reflected by a series of parallel arranged, long and flat mirrors that focus the radiation on a single line-collector that is placed above the

mirror field as shown in Figure 1.4. Studies [Häberle, et al., 2002] indicated that linear Fresnel collector systems achieve only approximately 70% of the thermal efficiencies accomplished with parabolic trough systems. But due to simpler component geometry and mechanics the capital and operating costs are also lower compared to the trough technology.

Figure 1-4: Compact Linear Fresnel Collector in Bakersfield, California by Ausra

1.3.4 Dish-Stirling Systems

The parabolic dish system uses a parabolic dish shaped mirror or a modular mirror system that approximates a parabola and incorporates two-axes tracking to focus the sunlight onto receivers located at the focal point of the dish, which absorbs the energy and converts it into thermal energy. This can be used directly as heat for thermal application or for power generation. The thermal energy can either be transported to a central generator for conversion, or it can be converted directly into electricity at a local generator coupled to the receiver (Figure 1.5).

The mirror system typically is made from a number of mirror facets, either glass or polymer mirror, or can consist of a single stretched membrane using a polymer mirror of thin metal stretched membrane. The PDCs (Parabolic Dish Collector) track the sun on two axes, and thus they are the most efficient collector systems. Their concentration ratios usually range from 600 to 2000, and they can achieve temperatures in excess of 1500^{O}C. Rankine-cycle engines, Brayton-cycle engines, and sodium-heat engines have been considered for systems using dish-mounted engines the greatest attention though was given to Stirling-engine systems.

The main challenge facing distributed-dish systems is developing a power-conversion unit, which would have low capital and maintenance costs, long life, high conversion efficiency, and the ability to operate automatically. Several different engines, such as gas turbines, reciprocating steam engines, and organic Rankine engines, have been explored, but in recent years, most attention has been focused on Stirling-cycle engines. These are externally heated piston engines in which heat is continuously added to a gas (normally hydrogen or helium at high pressure) that is contained in a closed system.

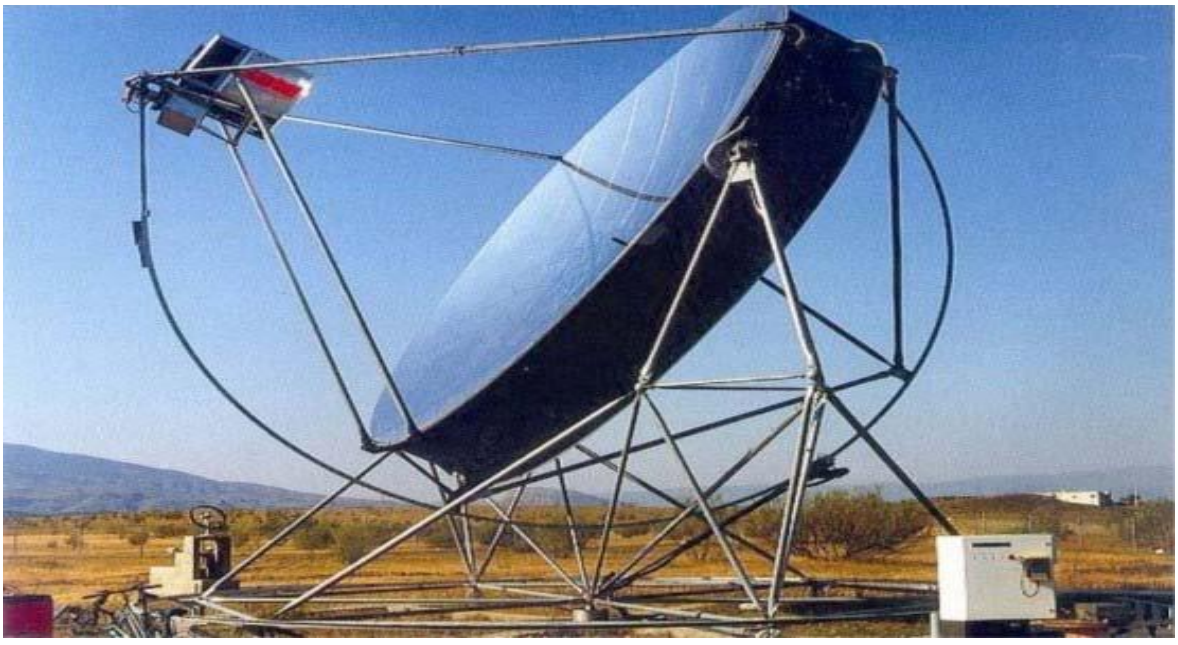

Figure 1-5: Parabolic Dish Systems

1.4 Objective of the Thesis

The major objective of this thesis is to model and simulate the central tower power generation system with thermal storage system. The objective of the model is to predict the transient behaviour of the thermodynamics variables associated to the thermohydraulic output power of the evaporator (mainly temperature, pressure, and specific enthalpy), when the external disturbances (concentrated solar radiation, ambient temperature, and wind speed and direction, etc…) change. The simulation processes could include the determination of temperature and mass flow rate variations of the circulating primary and secondary media, the solar energy absorbed, and total power output of the system as a function of time.

The specific objectives of the thesis are:

- Modeling of the central tower system power plant using appropriate software (EES and TRNSYS);
- Simulating to investigate the effects of varying parameters on the performance of the central tower system power plant using appropriate simulation software (TRNSYS);
- Cost and financial analysis of the power plant using appropriate software, (SAM)

1.5 Methodology

At the beginning, related literatures were collected from different electronic media and Addis Ababa university library catalogue. Then the weather data for plant analysis location was collected from energy plus weather website. Next to that, modeling of the power cycle was performed using EES software to obtain reference plant parameters. Following the power plant system modeling in TRNSYS16 simulation studio, the system was simulated to obtain a representative day power outputs. Financial and economic analysis of the power plant which includes different financial and economic parameters of the project was carried on using SAM software. Finally conclusions and recommendations were forwarded based on the thesis work performed.

1.6 Thesis Organization

There are seven chapters in this thesis. The first chapter covers the introduction part which deals with the background and objective of the thesis. The second chapter deals with the solar tower systems describing the main elements of the plant system namely heliostat field, tower, receiver, HTF and thermal storage. Chapter three is on modeling of power cycle using EES. This chapter yields the outputs that are used as reference values used either input or parameters during system simulation using TRNSYS. The discussion in this chapter is limited to steady state plant operation at rated capacity of 10MWe. The fourth chapter discusses the CRS power plant modeling in TRNSYS. It discusses the general overview of the software (TRNSYS) and its input and output parameters. It also covers the component-wise and overall system modeling of the plant in TRNSYS simulation studio. The fifth chapter deals with the simulation result analysis. This chapter shows the representative clear and cloudy day transient system simulation results for the design parameters from chapter three. Following this, the financial and economic analysis of the system is performed on chapter six. Finally, the conclusions and recommendations are forwarded in chapter seven.

CHAPTER TWO

THE SOLAR TOWER SYSTEM

2.1 Introduction

Solar Central Tower systems have a single receiver placed on top of a tower surrounded by hundreds of mirrors (heliostats) which follow the apparent motion of the sun in the sky and which re-direct and focus the sunlight onto the receiver. These plants are best suited for utility-scale applications in the 30 to 400 MW range. System design for a central receiver application is performed in a manner similar to that when other types of collector are used. Basically, the thermal output of the solar field is found by calculating collection efficiency and multiplying this by the solar irradiance falling on the collector (heliostat) field. The Power Tower system described in this chapter includes the major components of a central receiver system, their interaction in a particular field design and a 'molten salt' storage system.

2.2 The Power Tower System Background

Since the early 1980s, Power Towers have been fielded in Russia, Italy, Spain, Japan, France, and the United States. In Table 2.1, these experiments are listed along with some of their characteristics. These experimental facilities were built to prove that solar Power Towers could produce electricity. The Power Towers have also been built to get experience with individual system components to find out which parts need improvement (DOE IV, 1997).

California is one of the regions in the world that strongly promote the use of solar and wind energy. As a result of this promotion, a program that should use solar energy to make steam to drive turbines began near Barstow in the late 1970s. This program led to the building of Solar One. This is the most expensive solar power station, which started to produce electricity in 1982. Together with Solar Two, Solar One is the largest experimental Power Tower that has been built. The Solar One is a central receiving station or 'Power Tower' with 1818 mirrors of 39.3 m^2 reflective area each that are laid out in semi-circles around a 78 m

high tower. The mirrors focus sunlight on to a boiler at the top of the tower. As the Sun moves, the mirrors turn around, following it. The Solar One receiver heated sub-cooled water to superheated steam, which drove a turbine. The superheated steam was also used to charge an oil-rock thermocline storage system. The pressure of the steam turns a turbine, which drives a generator to produce 10 MW of electricity. Solar One was very expensive to built, and to replace a conventional power station on MW-basis, a lot more than one Solar Power Tower would be needed. Consequently, the produced solar kWh will be considerably more expensive than fossil or nuclear kWh (Grasse, 1992).

Several small pilot systems were constructed in Europe and the USA with outputs of 0.5 to 10 MW (Holl, 1989). These schemes used water as the heat transfer fluid, with the resulting steam passing directly to the turbine. This proved to be unreliable (thermal transients initiated generator shutdowns) and inefficient. Other pilot schemes utilised molten sodium salts, with the thermal storage facility separated from the receiver and the turbine (to reduce thermal transients). In these schemes, the collector area was in the range of 4000-12000 m^2 per MWe rating and the tower heights were 50 -100 m. From these early efforts, a second generation of Power Towers has been developed which uses air (e.g. the PHOEBUS plant at Alméria, Spain) or molten salt (e.g. the Solar Two plant in the US) as the heat transfer medium. Considerable progress has been made since the first schemes in the early 1980s so that many of the main aspects of this technology are now in the demonstration stage. Further research is required for advanced receivers based on absorption by thin films of salts (Léon et. al., 1994) or air (Haeger et. al., 1994) as well as new types of heliostats (Jiménez, 1995).

Table 2-1: Experimental Power Towers in the World [Romero, et al.2002]

Project	Country	Power (MWe)	Heat Transfer Fluid	Storage media	Beginning operation
SSPS	Spain	0.5	Liquid Sodium	Sodium	1981
EURELIOS	Italy	1	Steam	Nitrate Salt/water	1981

SUNSHINE	Japan	1	Steam	Nitrate Salt/water	1981
Solar One	U.S.A	10	Steam	Oil/Rock	1982
CESA-1	Spain	1	Steam	Nitrate Salt	1982
MSEE/Cat B	U.S.A	1	Nitrate Salt	Nitrate Salt	1983
THEMIS	France	2.5	Hitec Salt	Hitec Salt	1984
SPP-5	Russia	5	Steam	Water/Steam	1986
TSA	Spain	1	Air	Ceramic	1993
Solar Two	U.S.A	10	Nitrate Salt	Nitrate Salt	1996
Consolar	Israel	0.5**	Pressurized Air	Fossil Hybrid	2001
Solgate*	Spain	0.3	Pressurized Air	Fossil Hybrid	2002
PS10*	Spain	10	Air	Ceramic	2004
Solar Tres*	Spain	15	Nitrate Salt	Nitrate Salt	2004

***Project under development**

****Thermal**

To encourage the development of molten-salt Power Towers the Solar One plant was redesigned with a molten-salt heat-transfer system. After the rebuilding of Solar One the installation was entitled Solar Two. The objective of Solar Two was to mitigate the perceived technological and financial risks associated with the first commercial plants and to prove the molten-salt thermal storage technology. In Solar One, water was converted to steam in the receiver and used directly to power a conventional Rankine-cycle steam turbine. Solar Two

has a capacity of 10 MWe with enough thermal storage to continue to operate the turbine at full capacity for three hours after the sun has set (DOE IV, 1997).

2.3 System Description

The heliostats focus the solar energy onto a central receiver located on top of a tower see Figure 2.2. These mirrors cover typically 30-50 m^2 in area, although more modern designs cover 100- 150 m^2. They are slightly curved and are centrally controlled in order to track the sun in two dimensions. The temperature reached by the fluid in the receiver is tailored for the required purpose (e.g. 500-600^{O}C for electricity generation using a conventional steam turbine, 1000^{O}C for other purposes such as the testing of materials). In order to extend operation time, the schemes often incorporate a thermal storage facility (e.g. oil mixed with crushed rock or molten nitrate salts). The systems can be hybridised with a natural gas burner to provide better operating characteristics (Heliotech, 2000). The gas turbine produces power, which is fed to the grid, and steam, which is fed to the steam turbine of the Solar Tower System. Steam from the solar steam generator is blended with fossil steam from the gas turbine from the heat recovery steam generator before entering a steam turbine. With a gas turbine added, the Solar Tower system can still produce power when the sun is not strong enough to run the system solely. This is probably mainly the situation in the morning when the sun might not be strong enough to provide the needed start-up heat. In the evening, when the sun sets, a gas engine can upgrade the sun's last energy to a level, which is usable in the steam turbine.

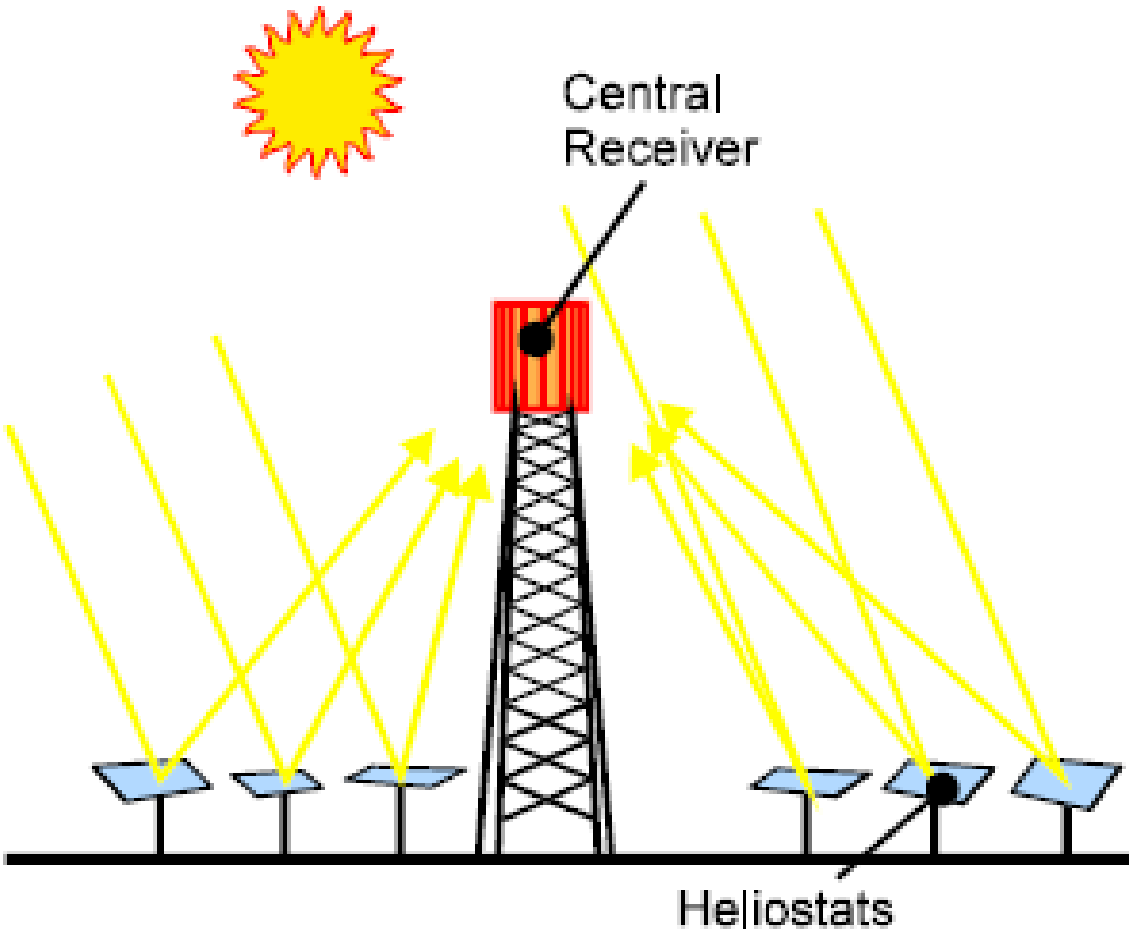

Figure 2-1: Principle of a Power Tower (SunLab, 2001)

In a Power Tower system the short wave sunlight is absorbed by a heat transfer fluid (HTF) in the central receiver and then transformed into long wave heat. The heat transfer fluid is pumped to a heat exchanger to produce high-pressure steam to drive a generator, see Figure 2.2. The heliostat field that surrounds the tower is laid out to optimize the annual performance of the plant. The field and the receiver sizes depend on the needs of the utility, in a maximum required energy to produce steam for the steam turbine. Consequently, a thermal storage system can be charged while the plant is producing power at full capacity (Eisenbeiß, 1996)

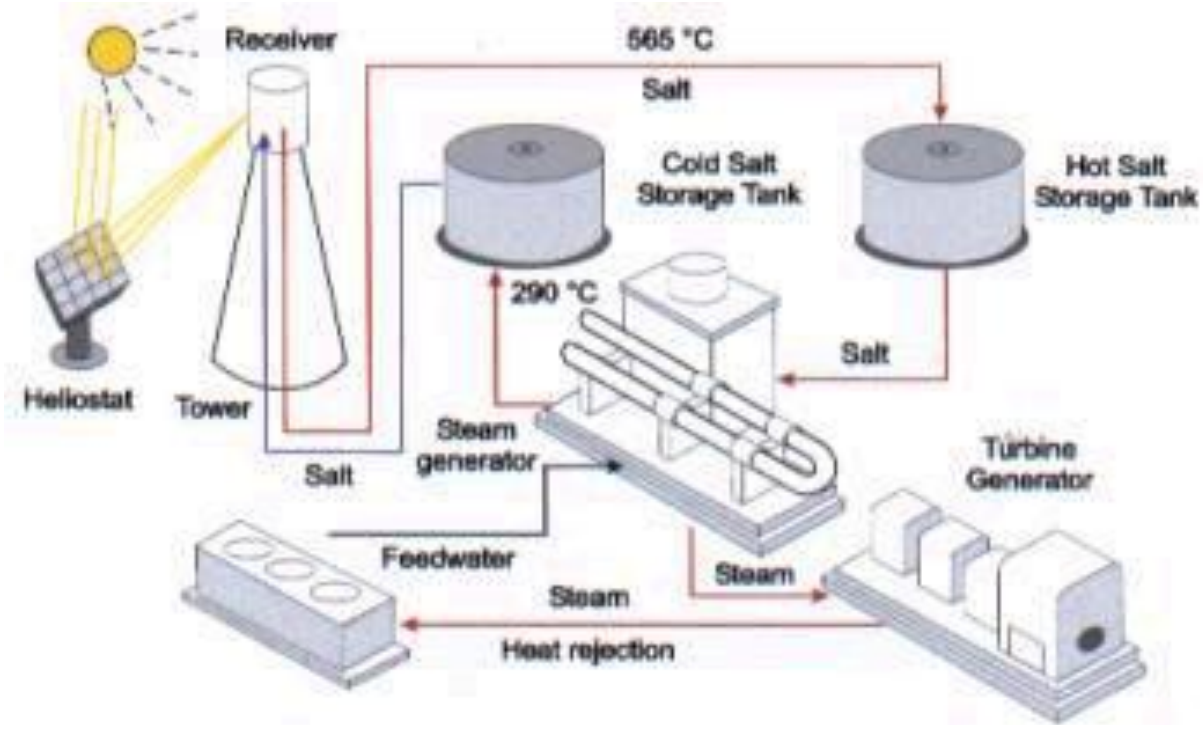

Figure 2-2: A Schematic Power Tower System (SunLab, 2001)

The heliostat field together with the receiver is called collector system. The ratio of the thermal power provided by the collector system to the peak thermal power that is required by the generator is called the solar multiple. With a solar multiple of approximately 2.7, a Power Tower with molten-salt storage tanks located in the California Mojave desert can be designed for an annual capacity factor of about 65%. This means that a Power Tower could potentially operate for 65% of the year without the need for a fossil fuel fired back-up installation. Without the molten salt storage tanks, concentrating solar technologies are limited to annual capacity factors near 25%. Because of the storage, power output from the generator remains constant through fluctuations in solar intensity until all energy stored in the hot tank is depleted (DOE IV, 1997).

2.4 Storage System

Energy storage and dispatchability are very important for the success of solar Power Tower technology. The Solar One thermal storage system stored heat from solar-produced steam in a tank filled with rocks and sand using oil as the heat transfer fluid. The system extended the plant's power-generation capacity into the night and provided heat for generating low-grade

steam for keeping parts of the plant warm during off-hours and for morning start-up. Unfortunately the storage system was complex and thermodynamically inefficient. During the operation of Solar One, research began on a molten salt Power Tower design that cumulated in the Solar Two project. It is believed that molten salt is the key to cost effective energy storage see Table 2.2

Table 2-2: Comparison of Solar Energy Storage Systems

	Installed cost of energy storage for 200MW plant [$/kWhr]	**Lifetime of storage system [years]**	**Round-trip storage efficiency [%]**	**Maximum operating temperature [^{O}C]**
Molten salt power tower	30	30	99	567
Synthetic oil parabolic trough	200	30	95	390
Battery storage grid connected	500 to 800	5 to 10	76	N/A

In a molten-salt solar Power Tower, liquid salt at 290°C is pumped from a 'cold' storage tank through the receiver where it is heated to 565°C and then on to a 'hot' tank for storage. When power is needed, hot salt is pumped to a steam generator that produces superheated steam for a conventional Rankine cycle turbine/generator. From the steam generator, the salt is returned to the cold tank where it is stored and eventually reheated in the receiver. Determining the optimum storage size to meet power-dispatch requirements is an important part of the system design process. Calculations have proven that storage tanks can be designed with sufficient capacity to power a turbine at full output for up to 13 hours (ConSolar, 1999). The salt storage medium is a mixture of 60% sodium nitrate and 40% potassium nitrate. It melts at 220°C and is maintained in a molten state (290°C) in the 'cold'

storage tank. Molten salt can be difficult to handle because it has a low viscosity (similar to water) and it adheres metal surfaces extremely well. Consequently, it can be difficult to contain and transport. An important consideration in successfully implementing this technology is the identification of pumps, valves, valve packing, and gasket materials that will work with molten salt. Accordingly, Solar Two is designed with a minimum number of gasket flanges and most instrument transducers, valves, and fittings are welded in place. The energy storage system for Solar Two consists of two 875,000 litre storage tanks. Thermal capacity of the system is 110 MW. A natural convection cooling system is used in the foundation of each tank to minimise overheating and excessive dehydration of the underlying soil. The steam generator system (SGS) and heat exchangers consist of a shell-and-tube superheater, a steam boiler, and a shell-and-tube preheater. Stainless steel cantilever pumps transport salt from the hot-tank through the SGS to the cold tank. Salt in the cold tank is pumped with multi-stage centrifugal pumps up the tower to the receiver (DOE IV 1997).

2.5 The Heliostat Field

The collectivity of heliostats located around the central tower is called the heliostat field. It represents a Fresnel-type concentrator. Since all heliostats are situated in the same plane they do not approximate one single parabola but each individual heliostat approximates a segment of a separate parabola. Thus, the achievable concentration ratio of CRSs is significantly lower than that of parabolic dish systems, reaching values of 500 to 1500 in practice.

The positioning of heliostats around the central tower requires a complex optimization process that depends mainly on the latitude of the site, the needed concentration, the power level and the quality as well as the size of the heliostats. It can be distinguished between a north field configuration, where heliostats stand only on one side of the tower (northwards in the northern hemisphere) to reflect the radiation to a southward direction aiming at the receiver at the top of the tower, and a surround field, where heliostats around the tower reflect the radiation to a cylindrical receiver or a number of individual receivers facing various directions. Which one of the both options is favored depends on the relative impact of two compensating effects:

- Heliostats to the north of the tower (for the northern hemisphere) can reflect more energy back to the tower because their projected area towards the sun is larger than for southern heliostats which have to be aligned much differently to reflect the radiation "backwards overhead" to the tower. This effect is called "cosine loss".

- The greater the distance between the heliostat and the tower the higher the losses due to atmospheric attenuation and the fraction of radiation that misses the receiver.

Thus, southern heliostats that are located close to the tower may provide more energy than northern heliostats that stand very far away despite their higher cosine losses. This leads to the fact, that for northern latitudes and for small power levels a northern field is the optimal choice whereas for sites closer to the equator and for larger power levels surround fields achieve a higher annual energy yield. Thus: based on the above discussion, the researcher decides to use the surrounding heliostat arrangement with cylindrical central receiver for this work.

The heliostat used in Solar One is shown in Figure 2.3. The reflecting element of a heliostat is typically a thin, back (second) surface, low-iron glass mirror. This heliostat is composed of several mirror module panels rather than a single large mirror. The thin glass mirrors are supported by a substrate backing to form a slightly concave mirror surface. Individual panels on the heliostat are also canted toward a point on the receiver. The heliostat focal length is approximately equal to the distance from the receiver to the farthest heliostat. Subsequent "tuning" of the closer mirrors is possible.

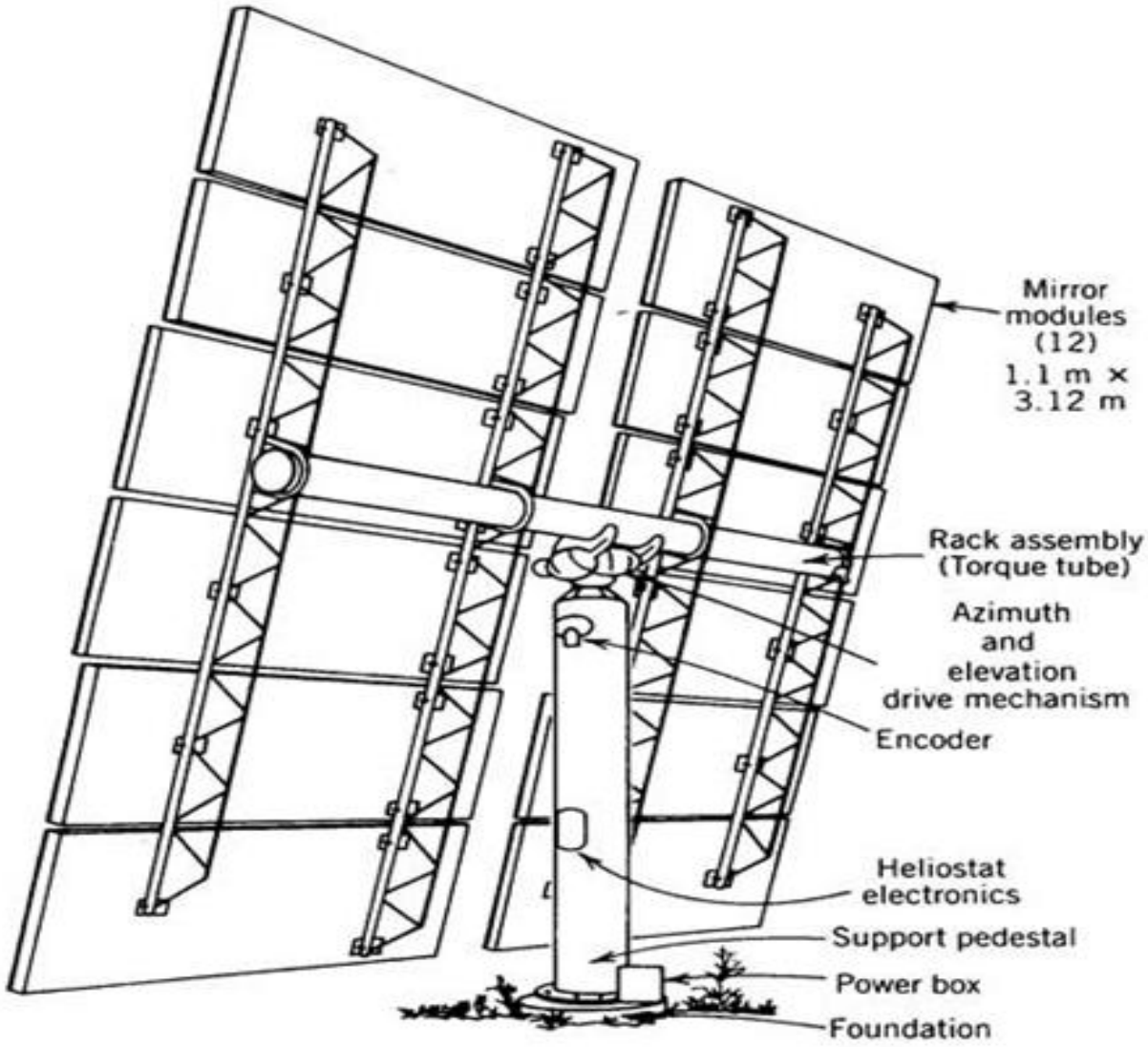
Mirror modules (12) 1.1 m × 3.12 m
Rack assembly (Torque tube)
Azimuth and elevation drive mechanism
Encoder
Heliostat electronics
Support pedestal
Power box
Foundation

(a)

(b)

Figure 2-3: (a) Backside of the Heliostat used at the Solar One Central Receiver Pilot Plant in Barstow, CA. (b) Front View of the PSI 120 Heliostat.

Another heliostat design concept, not so widely developed, uses a thin reflective plastic membrane stretched over a hoop. This design must be protected from the weather but requires considerable less expenditure in supports and the mechanical drive mechanism because of its light weight. Membrane renewal and cleaning appear to be important considerations with this design.

2.6 Angles for Heliostat Tracking System

The reflective surface of a heliostat is mounted or supported on a pedestal that permits movement about the azimuth and elevation axis. Movement about each axis is provided by a fractional-horsepower motor through a gearbox drive. These motors receive signals from a central control computer that accurately points the reflective surface normal halfway between the sun and the receiver. Figure 2.4 shows the arrangement of this half angle and subsequent equations are derived to get an expression for the two important angles (altitude and azimuth of the reflecting surface) for heliostat tracking system.

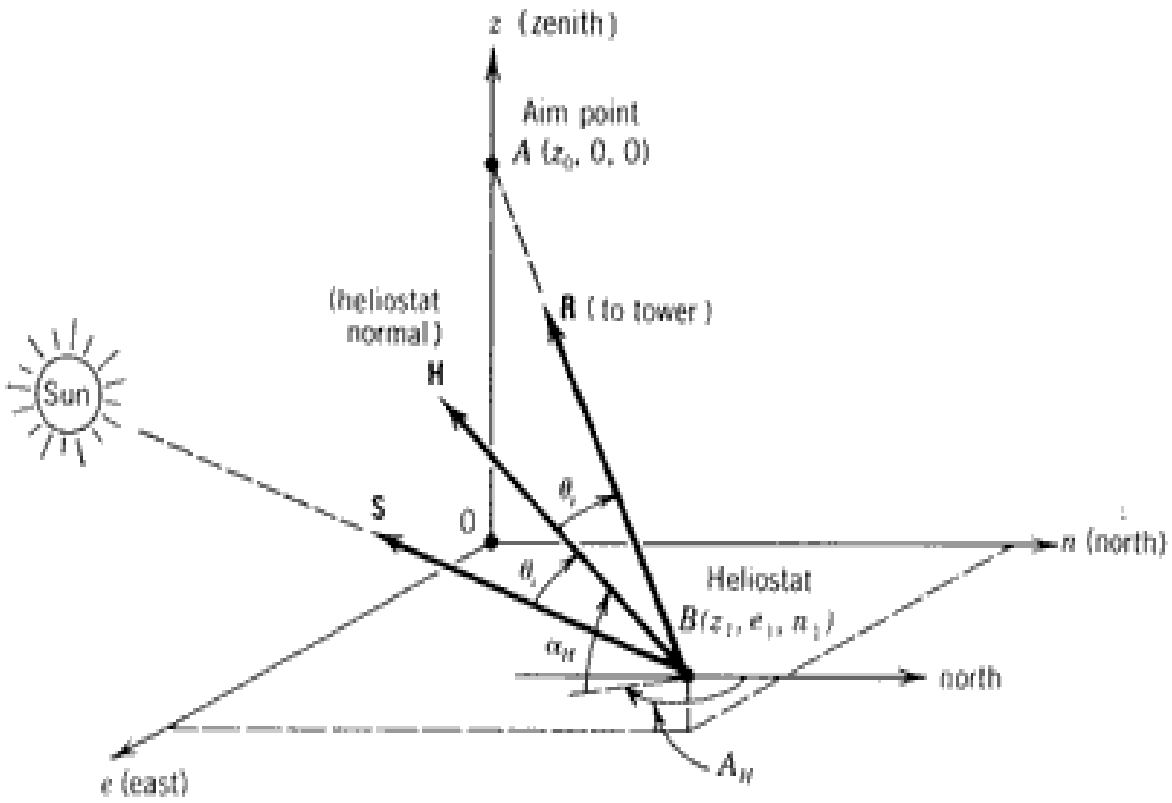

Figure 2-4: coordinates defining the reflection of the sun's rays by a heliostat to a single aim point. Vector H is normal to the heliostat reflecting surface

The appropriate geometry can be best described by using zenith, east, and north (z, e, and n) coordinates with their origin O at the base of the aim point A as shown in Figure 2.4. The location of a reflecting surface B can be defined as z_1, e_1 and n_1 and the aim point located at a distance z_{00} above the origin.

To predict the reflector (heliostat) altitude α_H and azimuth (A_H) angles, three unit vectors must be described. A central sun ray unit vector (**S)** pointing toward the sun and a unit vector pointing from the reflector toward the aim point (A) are defined as:

$$\boldsymbol{S} = S_z i + S_e j + S_n k \tag{2.1}$$

and

$$R = \frac{(z_0 - z_1)i - e_1 j - n_1 k}{\sqrt{(z_0 - z_1)^2 + e_1^2 + n_1^2}} \quad (2.2)$$

where *i*, *j*, and *k* are the unit vectors in the *z*, *e*, and *n* directions respectively.

Defining Equation (2.2) in terms of direction cosines:

$$\boldsymbol{R} = R_z i + R_e j + R_n k \quad (2.3)$$

The third vector of interest is a unit vector normal to the reflector surface. This is defined as:

$$\boldsymbol{H} = H_z i + H_e j + H_n k \quad (2.4)$$

Table 2.3 summarizes the sign conventions used to develop the angles related to heliostat design.

Table 2-3: Sign Convention for Important Heliostat Angles

Title	Symbol	Zero	Positive direction	Range	Equation number	Figure number
Heliostat Angles						
Angle of Incidence	θ_i	Perpendicular to surface	Toward surface	0 to 90^0	2.6	2.2
Surface Altitude	α_H	Horizontal	Up	0 to 90^0	2.8	2.2
Surface Azimuth	A_H	Due North	Clockwise	0 to 360^0	2.9	2.2

Since the laws of specular reflection require that the angle of incidence (θ_i) is equal to the angle of reflection, an expression for this angle can be written in terms of the central sun ray unit vector (**S**) and the aim point unit vector (**R**) as

$$\cos 2\theta_i = \boldsymbol{S}.\boldsymbol{R} \tag{2.5}$$

Using Equations (2.1) and (2.2):

$$\cos 2\theta_i = R_z \sin\alpha + R_e \cos\alpha \sin A + R_n \cos\alpha \cos A \tag{2.6}$$

From which the angle of incidence or reflection can be obtained, if the position of the sun and the position of the aim point relative to the reflection surface are known.

The reflection surface unit normal (**H**) can be found by adding the incidence and reflection vector and dividing by the appropriate scalar quantity. This gives:

$$H = (R+S)/(2\cos\theta i) = ((Rz+Se)i + (Re+Se)j + (Rn+Sn)k)/(2\cos\theta i) \tag{2.7}$$

Substituting Equation (2.1) and describing the altitude and azimuth of the reflecting surface (α_H) and (A_H) respectively, in terms of the orthogonal coordinates, the following relation is obtained:

$$\sin\alpha_H = \frac{Rz+\sin\alpha}{2\cos\theta i} \tag{2.8}$$

and

$$\sin A_H = \frac{Re+\sin\alpha\sin A}{2\cos\theta i\cos\alpha_H} \tag{2.9}$$

The third expression is redundant but is written here for completeness:

$$\cos A_H = \frac{Rn+\cos\alpha\cos A}{2\cos\theta i\cos\alpha_H} \tag{2.10}$$

When the reflector azimuth is found by using the arc sine and arc cosine functions, the problem of quadrant ambiguity must again be recognized. It could be handled with simpler logic i.e. it is obvious that the angle of incidence (θi) cannot exceed 90 degrees.

2.7 Azimuth / Elevation Tracking

With azimuth / elevation tracking, the collector aperture must be free to rotate about the zenith axis and an axis parallel to the surface of the earth. The tracking angle about the zenith axis is the solar azimuth angle (A), and the tracking angle about the horizontal axis is the solar altitude angle (α).

Of primary interest to the designer of a two-axis tracking system is the rate at which these angles change called the slew rate. For the azimuth / elevation system, the rates of change of both the azimuth and elevation angles are not constant and depend on the location, time of day, and season. An expression for the slew rate about the horizontal axis may be found by taking the derivative of Equation for solar altitude with respect to time. Neglecting the very slow variation in declination angle, the result is:

$$\frac{d\alpha}{dt} = \frac{-\cos\emptyset \sin\delta \sin\omega}{\cos\alpha}\left(\frac{d\omega}{dt}\right) \tag{2.13}$$

The slew rate about the vertical axis is found similarly by derivation of solar azimuth Equation with respect to time and is

$$\frac{dA}{dt} = \frac{\cos\delta}{\cos A \cos^2\alpha}\left(\cos\delta \sin^2\omega \tan\alpha \cos\emptyset - \cos\alpha \cos\omega\right)\frac{d\omega}{dt} \tag{2.14}$$

2.8 Field Layout

Decisions regarding the best position for locating heliostats relative to the receiver and how high to place the receiver above the field constitute a multifaceted problem, in which costs and heliostat "loss" mechanisms are the variables. Some of these loss mechanisms and how they interact in shaping an optimum heliostat field are discussed in section 2.10.

Optimum field layouts are made by use of ray tracing techniques in an extensive computer analysis. These programs study representative heliostats in a field and check them for both blocking and shadowing by the heliostats in the two rows in front of the heliostat in

question. Two central receiver performance programs that have this capability are HELIOS (Biggs and Vittitoe, 1979) and DELSOL2 (Dellin et al., 1981).

This type of analysis is beyond the scope of this thesis; however, some general field layout guidelines have been discussed. It is generally best to arrange heliostats in a radial stagger pattern as shown in Figure 2.5. This pattern minimizes land usage as well as shadowing and blocking losses. The heliostats are tightly packed near the tower but must be sufficiently separated to prevent mechanical interference. For heliostats located farther from the tower, the spacing increases in order to minimize blocking of the reflected beams. Going out a long a radius, additional heliostats are added when spacing becomes too great and a new stagger pattern is established.

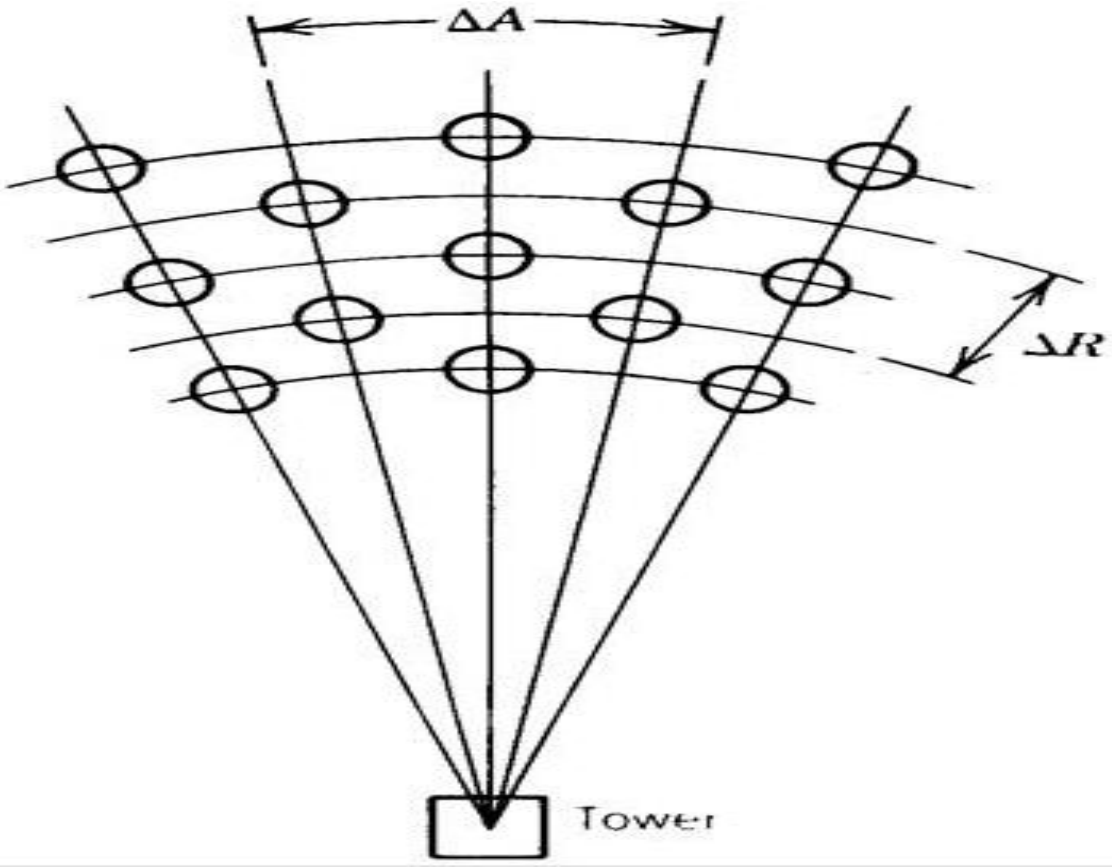

Figure 2-5: The Radial Stagger Heliostat Layout Pattern Developed By The University of Houston.

Heliostat packing density is the ratio of mirror area to field area. The average heliostat packing density from optimized ray trace analyses of shadowing and blocking is typically in the range of 0.2 to 0.25 (Battleson, 1981).

Optimized heliostat layouts developed at the University of Houston (Lipps and Vant-Hull, 1978) have produced a means of determining spacing and average field density for preliminary field layouts. The radial spacing ΔR and the azimuthal spacing ΔA, defined in Figure 2.5, are given by Dellin et.al. (1981) for high-reflectance heliostats (about 90 percent) in large fields as

$$\Delta R = HM\left(1.44\cot\theta_L - 1.094 + 3.068\theta_L - 1.1256{\theta_L}^2\right) \quad (m) \tag{2.13}$$

and

$$\Delta A = WM(1.749 + 0.6396\theta_L) + \frac{0.2873}{\theta_L - 0.04902} \quad (m) \tag{2.14}$$

where *HM* and *WM* are the height and width of the heliostat, respectively as depicted in Figure 2.3. The angle θ_L is the altitude angle to the receiver from the heliostat location of interest and may be calculated as

$$\theta_L = \tan^{-1}\left(\frac{1}{r}\right) \ (deg) \tag{2.15}$$

where *r* is the normalized distance from the tower to the heliostat location measured in "*tower heights*."

The local field density is the ratio of mirror area to land area at a particular point in the field. This may be calculated as

$$\rho_F = \frac{2DM\ WM\ HM}{\Delta R \Delta A} \tag{2.16}$$

where *DM*, the mirror density, is the ratio of mirror area to overall heliostat area.

The process of laying out a heliostat field consists of segmenting the land area around the tower into a number of concentric zones. Equations (2.13) and (2.14) are used to determine

the average or central radial stagger pattern within these zones, and Equation (2.16) is used to calculate the local field density. If large zones are selected, it may not be possible to maintain the azimuthal spacing defined in Equation (2.14) for all rings. Heliostats near the inner ring of the zone may produce mechanical interference or unacceptable blocking or shadowing. When this is the case, every fourth heliostat is normally removed from a ring in what is called a *slip plane* and the radial stagger pattern is restarted.

Figure 2.6 shows the spacing predicted by Equations (2.13) and (2.14). Note that for the heliostats farther from the tower, the radial spacing increases dramatically, whereas the azimuthal spacing decreases to the point where the heliostats at a particular radial distance have one heliostat width between them. Figure 2.7 shows the decrease in local field density as distance from the tower increases.

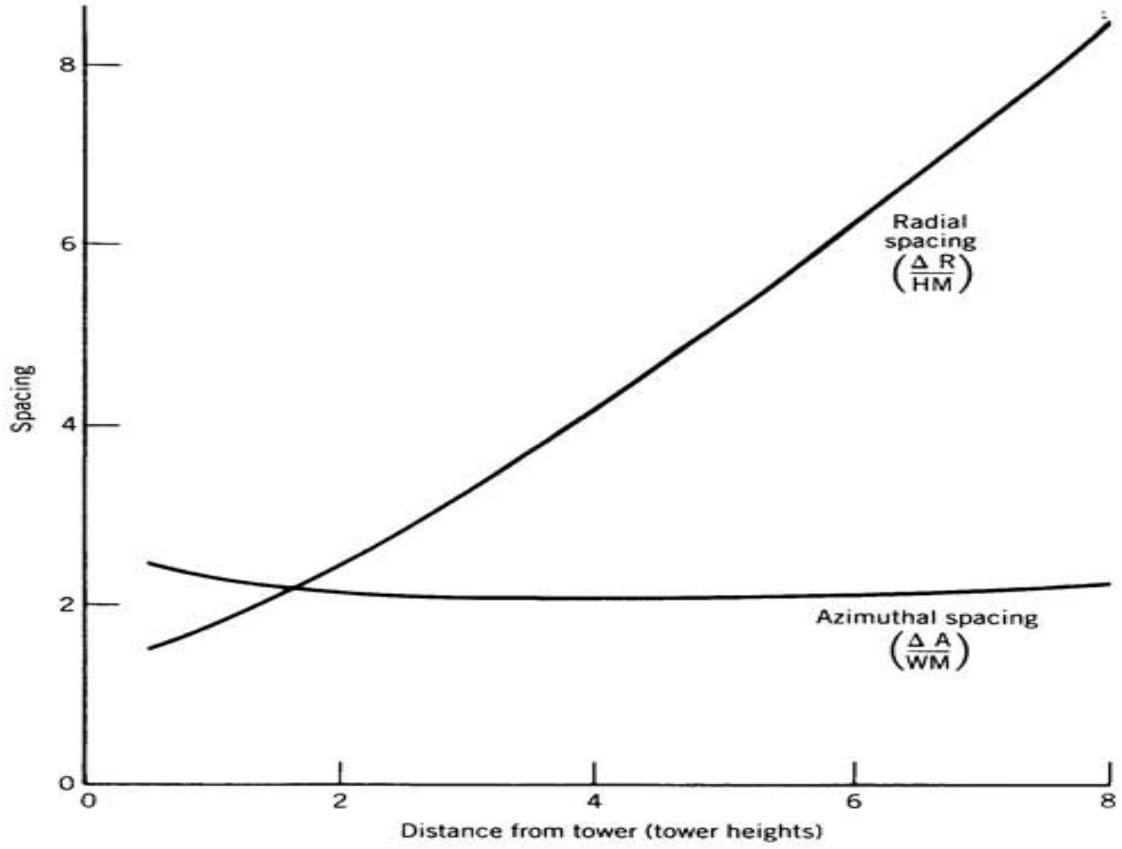

Figure 0-6: Heliostat Spacing for a Field using the Radial Stagger Layout Pattern.

Figure 2-7: Local Heliostat Densities as Predicted by Equation (2.16) for Radial-Stagger Field Layouts

2.9 Receiver and Tower Components

2.9.1 Receiver Design

There are two different receiver designs in CRSs, the external and the cavity design. In cavity receivers, the heat absorbing elements are located inside of an insulated cavity. The focal spot of the heliostat field coincides with the aperture of the cavity. In external receivers the heat transferring surfaces are exposed to the ambient and are located directly in the focal point of the heliostat field. Cavity receivers offer the benefit of lower heat losses but generally constrain the direction of the incoming radiation and thus impact the heliostat field arrangement. They also restrict the benefits of selective absorber surfaces when they may become available in the future and are generally costlier. External receivers allow for an

easier scale-up to higher power levels. In particular, cylindrical designs offer a flexible design of surround heliostat fields. However, in contrast to cavity receivers, the maximum concentration of the heliostat field that could be exploited is limited by the material constraints of the heat absorbing elements, because they are located directly in the focal point. Figure 2.8 shows the two types of receiver configuration.

A second criterion for the receiver design is the selected heat transfer fluid. Liquids like molten salt, liquid sodium or water/steam use irradiated tubular designs similar to those in conventional boilers, whereas for gaseous media also so-called "volumetric" absorbers are applied. They consist of high temperature resistant irradiated porous structures like wire meshes or ceramic foams. The radiation is absorbed by the material in the volume of the structure. Gas is driven through the porous material and is heated convectively. The high inner surface combined with the very small structures lead to a very efficient heat input into the gas, allowing us to transfer very high concentrated heat fluxes (0.5 MW/m^2 to 2.5 MW/m^2) [Robert Pitz-Paal] in spite of the poor heat conductivity of the gas. The high concentration heat fluxes lead to high receiver efficiencies even at high gas temperatures. Temperatures of more than 1000 °C could be demonstrated in prototype receivers at the Plataforma Solar in Almería (PSA).

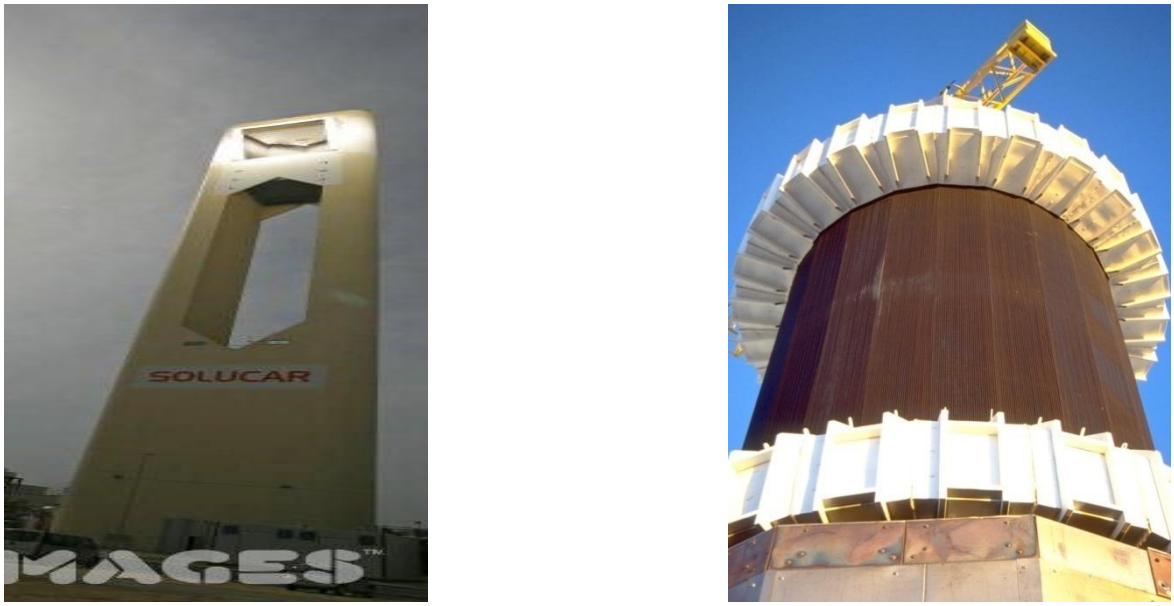

Figure 2-8: Two Possible Receiver Geometries Include the External Receiver (Right) and the Cavity Receiver (Left) (The external receiver is modeled in this thesis)

2.9.2 Heat Flux Considerations

The primary limitation on receiver design is the heat flux that can he absorbed through the receiver surface and into the heat transfer fluid, without overheating the receiver walls or the heat transfer fluid within them. A survey of typical design peak values is given in Table 2.4. The average flux over the entire absorber wall is typically one-half to one-third of these peak values. Two other important considerations are: (1) limiting the temperature gradients along the receiver panels and (2) the daily heat-cycling of the receiver tubes.

Table 2-4: Typical Receiver Peak Flux Design Values

Heat transfer fluid	Configuration	Peak Flux (MW/m^2)
Liquid sodium	In tubes	1.5
Liquid sodium	In heat pipes (transferring to air)	1.2
Molten nitrate salt	In tubes	0.7
Liquid water	In tubes	0.7
Steam vapor	In tubes	0.5
Air	In tubes	0.22

Source; Battleson (1981)

2.9.3 Tower Design

The height of the tower is limited by its cost. The weight and windage area of the receiver are the two most important factors in the design of the tower. Seismic considerations are also important in some locations. The weight and size of a receiver are affected by the fluid choice. Typical weights for a 380 MW receiver range from 250,000 kg for an external receiver using liquid sodium to 2,500,000 kg for a cavity air receiver [www.powerfromsun]. These would be placed at the top of a 140 to 170 m) tower if a surrounding heliostat field is used.

Proposed tower designs are of steel frame construction, using oil derrick design techniques, or concrete, using smokestack design techniques. Cost analyses indicate that steel frame towers are less expensive at heights of less than about 120 m and that concrete towers are less expensive for higher towers. The results of such a cost analysis described in Sterns Roger Engineering (1979) are shown in Figure 2.9.

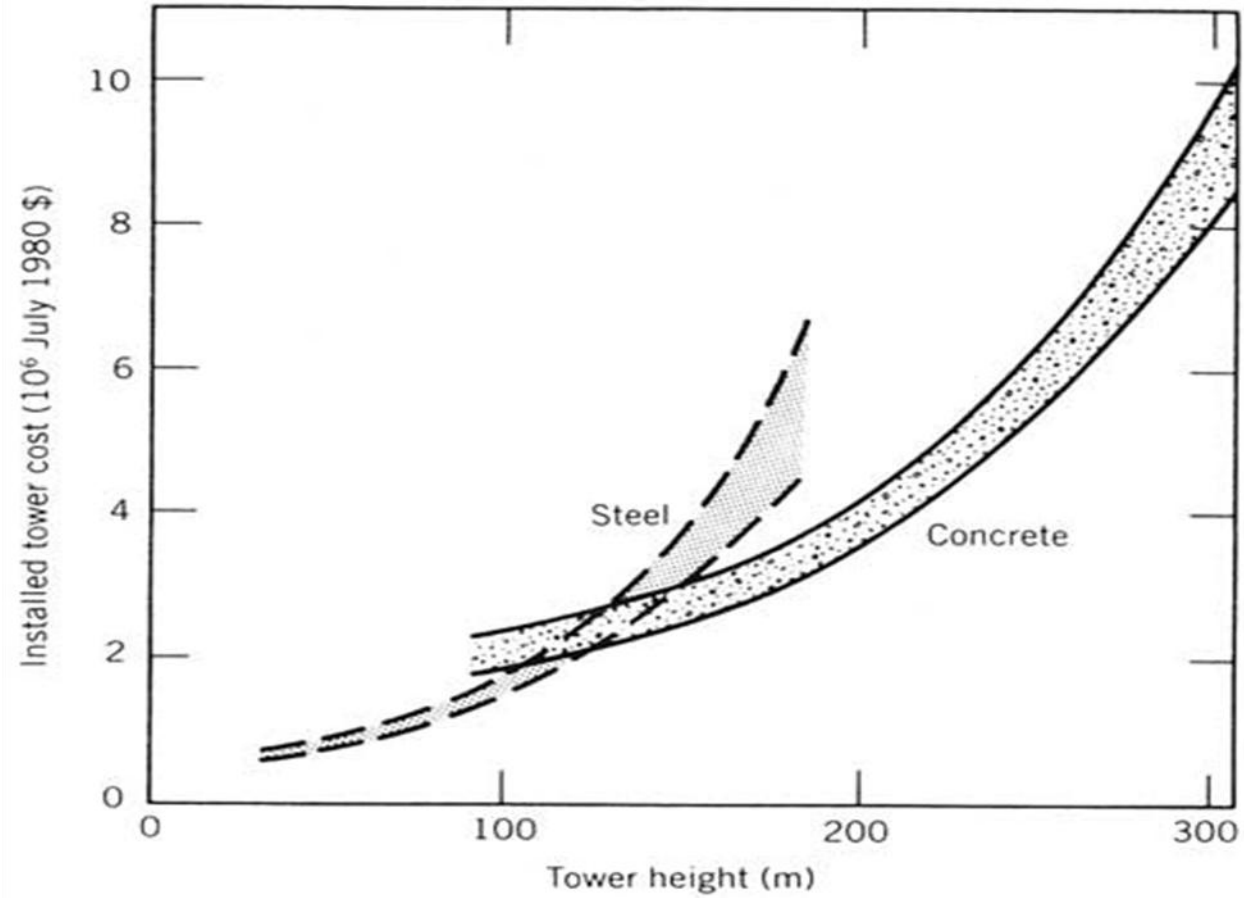

Figure 2-9: Tower Cost Data for Towers of Different Heights.

The band reflects use of different receivers having different windage and weight. These designs were made to withstand a 40 m/s wind (Battleson, 1981).

2.9.4 Beam Characterization Targets

Prominent on any photograph or drawing of a central receiver tower are the white targets located just below the receiver. These are beam characterization system (BCS) targets used to aid in periodic calibration and alignment of individual heliostats. They are coated with a

diffusely reflecting white paint, and are not designed to receive the flux of more than one or two heliostats. Instrumentation within the target area is used to determine the centroid and flux density distribution of the beam from a selected heliostat. If the centroid of the beam is not located where the field tracking program predicts it to be, tracking program coefficients are modified appropriately.

2.10 Energy Losses

As with the solar collector modules of other solar thermal power plant systems, the thermal performance of a central receiver system may be defined in terms of overall system efficiency. It is common to define this efficiency in terms of the beam (direct) normal solar irradiance $I_{b,n}$ and the total surface area of all of the heliostats in the field. The overall energy collection efficiency of a central receiver system therefore is

$$\eta_{col} = \frac{\dot{Q}_{useful}}{I_{b,n} n_h A} \tag{2.15}$$

Where $\dot{Q}_{useful}$ is the rate of energy addition to the working fluid (measured at the bottom of the receiver tower), n_h is the total number of heliostats in the field, and A_h is the total area of the heliostat (based on outside dimensions, not the reflective portion).
In this section the modes of energy loss which make up the overall efficiency term η_{col} and then how they are predicted is discussed in detail.

There are ten important sources of loss in a central receiver system that combine together to form the overall system energy collection efficiency. These losses, cast in terms of efficiencies, may be allocated to either field efficiency or receiver efficiency.
Field losses:

- Cosine
- Shadowing and blocking
- Reflectance
- Attenuation

Receiver losses:

- Spillage
- Absorptance
- Radiation
- Convection and conduction

2.10.1 Field Losses

The energy losses associated specifically with the heliostat field include four of the five greatest sources of energy loss. Among most of these losses that are going to be discussed in detail in this section, the largest loss term is the cosine loss. The cosine losses may be minimized through proper field design; however, they still represent the single most important loss mode.

Following the cosine effect in importance is the mirror reflectance loss. Although new low-absorption glass mirrors can be made with a reflectance of about 94 percent, age and dust soon reduce this to an average value of about 90 per cent. Keeping the mirrors washed, clean and in good repair is essential to maximize annual energy output.

The third most important loss factor for the losses is the atmospheric attenuation. As will be discussed in this section, atmospheric attenuation becomes significant for very large heliostat fields where the outer heliostats are far from the receiver.

Blocking and shadowing represent the next most important loss factor in central receiver system performance. Although at noon, when the sun's altitude is a maximum, there is usually no blocking or shadowing for a well designed field, significant blocking and shadowing does take place in the mornings and afternoons, especially in the winter, when the sun is low in the sky. Because of this, the annual average blocking and shadowing losses are also significant.

Defining each of these losses in terms of efficiency, the field efficiency is expressed as:

$$\eta_{field} = \eta_{cos}\eta_{shadow}\eta_{block}\eta_{refl}\eta_{atten} \quad (2.16)$$

where η_{cos}, η_{shadow}, η_{block}, η_{refl} and η_{atten} are efficiencies (i.e., 1 minus the fraction of energy lost in the process) based on cosine, shadowing, blocking, mirror reflectance, and atmospheric attenuation losses, respectively.

One loss source, receiver spillage, is a function of both the heliostat field (heliostat beam focus and distance from the tower) and the receiver (size of absorbing surface or aperture). This factor has been arbitrarily included with the receiver loss rather than with the field loss.

2.10.1.1 Cosine Effect

The major factor determining an optimum heliostat field layout is the cosine "efficiency" of the heliostat. This efficiency depends on both the sun's position and the location of the individual heliostat relative to the receiver. The heliostat is positioned by the tracking mechanism so that its surface normal bisects the angle between the sun's rays and a line from the heliostat to the tower. The effective reflection area of the heliostat is reduced by the cosine of one-half of this angle. This may be visualized by considering heliostats at two positions in a field as shown on Figure 2.10. Heliostat A has a small cosine loss since its surface normal is almost pointing toward the receiver. Heliostat B has a larger cosine loss because of the position it must assume in order to reflect the sun's rays onto the receiver. Note that the most efficient heliostats are located opposite the sun.

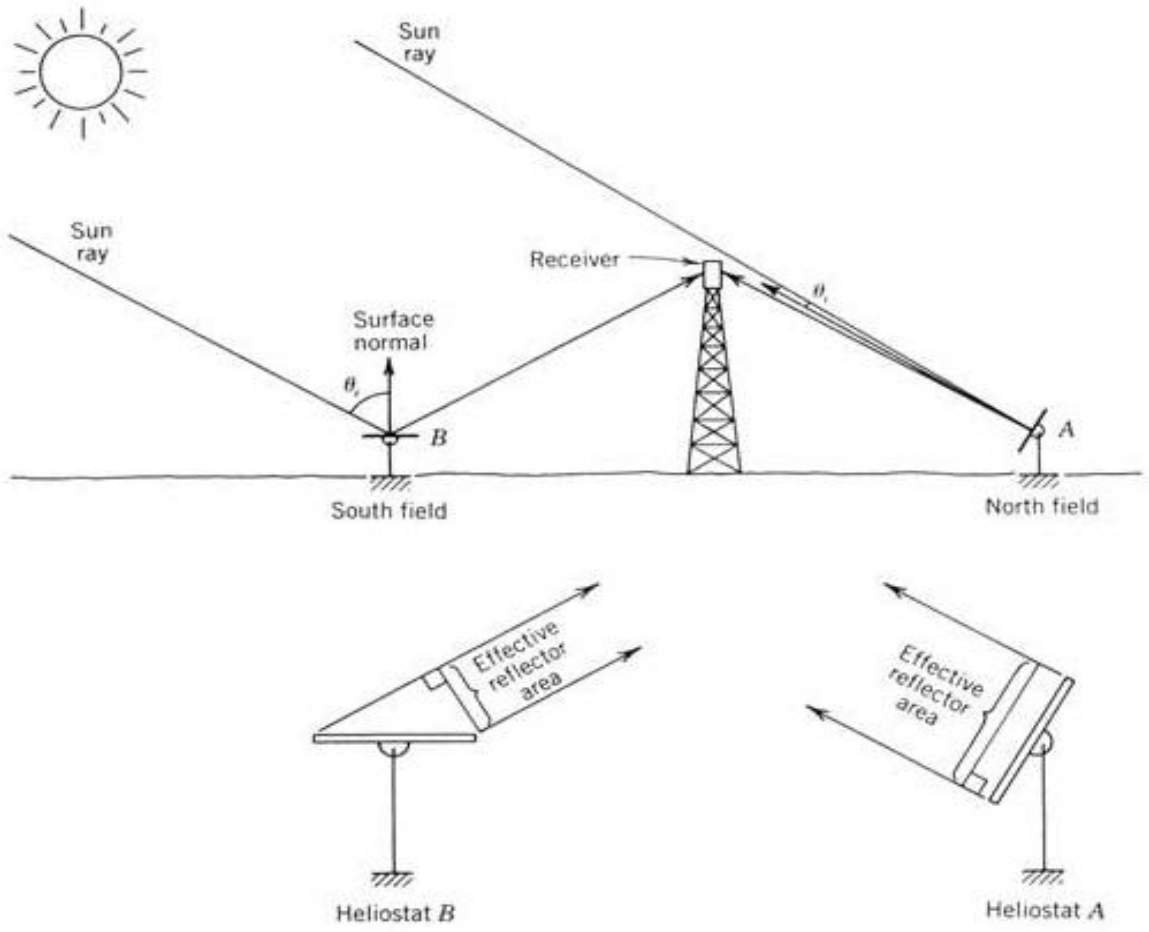

Figure 2-10: The cosine effect for two heliostats in opposite directions from the tower

For the noontime sun condition shown, heliostat A in the north field has much greater cosine efficiency than does heliostat B.

An expression for calculation of the cosine of this half angle incorporating the appropriate tower and heliostat position coordinates defined in Figure 2.4, is given as

$$\cos 2\theta_i = \frac{(z_0 - z_1)\sin\alpha - e_1\cos\alpha\sin A - n_1\cos\alpha\cos A}{[(z_0 - z_1)^2 + e_1^2 + n_1^2]^{1/2}} \tag{2.17}$$

where α and A are the sun's altitude and azimuth angles, respectively, and z, e, and n are the orthogonal coordinates from a point on the tower at the height of the heliostat mirrors as depicted in Figure 2.4.

Averaged over the entire year, the cosine efficiency of a field resembles that shown in Figure 2.11. As can be seen from the figure, the north field efficiency is dominant. In some designs as Solar One in Barstow, California, the south field heliostats are used only to preheat the water, which is subsequently turned into superheated steam in the rest of the receiver. This is done because of the reduced flux being reflected to this part of the receiver.

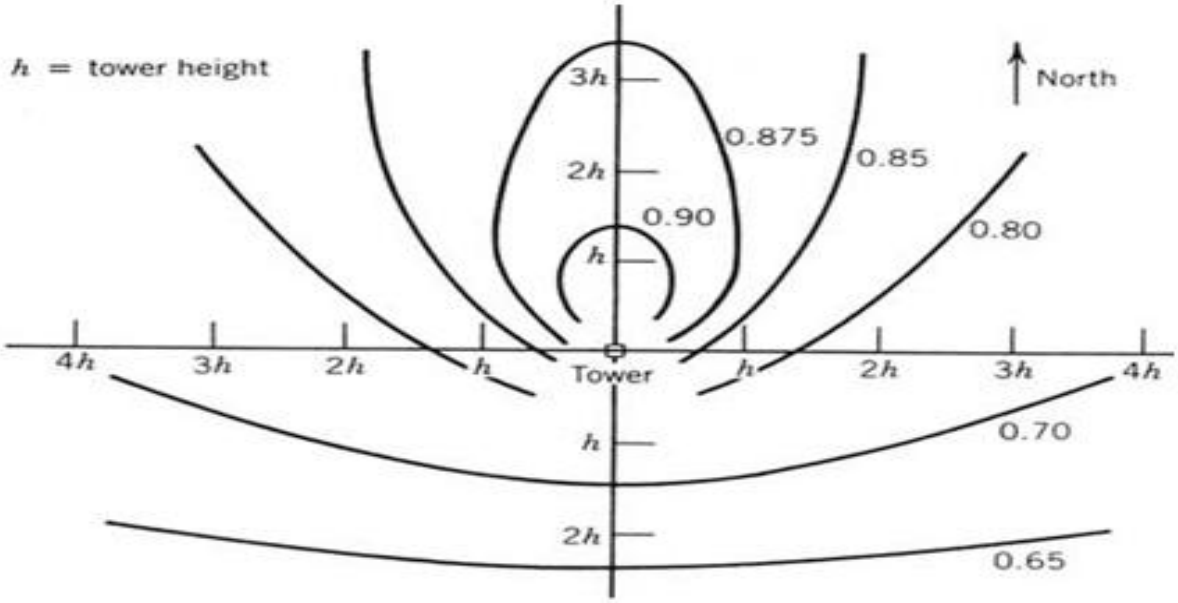

Figure 2-11: Annual Cosine Efficiency at Barstow, CA (Holl, 1978)

2.10.1.2 Shadowing and Blocking

The problem of one collector casting a shadow on an adjacent collector reduces the energy output of the shaded collector. For central receiver systems, there are two such interaction processes that reduce the amount of energy reaching the receiver. These are shadowing and blocking by adjacent heliostats.

Shadowing occurs at low sun angles when a heliostat casts its shadow on a heliostat located behind it. Therefore, not all the incident solar flux is reaching the reflector. Blocking occurs when a heliostat in front of another heliostat blocks the reflected flux on its way to the receiver. Both processes are illustrated in Figure 10.9. Blocking can be observed in a heliostat field by noting reflected light on the backs of heliostats.

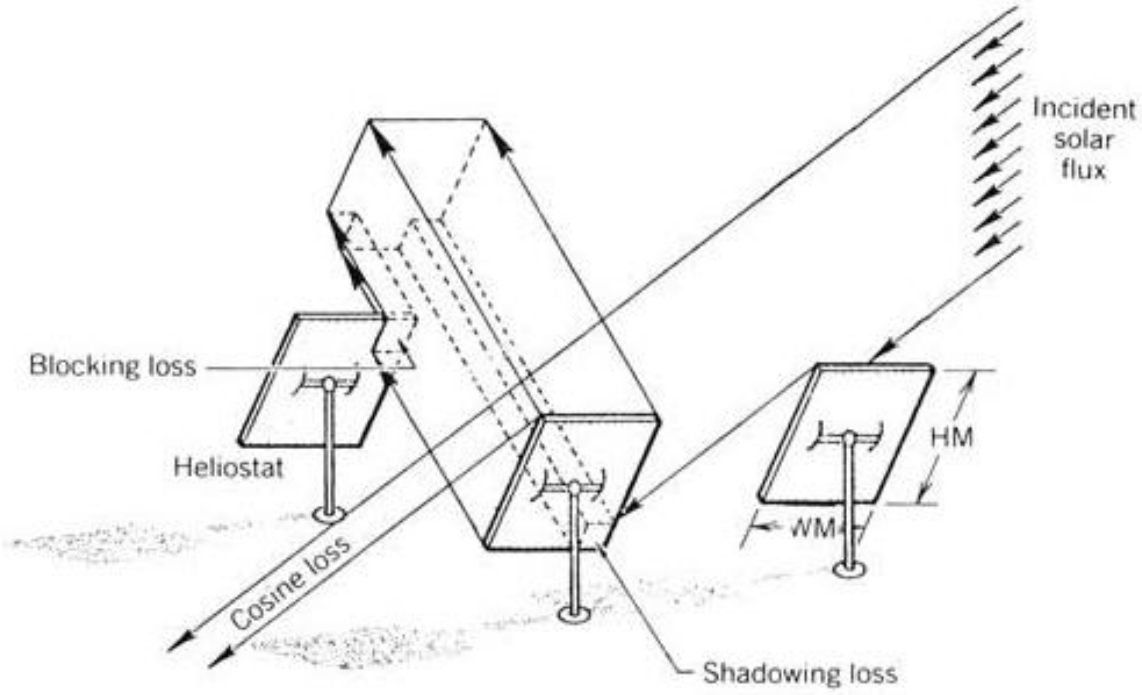

Figure 2-12: Shadowing and Blocking Loss of Solar Flux.

The amount of shadowing and blocking in a particular field layout is a function of the heliostat spacing, tower height, and sun angle.

2.10.1.3 Atmospheric Attenuation

Many factors in field layout suggest that the field should extend far to the north of a very high tower. One major limitation on the distance a heliostat is placed away from the tower is the attenuation of the reflected beam as it travels from the heliostat to the receiver.
Atmospheric transmittance has been approximated by Vittitoe and Biggs (1978) for a clear day (23-km visibility) and a hazy day (5-km visibility). For a clear day with 23-km visibility, the atmospheric transmittance is

$$\tau_a = 0.99326 - 0.1046S + 0.017S^2 - 0.002845S^3 \qquad (2.18)$$

where S is the slant range from heliostat to receiver in kilometers. For a hazy day with only 5-km visibility, the atmospheric transmittance is

$$\tau_a = 0.98707 - 0.2748S + 0.03394S^2 \quad (2.19)$$

Although these expressions were derived for a specific site altitude, they are strongly dependent on the aerosol distribution at ground level (visibility) and only slightly dependent on site altitude.

The effect of atmospheric attenuation is presented graphically in Figure 2.13. The maximum slant range for Solar One is 0.44 km (1440 ft); however, larger fields are envisioned in the near future where atmospheric attenuation will be even more significant.

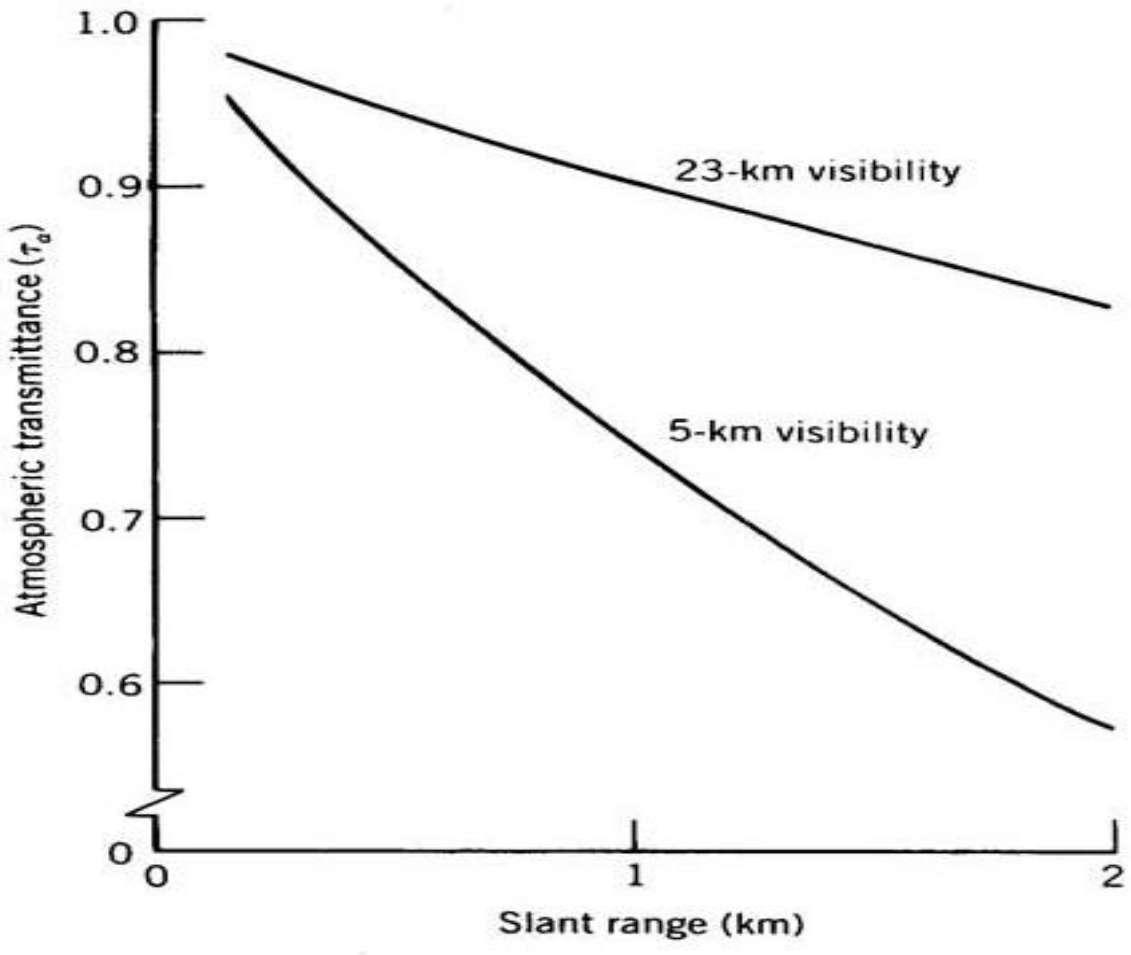

Figure 2-13: Atmospheric Transmittance for a Clear and a Hazy Atmosphere

2.10.2 Receiver Losses

The remainders of the losses are associated with the receiver. The various modes of receiver loss are depicted in Figure 2.14.

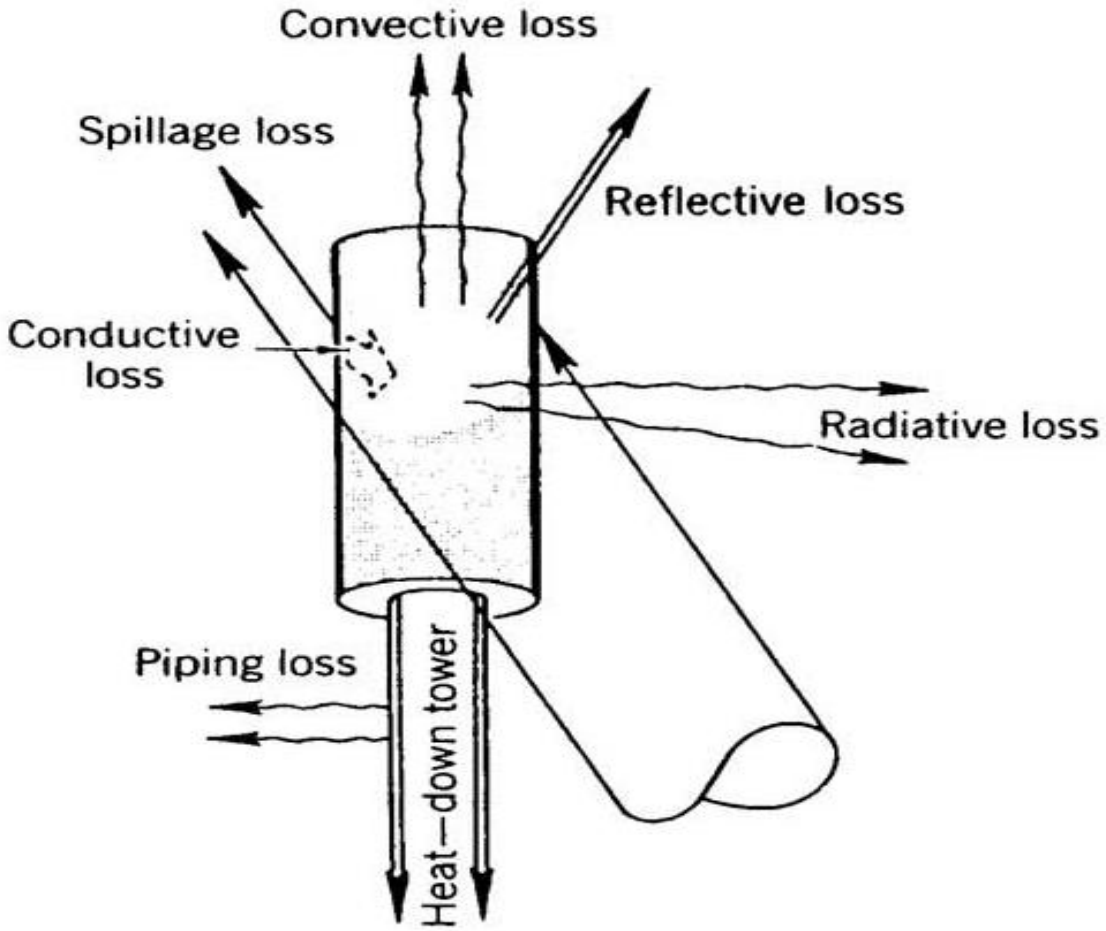

Figure 2-14: Receiver Heat Loss Modes.

Receiver efficiency may be defined as the product of each loss mode of efficiency as:

$$\eta_{receiver} = \eta_{cos}\eta_{spill}\eta_{absorp}\eta_{rad}\eta_{conv}\eta_{cond} \quad (2.20)$$

Where η_{spill},η_{absorp}, η_{rad}, η_{conv} andη_{cond} are efficiencies based on receiver spillage, absorption, radiation, convection, and conduction losses, respectively.

The important energy loss for the receiver originates from convection and radiation heat transfer to the surroundings. These losses depend on the design of the receiver, whether it is a cavity or external receiver, its heated (or aperture) area, and its operating temperature. Additional factors include the local wind velocity, ambient temperature, and the orientation of the receiver.

Studies have been made on the combined radiation, free and forced-convection losses from large surfaces, and tilted cavities. Siebers et al. (1982) have performed experiments on large vertical surfaces in horizontal flow, and their data are being used to predict losses from external receivers. Clausing (1981) has developed a method for predicting the natural convective loss from cavity receivers. A summary of these studies may be found in Siebers and Kraabel (1984).

Radiation and convection losses are primarily functions of the size of the receiver and the operating temperature of the system. For most currently conceived central receiver system designs, the receiver operates at a constant temperature. Therefore, the rate of energy being lost from the receiver is essentially constant throughout the day (and year) and the percentage loss increases in the morning and evening. This makes the annual average percentage loss greater than the design point (noon).

It is this constant receiver thermal loss rate that defines the operating threshold for the system. The system will operate only when the sun's energy is sufficient to overcome the receiver heat loss. This threshold usually occurs when the sun's altitude angle is about 15 degrees. Operation at sun angles below this is also constrained because of the rapid increase of heliostat blocking and shadowing.

Spillage loss or energy directed toward the receiver that does not fall on the absorbing area is a parameter of both the heliostat field and the receiver design. The heliostat surface accuracy, beam spread, mirror canting accuracy, and tracking accuracy all have a major effect on the flux distribution at the receiver and, therefore, on the spillage.

Spillage loss can be reduced by increasing the size of the receiver. The receiver is normally made large enough to intercept most of the reflected irradiance from the heliostat field and to keep peak incident flux values low enough for the heat transfer fluid. However, its size is limited because both radiation and convection heat losses are directly proportional to the receiver area. Determination of the optimum receiver size requires numerous optimization studies with field receiver computer models.

In contrast to spillage, receiver absorptance is only a function of the type of coating on the absorbing surface. Many current designs use a high-absorptance paint commercially marketed as Pyromark®. This paint is formulated for high temperature surfaces and has an absorptance of approximately 0.95. If the absorbing surface is inside a cavity, the effective absorptance (based on reflection back through the cavity aperture) increases to about 0.98.

The final receiver heat loss term represents the heat conducted away from the receiver. Most of this heat is lost through the receiver supporting brackets that connect the receiver to the tower structure. This is normally a small fraction of the total receiver heat loss and is kept small by minimizing the number and size of receiver attach points and using low thermal conductance metals such as stainless steels in their construction.

10.11 Heat Transfer Fluids

The choice of the heat transfer fluid to be pumped through the receiver is determined by the application. The primary choice criterion is the maximum operating temperature of the system followed closely by the cost-effectiveness of the system and safety considerations. Five heat transfer fluids have been studied in detail for application to central receiver systems. They are discussed separately in the paragraphs which follow.

The heat transfer fluids with the lowest operating temperature capabilities are heat transfer oils. Both hydrocarbon and synthetic-based oils may be used, but their maximum temperature is around 425°C. However, their vapor pressure is low at these temperatures, thus allowing their use for thermal energy storage. Below temperatures of about -10°C, heat must be supplied to make most of these oils flow. Oils have the major drawback of flammable and thus require special safety systems when used at high temperatures. Heat transfer oils cost about $0.77/kg.

Steam has been studied for many central receives applications and is the heat transfer fluid used in the Solar One power plant. Maximum temperature applications are around 540°C where the pressure must be about 10 MPa (1450 psi) to produce a high boiling temperature. Freeze protection must be provided for ambient temperatures less than 0°C. The water used in the receiver must be highly deionized in order to prevent scale buildup on the inner walls of the receiver heat transfer surfaces. However, its cost is lower than that of other heat transfer fluids. Use of water as a high-temperature storage medium is difficult because of the high pressures involved.

Nitrate salt mixtures can be used as both a heat transfer fluid and a storage medium at temperatures of up to 565°C. However, most mixtures currently being considered freeze at temperatures around 140 to 220°C and thus must be heated when the system is shutdown. They have a good storage potential because of their high volumetric heat capacity. The cost of nitrate salt mixtures is around $0.33/kg, making them an attractive heat transfer fluid candidate.

Liquid sodium can also be used as both a heat transfer fluid and storage medium, with a maximum operating temperature of 600°C. Because sodium is liquid at this temperature, its vapor pressure is low. However, it solidifies at 980°C, thereby requiring heating on shutdown. The cost of sodium-based systems is higher than the nitrate salt systems since sodium costs about $0.88/ kg.

For high-temperature applications such as Brayton cycles, it is proposed to use air or helium as the heat transfer fluid. Operating temperatures of around 850°C at 12 atm pressure are being proposed. Although the cost of these gases would be low, they cannot be used for storage and require very large diameter piping to transport them through the system.

According to SENER estimates, CRS power plants with molten-salt storage are, even at the design stage, the winning-choice for solar thermal power plants, in terms of energy efficiency, cost per unit produced, and surface required for power production. Moreover, high-capacity molten-salt storage makes it possible for the plant to provide dispatchable power, which, from the utilities' point of view, is crucial for the deployment of these plants

as capable of secure, predictable and programmable power supply, avoiding the problems for the national grid caused by other renewable sources of power, such as wind or photovoltaic.

According to the European Concentrated Solar Thermal Road Mapping study entitled ECOSTAR [Robert Pitz-Paal]; co-funded by the EC, the US 10-MW pilot plant experience has made the molten salt technology the best developed central receiver system today. Based on cost estimates provided by U.S. colleagues and the ECOSTAR evaluation, even small-scale (17 MWe) costs (LEC 18-19 cents/kWh) look relatively attractive. This is mainly attributable to very low thermal energy storage costs, which benefit from a three times larger temperature rise in the CRS compared to the parabolic trough systems. Furthermore, a higher annual capacity factor than in parabolic trough systems is possible, due to the smaller difference between summer and winter performance. Based on the above discussion, a mixture of 60% sodium nitrate and 40% potassium nitrate molten salt is used as a heat transfer fluid in this thesis.

CHAPTER THREE

POWER CYCLE MODEL USING EES

3.1 Overview of Engineering Equation Solver (EES)

EES (pronounced 'ease') is an acronym for Engineering Equation Solver. The basic function provided by EES is the solution of a set of algebraic equations. EES can also solve differential equations, equations with complex variables, do optimization, provide linear and non-linear regression, generate publication-quality plots, simplify uncertainty analyses and provide animations.

There are two major differences between EES and existing numerical equation-solving programs. First, EES automatically identifies and groups equations that must be solved simultaneously. This feature simplifies the process for the user and ensures that the solver will always operate at optimum efficiency. Second, EES provides many built-in mathematical and thermophysical property functions useful for engineering calculations.

The library of mathematical and thermophysical property functions in EES is extensive. EES allows the user to enter functional relationships in three ways. First, a facility for entering and interpolating tabular data is provided so that tabular data can be directly used in the solution of the equation set. Second, the EES language supports user-written Functions and Procedures similar to those in Pascal and FORTRAN. EES also provides support for user-written routines, which are self-contained EES programs that can be accessed by other EES programs. The Functions, Procedures, Subprograms and Modules can be saved as library files which are automatically read in when EES is started. Third, external functions and procedures, written in a high level language such as Pascal, C or FORTRAN, can be dynamically-linked into EES using the dynamic link library capability incorporated into the Windows operating system. These three methods of adding functional relationships provide very powerful means of extending the capabilities of EES.

EES is particularly useful for design problems in which the effects of one or more parameters need to be determined. The program provides this capability with its Parametric Table, which is similar to a spreadsheet. The user identifies the variables that are independent by entering their values in the table cells. EES will calculate the values of the dependent variables in the table. The relationship of the variables in the table can then be displayed in publication-quality plots. EES also provides capability to propagate the uncertainty of experimental data to provide uncertainty estimates of calculated variables. With EES, it is no more difficult to do design problems than it is to solve a problem for a fixed set of independent variables.

3.2 Rankine Cycle for the Central Receiver Power Plant

A Rankine cycle describes a model of steam operated forward heat engine most commonly found in power generation plants. Common heat sources for power plants using the Rankine cycle are the combustion of coal, natural gas and oil, and nuclear fission. The efficiency of a Rankine cycle is usually limited by the working fluid. Without the pressure reaching super critical levels for the working fluid, the temperature range the cycle can operate over is quite small: turbine entry temperatures are typically 565°C (the creep limit of stainless steel) and condenser temperatures are around 30°C. This gives a theoretical Carnot efficiency of about 63% compared with an actual efficiency of 42% for a modern coal-fired power station. This low turbine entry temperature (compared with a gas turbine) is why the Rankine cycle is often used as a bottoming cycle in combined cycle gas turbine power stations.

Except a few technologies such as hydrogen generation and thermal process heat generation, the thermal power from the central receiver system is used to drive an electric power generation cycle. The most common generation cycle for this application is the steam Rankine cycle. As with any steam Rankine power generation cycle, the central receiver power cycle can include any variety of configurations to ease implementation and boost efficiency. The following discussion introduces a Rankine cycle modeling tool that is intended for general use with multiple stage cycle design configurations.

One of the principal advantages the Rankine cycle holds over others is that during the compression stage relatively little work is required to drive the pump, the working fluid being in its liquid phase at this point. By condensing the fluid to liquid, the work required by

the pump consumes only 1% to 3% of the turbine power and contributes to a much higher efficiency for a real cycle. The benefit of this is lost somewhat due to the lower heat addition temperature. Gas turbines, for instance, have turbine entry temperatures approaching 1500°C. Nonetheless, the efficiencies of actual large steam cycles and large modern gas turbines are fairly well matched.

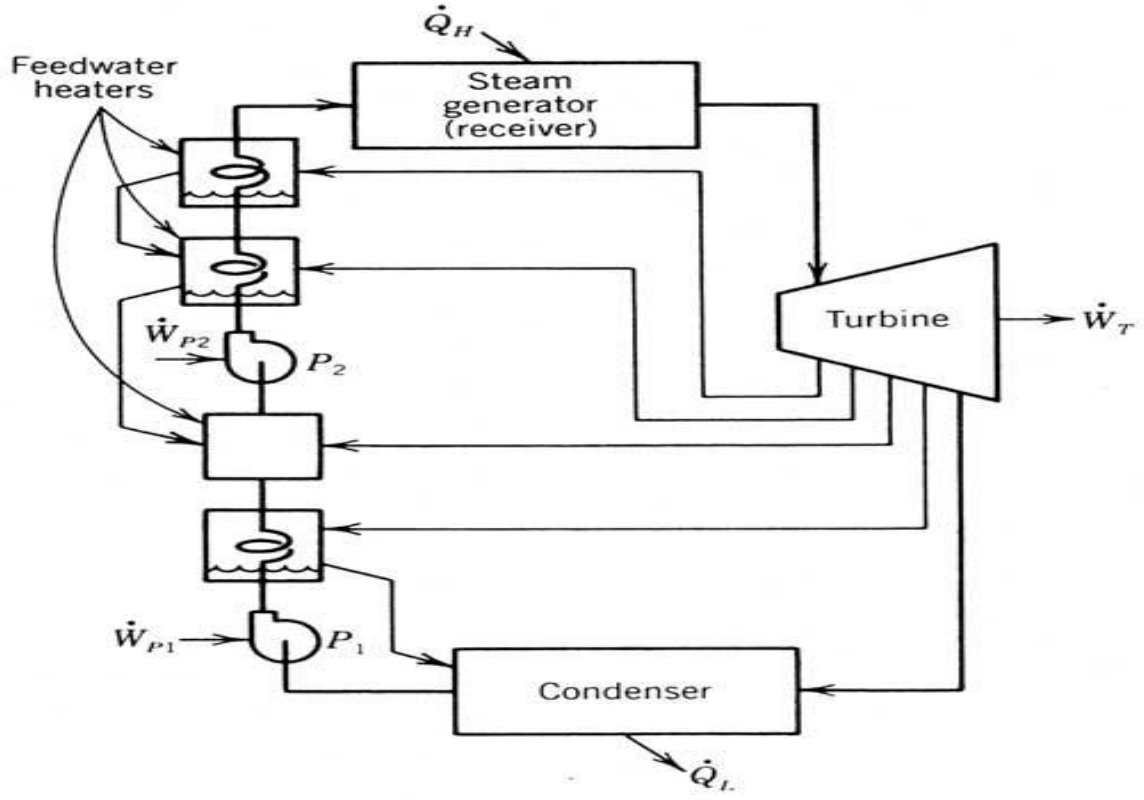

Figure 3-1: Schematic of the l0-MWe steam Rankine cycle at the Solar One pilot plant at Barstow, California.

Solar energy-driven power cycles present a set of unique challenges and constraints. Unlike conventional base-load power cycles typical of a fossil-fuel fired plant that often see very little if any variation in operating conditions over the course of their operation lifetime, the CRS power cycle is subject to frequent transients in weather, daily shutdown and startup, and varying heat transfer fluid flow rates and temperatures. The ability of a long-term simulation to accommodate these variances is paramount to the accuracy of that simulation, since deviations from the design conditions of a power cycle adversely affect performance.

Using a Rankine cycle with deaerator, feed-water heater, pre-heat, and super-heat, a nominally 10MW cycle is constructed. The results of this analysis indicate that the Rankine cycle can successfully be modeled for a range of design points and equipment sizes using a single set of correlations. It should be noted that this model has been developed for only steam Rankine cycles with superheat.

3.3 Design Analysis of Rankine Cycle

The cycle under consideration is intended to accommodate the conversion of heat provided by the central receiver heat transfer fluid flow to electric power in the turbines with a combined output of 10 MWe. The heat transfer fluid is supplied from the tower at 565°*C* under design conditions, while the cooling water is supplied to the condenser at 20°C, both at flow rates yet to be calculated. Figure 3.2 shows a simplified version of the design cycle configuration adapted from the Solar II power cycle schematic presented by Lippke (1995).

A preheater, boiler, and superheater handle the heat addition portion of the cycle. Each of these is modeled as a separate component since the heat transfer relationships that govern these three stages differ.

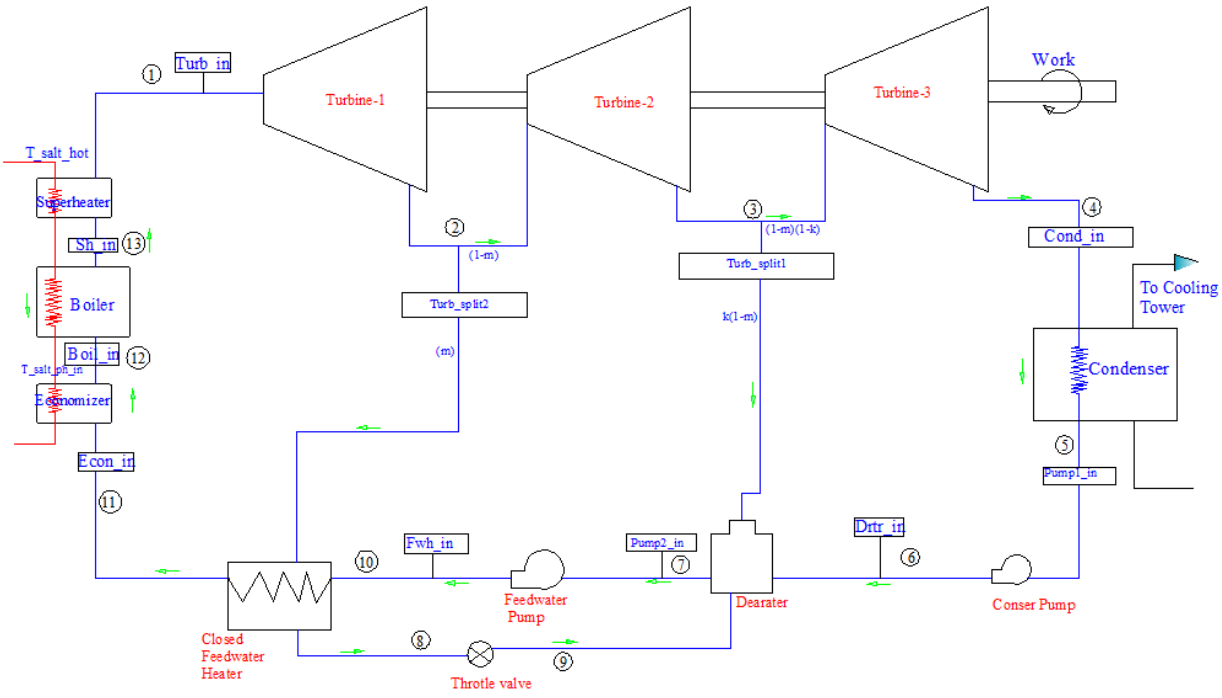

Figure 3-2: The Rankine Cycle Configuration Used in the Modeling of the Power Block

The cycle begins by receiving thermal energy from hot thermal storage tank which in turn receives thermal energy from central receiver component though the use of molten salt heat transfer fluid. The HTF receives pre-heated feedwater and generates dry steam at a temperature and pressure of 510 ^{O}C and 100 bar (at rated power conditions) by heat exchange with the HTF in the steam preheater (Economizer), steam generator (Boiler) and superheater. The superheated steam passes first through the high pressure turbine, where it expands and propels the turbine blades. A single extraction takes place from the exit of high pressure turbine which is used to preheat feedwater in a closed feedwater heater. The major part of the steam exiting the high pressure turbine is directed to low pressure turbine (Turbine 2 in Figure 3.2), The steam then passes through the low pressure turbine, where again the steam expands and propels the turbine blades. Another extraction from the exit of Turbine-2 is taken to preheat and deaerate the feedwater at the deaerator while the remaining major part goes to Turbine-3 for further power generation. The steam leaving the low pressure turbine (Turbine-3 in Figure 3.2) is condensed in a surface condenser by heat exchange with circulating water. The condenser water is then cooled using cooling tower. The condensed steam is pumped to deaerator and then pumped by Pump2 from outlet of deaerator to a pressure slightly higher than the boiling pressure in the steam generator (Boiler).

3.3.1 Thermodynamic Analysis of a Rankine Cycle

The analysis begins by writing procedures for turbines and pumps of the power cycle. These procedures can later be called in the main body of the program. Next to that, assigning state points for the cycle components at each point of interest becomes important. In this case, arrays containing the temperatures, pressures, enthalpies, and entropies will be denoted by the integers representing each of the points. In addition, the heat transfer fluid inlet temperature, outlet temperature, and type must be specified, and the desired output power is specified. Typical turbine and pump efficiencies are specified, with the pump and turbine efficiencies equal to the value of an isentropic efficiency calculated from the Solar II cycle analyzed by Lippke (1995) for this work.

3.3.1.1 Turbine and Splitter Stages

The calculations for the cycle begin at the high pressure turbine inlet (Turb_in), where desired pressure and temperature conditions are specified. The pressure at the turbine inlet is equal to the boiler pressure, since the pressure drop of the steam across the heat exchangers is neglected. The boiler pressure can be controlled in plant operation, and so this pressure is specified in the model. From maximum temperature resisting property of Rankine cycle turbine material discussed above and existing practice of molten salt HTF power tower technology, the high pressure turbine inlet temperature is set to be 510^{O}C at a pressure of 100 bar while the HTF inlet temperature to superheater is 565 ^{O}C and its exit at preheater is set to be 290 ^{O}C for this work.

As a usual case of power generation through Rankine cycle, steam enters the turbine at a high temperature and high pressure superheated state. The expansion of the steam as it moves from high pressure to lower pressure converts the potential energy (in the form of pressure) to kinetic energy by imparting its momentum to the turbine blades, thereby causing the connected shaft to rotate. The mechanical work created by the rotating shaft is converted to electrical energy through a generator.

The high pressure turbine inlet condition is:

$$T_{turb,in} = 510\ ^{0}\text{C}$$

$$P_{turb,in} = 100\ bar$$

$$h_{turb,in} = enthalpy\ of\ steam_{@\ T=T_{turb,in}\ and\ P=P_{turb,in}}$$

$$s_{turb,in} = entropy\ of\ steam_{@\ T=T_{turb,in}\ and\ P=P_{turb,in}}$$

The turbine splitter extraction phases can be fixed at a desired pressure to maximize cycle efficiency. The pressure can be estimated as the saturation pressure of the temperature at the stage outlet. At this pressure, the corresponding saturation temperature is calculated, and the intermediate splitter stage pressure is calculated by evenly dividing the difference in temperature between the first turbine inlet stage and the last turbine outlet stage into even

increments (El Wakil, 1984). The resulting temperature at saturation is associated with the actual saturation pressure to be used at that splitter stage.

The saturation temperatures corresponding with the pressures at the inlet and outlet of the turbine stages are calculated, and require the specification of the condensing pressure. The enthalpy at the outlet of the first turbine stage can be calculated using the known inlet conditions, the known pressure at the splitter stage, and the known isentropic efficiency. The mathematical expressions or thermodynamic relations governing the above statements are given as:

$$P_{cond,in} = 0.085\ bar$$

$$T_{sat@HI} = saturation\ temperature\ of\ steam_{@\ P=P_{turb,in}}$$

$$T_{sat@LO} = saturation\ temperature\ of\ steam_{@\ P=P_{cond,in}}$$

Hence the outlet enthalpy and temperature of high pressure turbine can be evaluated from the known turbine splitter stage-2 pressure and isentropic enthalpy of turbine as:

$$P_{turb\_split2} = P_{sat_{steam}@\ T=T_{satHI}-(T_{satHI}-T_{satLO}/3)}$$

$$h_{s\_turb\_split2} = enthalpy\ of\ steam_{@\ P=P_{tur\_split2}\ and\ s=s_{turb,in}}$$

$$h_{turb\_split2} = h_{turb\_in} - \eta_{turb\_1} * (h_{turb_{in}} - h_{\_s\_turb\_split2})$$

$$T_{turb\_split2} = temperature\ of\ steam_{@\ h=h_{turb\_split2}\ and\ P=P_{turb\_split2}}$$

$$s_{turb\_split2} = entropy\ of\ steam_{@\ h=h_{turb\_split2}\ and\ P=P_{turb\_split2}}$$

Now for a given steam mass flow rate, the specific work and power from the first turbine respectively are:

$$W_{turb1} = h_{turb,in} - h_{turb\_split2}$$

$$\dot{W}_{turb1} = W_{\_turb1} * \dot{m}_{\_steam}$$

At each of the two splitter stages, a portion of the steam mass flow rate is diverted into an open feed-water heater, as shown in the cycle schematic in Figure 3.2 above. The fractions

that are extracted are denoted as *m* for the higher pressure feed-water heater and k for the lower pressure feed-water heater. The remaining fraction passes through the subsequent turbine stage(s) and condenser, with the total remaining fraction passing through the condenser being (1- *m*)(1-*k*).

In the same way that the high-pressure turbine outlet properties were calculated, the intermediate turbine outlet properties at the low-pressure feed-water heater can be evaluated. While the outlet of the high-pressure turbine was fixed at a pressure representing the saturation temperature 1/3 of the way from *TsatHI (saturation temperature at high pressure turbine inlet)* to *TsatLO (saturation temperature at low pressure turbine outlet)*, the outlet of the intermediate turbine is evaluated at a saturation temperature 2/3 of the distance between these values. Finally the power obtained from the remaining low pressure turbine stages is given as:

$$\dot{W}_{turb2} = W_{turb2} * \dot{m}_{\_steam} * (1 - m) \qquad \text{from Turbine-2 and}$$

$$\dot{W}_{turb3} = W_{turb3} * \dot{m}_{\_steam} * (1 - m)(1 - k) \qquad \text{from Turbine-3 respectively}$$

And at the end all of the turbine power rates are summed to provide the total power generated by the turbines.

$$\dot{W}_{total} = \dot{W}_{turb1} + \dot{W}_{turb2} + \dot{W}_{turb3}$$

3.3.1.2 Condenser

Having done work through expansion in the low pressure turbine, the working fluid or the steam proceeds to the condenser, located after the turbine. The condenser is a closed shell-and-tube heat exchanger, with cooling water flow on the tube side and condensing steam from the turbine on the shell side to give greater heat transfer by forcing the fluid to flow in a more turbulent fashion around the piping. The function of the condenser is to condense the turbine exhaust from vapor to liquid, so the working fluid can be pumped back to the boiler.

The condenser pressure at the outlet of the lowest pressure turbine has been specified based on literatures as 8.5 kPa for better extraction of energy from low pressure stage turbine, so that the steam conditions at the condenser inlet are easily calculated.

The outlet condition of the steam from the condenser is known to be saturated or slightly sub-cooled liquid. To maintain this condition, a temperature is specified such that the steam leaves as slightly sub-cooled liquid. The pressure at the outlet of the condenser is known since any pressure losses in the heat exchange equipment is neglected in this analysis. The thermodynamic relations for condenser outlet and pump1 inlet are given by:

$$P_{steam,in} = P_{feedwater,out} \text{ or } P_{cond\_in} = P_{pump1\_in}$$

$$h_{feedwater,out} = h(P_{feedwater,out}, X = 0)$$

$$T_{pump1\_in} = saturation\ temperature\ of\ steam_{@\ P=P_{cond,in}} - T_o$$

where:

T_o is some constant temperature value to insure slight sub-cooled condition of steam at condenser outlet

The enthalpy, entropy, and specific volume of steam at exit of condenser and inlet of pump1 are evaluated as:

$$h_{pump1\_in} = enthalpy\ of\ steam_{@\ T=T_{pump1\_in}\ and\ P=P_{pump1\_in}}$$

$$s_{pump1\_in} = entropy\ of\ steam_{@\ T=T_{pump1\_in}\ and\ P=P_{pump1\_in}}$$

$$v_{pump1\_in} = sp.volume\ of\ steam_{@\ T=T_{pump1\_in}\ and\ P=P_{pump1\_in}}$$

From energy balance with negligible change in potential, internal and kinetic energy terms, the work done is equal with the heat transferred per unit mass as given by:

$$q_{cond} = h_{cond\_in} - h_{pump1\_in}$$

From which the heat transfer rate in the condenser is computed as:

$$\dot{q}_{cond} = q_{cond} * \dot{m}_{steam} * (1 - m) * (1 - k)$$

3.3.1.3 Pumps

The parasitic electric power required to run the pumps is virtually insignificant in the overall energy balance; however, it is likely of interest for sizing purposes. The following relationship is used to calculate the work done by the pump in compression of the working fluid:

$$W_p = v_{in}.(\frac{P_{in} - P_{out}}{\eta_{pump}}) \tag{3.1}$$

All the state points of the pumps are evaluated for saturated liquid or x=0 quality at given pressure. The pump efficiency and the relationship presented in Eq. (3.1) provide enough information to calculate the work per-unit-mass done in compression process by the low pressure pump, and the actual outlet state of the steam from the pump. However, the fraction ((1-*m*)(k) of the steam mass-flow that is extracted through the low-pressure feed-water heater is required to calculate the corresponding pump parasitic power. The pump power is scaled by this mass flow fraction, since the steam mass flow rate through the pump is decreased by the amount that is diverted before reaching the pump.

An energy balance on the low-pressure feed-water heater yields the fraction of steam entering the feedwater heater -1. The pressure throughout the low-pressure feed-water system has been specified at the turb_split1 state. The intermediate pump calculations are identical to the low-pressure pump, and another energy balance across the high-pressure feed-water heater is used to determine the fraction of steam entering feedwater heater -2. High pressure pump conditions are calculated in the same way as the previous pumps, except that the boiler pressure is used as the steam pressure at the pump outlet. Based on equation 3.1 and amount of steam to be conveyed through each pump, a summary of power consumption of the three pumps is given below.

$$\dot{W}_{p1} = W_{p1} * \dot{m}_{steam} * (1 - m) * (1 - k)$$
$$\dot{W}_{p2} = W_{p2} * \dot{m}_{steam} * (1 - m)$$
$$\dot{W}_{p3} = W_{p3} * \dot{m}_{steam}$$

3.3.1.4 Closed Feed-water heater

A feedwater heater is a heat exchanger designed to preheat boiler feedwater by means of condensing steam extracted (or "bled") from a steam turbine. The heater discussed here is classified as closed, since the tube side fluid remains enclosed by the tubes and channel, and does not mix with the condensate, as is the case with open feedwater heaters. They are unfired since the heat transfer within the vessel does not occur by means of combustion, but by convection and condensation.

Closed feedwater heaters are typically shell and tube heat exchangers where the feedwater passes throughout the tubes and is heated by turbine extraction steam. These do not require separate pumps before and after the heater to boost the feedwater to the pressure of the extracted steam as with an open heater. However, the extracted steam (which is most likely almost fully condensed after heating the feedwater) must then be throttled to the deaerator pressure, an isenthalpic process that results in some entropy gain with a slight penalty on overall cycle efficiency.

The steam extraction process in a closed feedwater is referred to as uncontrolled extraction. The flow rate of steam into a feedwater heater is not limited by the amount of available steam (as opposed to a surface condenser, for instance). The shellside operating pressure in a feedwater heater is determined by the pressure of the steam supplied to it, not by the amount of heat transfer surface.

The heating process by means of extraction steam is referred to as being regenerative. The feedwater heaters are an integral portion of the power plant thermodynamic cycle. Normally, there are multiple stages of feedwater heating. Each stage corresponds to a turbine extraction point. These extraction points occur at various stages of the expansion of steam through the turbines. The presence of the heaters in the cycle enhances the thermal efficiency of the power plant; the greater the number of extraction stages, the lower the amount of thermal energy required to generate a given amount of electrical energy. A beneficial by-product of the energy extracted by the heaters is the reduced rate of rejection of energy to the environment.

There are three zones or separate areas within the shell in a feedwater heater namely: Condensing Zone, which is a characteristic figure of all feedwater heaters in the cycle. All of the steam is condensed in this area, and any remaining non condensable gases must be removed. A large percentage of the energy added by the heater occurs here. The next one is Subcooling Zone: (Optional) the condensed steam enters this zone at the saturation temperature and is cooled by convective heat transfer from the incoming feedwater. The final one is Desuperheating Zone: (Optional) the incoming steam enters this zone, giving up most of its superheat to the feedwater exiting from the heater (dearator). The size and conductance of heat exchangers are characterized by an overall heat transfer coefficient (UA). Each zone in the closed feedwater heater will have an associated UA value. It is assumed here that the condensing zone of each feedwater heater is sufficiently large in comparison to the desuperheating and subcooling zones that the desuperheating and subcooling zones can be neglected. An overall UA for each feedwater heater is defined assuming steam is condensing throughout the length of the feedwater heater.

The exit enthalpy of the condensed steam (condensate) is that of saturated liquid at the inlet pressure to the feedwater heater, assuming that no pressure drop occurs over the condensing steam:

$$P_{steam,in} = P_{steam,out}$$

$$h_{steam,out} = h(P_{steam,out}, x = 0)$$

The mass flow rate of extracted steam/condensate through the heater may be determined from the heat transfer between fluids over the difference in enthalpy from steam inlet to condensate outlet:

$$\dot{m}_{steam} = \frac{Q}{(h_{steam,in} - h_{steam,out})}$$

The exit enthalpy of the feedwater is determined from the inlet enthalpy of the feedwater plus the heat transfer per unit feedwater mass flow rate:

$$h_{feedwater,out} = h_{feedwater,in} + \frac{Q}{\dot{m}_{feedwater}}$$

The outlet feedwater temperature may be determined as a function of the outlet pressure and outlet enthalpy using a property relation for water:

$$T_{feedwater,out} = T(P_{feedwater,out}, h = h_{feedwater,out})$$

The mass flow rates of the feedwater and steam/condensate at the outlet will equal the mass flow rates of the streams at the inlet.

$$\dot{m}_{feedwater,out} = \dot{m}_{feedwater,in}$$
$$\dot{m}_{steam,out} = \dot{m}_{steam,in}$$

3.3.1.5 Deaerator (Open Feed-water heater)

A deaerator is a device that is widely used for the removal of air and other dissolved gases from the feedwater to steam-generating boilers. In particular, dissolved oxygen in boiler feedwaters will cause serious corrosion damage in steam systems by attaching to the walls of metal piping and other metallic equipment and forming oxides (rust). Water also combines with any dissolved carbon dioxide to form carbonic acid that causes further corrosion. The deaerators in the steam generating systems of most thermal power plants use low pressure steam obtained from an extraction point in their steam turbine system.

The open feedwater heater, like the closed feedwater heaters, uses extracted steam from the turbine to preheat feedwater to the steam generator. Unlike the closed feedwater heaters, however, in the open feedwater heater the extracted steam is directly mixed with the feedwater. Open feedwater heaters are more effective than closed feedwater heaters, and are beneficial for the removal of non-condensables from the feedwater (El-Wakil, 1984). The disadvantage of open feedwater heaters is that the outlet pressure cannot exceed the pressure of the extracted steam; an additional pump is required at the feedwater exit to increase fluid pressure to boiling pressure.

The open feedwater heater (deaerator) is modeled as a fluid mixer with three inlet streams and a single outlet stream. The three inlet streams are the extracted steam from the first stage of the low pressure turbine (split1_stage or state 3), the condensate from the high pressure feedwater heaters (state 9), and the feedwater from the condenser or pump1_exit (state 6). The mass flow rate of the outlet stream is the sum of the mass flow rates of the three inlet streams:

$$\dot{m}_{feedwater,out} = \dot{m}_{steam,extract} + \dot{m}_{condensate,in} + \dot{m}_{feedwater,in}$$

An energy balance indicates that the enthalpy of the feedwater at the outlet is equal to the weighted average of the enthalpies of the three streams entering the heater:

$$h_{out}\dot{m}_{feedwater,out} = h_{extract}\dot{m}_{steam,extract} + h_{cndst,in}\dot{m}_{cndnste,in} + h_{feed,in}\dot{m}_{feedwater,in}$$

Assuming that the feedwater exits as saturated liquid (x = 0), the enthalpy of the outlet is also equal to the saturated liquid enthalpy at the outlet pressure:

$$h_{feed,out} = h(P_{feed,out}, x = 0)$$

Where the pressure at the feedwater outlet is assumed to be the pressure of the extracted steam (the outlet pressure cannot exceed this pressure):

$$P_{steam,extract} = P_{feedwater,out}$$

Since the outlet state is saturated liquid, the temperature at the heater outlet is the saturation temperature at the outlet pressure:

$$T_{sat,out} = T\_sat(P_{feedwater,out})$$

3.3.1.6 Heat Addition Portion of the cycle

The following inventory of available information and modeling considerations for the heat-addition phase of the cycle is provided to clarify the calculation process. The heat addition to the Rankine cycle occurs by means of a preheater heat exchanger, a steam boiler, and a superheater heat exchanger. The preheater is placed at the low temperature end of the heat transfer fluid flow, and at the low-energy end of the steam flow (following the high-pressure pump). The preheater provides thermal energy to the subcooled steam such that the steam flow leaving the preheater under design conditions is at saturated liquid conditions.

Physically, the preheater and boiler may exist as the same piece of equipment. However, the heat-transfer correlations that apply to sub-cooled liquid heat transfer and the correlations that apply to heat transferred with one side undergoing a phase change (the steam in the boiler) are different, and so must be modeled differently. The superheater heat exchanger is also modeled as a separate piece of equipment. Steam generated in the boiler is extracted into the superheater where heat transfer between the steam vapor and the hottest portion of the heat transfer fluid takes place. Therefore, from the preceding discussion, from previous calculations, and from the related literatures, the following conditions are known:

- Preheater inlet steam condition
- Preheater outlet / boiler inlet steam quality ($x=0$)
- Preheater outlet heat transfer fluid temperature ($T_{htf,cold}$ $T_{htf,cold}$)
- Boiler outlet / superheater inlet steam condition
- Superheater heat transfer fluid inlet temperature ($T_{htf,hot}$)
- Superheater outlet / high-pressure turbine inlet steam condition
- Steam mass flow rate

Among the unknown information in the heat-addition portion of the cycle are the following parameters: UA_{econ}, UA_{boil} UA_{sh}

- Heat transfer fluid mass flow rate ($\dot{m}_{htf}$)
- Heat transfer fluid boiler inlet temperature ($T_{htf,boil,in}$ $T_{htf,boil,in}$)
- Heat transfer fluid preheater inlet temperature ($T_{htf,ph,in}$ $T_{htf,ph,in}$)

- Preheater, boiler, and superheater conductance (UA_{econ}, UA_{boil}, UA_{sh}),respectively

To proceed with the analysis, the preheater outlet/boiler inlet conditions are calculated with known quality and pressure. The heat flow in the preheater can then be determined, and the heat transfer rate follows.

$x_{boil\_in} = 0$, quality at boiler inlet is set to be zero

With the assumption of negligible pressure drop, $P_{boil\_in} = P_{turb\_in}$ from which the boiler inlet temperature and inlet enthalpy are evaluated as:

$$T_{boil\_in} = temperature\ of\ steam_{@\ P=P_{boil\_in}\ and\ x=x_{boil\_in}}$$

$$h_{boil\_in} = enthalpy\ of\ steam_{@\ P=P_{boil\_in}\ and\ x=x_{boil\_in}}$$

Since the heat transfer fluid conditions at the preheater are needed to determine the conductance of the heat exchanger, the mass flow rate of the heat transfer fluid should be calculated at this point. With the known preheater inlet steam enthalpy and the known turbine inlet steam enthalpy, the total heat flow per-unit-mass into the steam is calculated. The mass flow rate of the heat transfer fluid can then be obtained by employing the energy balance shown in Eq. (3.2) below, where $C_{htf,ave}$ is evaluated at the average heat transfer fluid temperature in the cycle. This energy balance assumes that there are no thermal losses from the jacket of the boiler heat exchangers.

$$\dot{m}_{htf} = \frac{(h_{turb,in} - h_{ph,in}) \cdot \dot{m}_{steam}}{C_{htf,ave} \cdot (T_{htf,hot} - T_{htf,cold})} \tag{3.2}$$

With all of the information about the flows passing through the preheater defined, the heat exchanger size can be determined. The Effectiveness-NTU method is the most convenient for characterizing the simple heat exchanger models used in this evaluation. The heat-exchanger

effectiveness (ε) is defined as in Eq. (3.3) such that it indicates the fraction of heat exchanged between the hot and cold streams compared to the maximum heat flow possible.

$$\dot{q} = \varepsilon \dot{q}_{max} \tag{3.3}$$

The maximum heat flow is defined in terms of the capacitance rate and the maximum temperature difference between hot and cold side streams as shown in Eq. (4.4).

$$\dot{q}_{max} = \dot{C}_{\min} (T_{H,in} - T_{C,in}) \tag{3.4}$$

where:

$$\dot{C}_{\min} = \min [(C_{p,steam}.\dot{m}_{steam}), (C_{htf}.\dot{m}_{htf})]$$

Since the specific heat of a fluid undergoing a phase change (as in the condenser or boiler) is effectively infinite, the minimum capacitance rate for the heat transfer relationship in these components will always be on the non-steam side. Combining Eqs (3.3) and (3.4), a useful relationship between the effectiveness, stream inlet temperatures, and the heat transfer in the heat exchanger is obtained.

$$\dot{q} = \varepsilon.\dot{C}_{\min} (T_{H,in} - T_{C,in}) \tag{3.5}$$

The number of transfer units (NTU) represents the dimensionless size of the heat exchanger. The UA associated with the particular heat exchanger is scaled by the minimum capacitance rate described in Eq. (3.4).

$$NTU = \frac{UA}{C_{min}} \tag{3.6}$$

A final consideration in calculating the heat exchanger size is the relationship between effectiveness and *NTU*, which can be determined based on the heat exchanger configuration and the capacitance ratio. This ratio is defined as the minimum capacitance rate divided by the maximum capacitance rate. For streams that are undergoing a phase change, the effective specific heat of the fluid is infinite since the energy flow is latent heat. Therefore, the

maximum capacitance rate is infinite, and the ratio (*CR*) is zero. For this situation, the *NTU* can be calculated as in Eq. (3.7), and is independent of heat exchanger configuration (Nellis & Klein, 2009).

$$NTU = -ln(1 - \varepsilon) \tag{3.7}$$

For heat exchangers where both flows are single-phase, the relationship between *NTU* and effectiveness depends on the configuration of the heat exchanger. In this analysis, a counter-flow heat exchanger is used. The *NTU* is calculated with the following relationship (Nellis & Klein, 2009)

$$NTU_{PH} = \frac{ln(\frac{\varepsilon_{ph}-1}{\varepsilon_{ph}C_{R,PH}-1})}{C_{R,PH}-1} \tag{3.8}$$

Now the preheater heat exchanger product of overall heat transfer coefficient by area can be computed using the relationship between the *NTU* and effectiveness shown in Eq. (3.8). The preheater *UA* is then calculated. With a previously calculated heat transfer fluid mass flow rate and preheater inlet temperature, as well as known steam conditions, the boiler product of overall heat transfer coefficient by area calculation is relatively straight-forward. Figure 3.3 shows an energy balance on the boiler. Note the effectively infinite specific heat capacity of the steam flow that results from the latent heat addition through a phase change from liquid to vapor.

The effectively infinite capacitance rate on the steam side of the heat exchanger requires the use of the effectiveness-*NTU* relationship shown above in Eq. (3.7). The heat flow in the preheater is calculated with the steam inlet and outlet enthalpies on a per-unit-mass basis as Q_{boil}. The heat transfer rate can then be determined as the product of the heat per unit-mass by the steam mass flow rate. The heat transfer fluid boiler inlet temperature can be determined with an energy balance on the HTF side of the boiler heat exchanger.

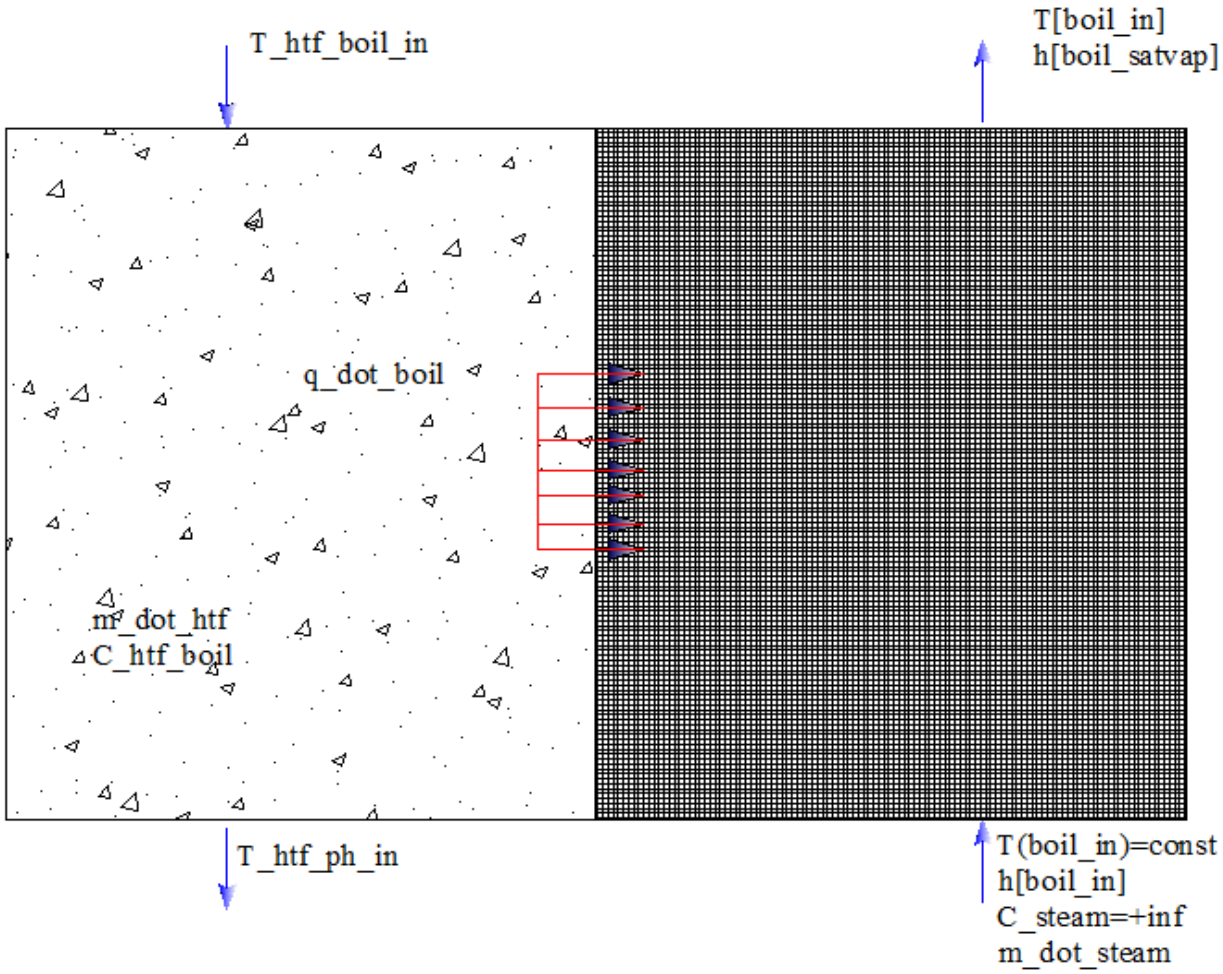

Figure 3-3: Energy Balance Representing the Heat Flow across the Boiler from the Heat Transfer Fluid to the Boiling Steam Flow

The final calculation in the heat-addition portion of the Rankine cycle is the computation of the superheater heat exchanger product of overall heat transfer coefficient by area. This heat exchanger is similar to the preheater in configuration and in analysis with the relationship shown previously in Eq. (3.8) also applying to the superheater. Once the superheater heat flow has been calculated, the unknown heat transfer fluid boiler inlet temperature is established.

Now the remaining design-cycle computations are the product of overall heat transfer coefficient by area of the condenser and the flow rate of the cooling water through the condenser. For the design case, both the cooling water inlet and outlet temperatures must be

specified. Expressed in terms of the difference between the saturation temperature of steam entering condenser and the cooling water circulating temperature, the recommended temperature range for the inlet temperature is between 11 to 17°C below saturation temperature (El Wakil, 1984). The difference between the outlet temperatures should not be less than about 5°F (2.8°C). The actual temperature can be calculated according to:

$$T_{cw} = T_{sat}\left('Steam', P = P_{cond,in}\right) - \Delta T \tag{3.9}$$

where: ΔT represents the specified temperature difference between the saturation temperature and the cooling water temperature. For this specific case, the temperature difference for inlet and outlet cases are taken as 15^0C and 4^0C respectively based on the above recommendation.

Finally, the total cycle heat addition, total cycle work minus parasitic, and the total thermal efficiency are analyzed as:

$$\dot{q}_{hot,tot} = \dot{q}_{ph} + \dot{q}_{boil} + \dot{q}_{sh} \tag{3.10}$$

$$\dot{W}_{cycle} = \dot{W}_{turb1} + \dot{W}_{turb2} + \dot{W}_{turb3} + \dot{W}_{pump1} + \dot{W}_{pump2} + \dot{W}_{pump3} \tag{3.11}$$

$$\eta_{cycle} = \dot{W}_{cycle} \Big/ \dot{q}_{hot,tot} \tag{3.12}$$

3.4 Result of EES Model of the Power Cycle

Cycle parameters such as heat exchanger product of overall heat transfer coefficient by area and fluid mass flow rates that are determined in the design phase can now be used in building the cycle model in TRNSYS. Tables and plots below are results obtained from EES program written for this thesis giving the reference state values to be used in TRNSYS power plant simulation in chapter five

Table 3-1: Reference State Point Properties of Steam for the Power Cycle Analyzed

State Point	Property				
	h_i [kJ/kg]	P_i [bar]	s_i [kJ/kg-k]	T_i [^{0}C]	x_i [-]
1	3400	100	6.63	510	-
2	3113	23.88	6.839	343.3	-
3	2793	2.875	7.171	164.6	
4	2414	0.085	7.685	42.65	
5	178.6	0.085	0.6075	42.65	0
6	178.6	2.875	0.6066	42.59	0
7	555.3	2.875	1.657	132.1	0
8	950.7	23.88	2.532	221.6	0
9	950.7	2.875	2.632	132.1	0
10	555.5	100	1.631	130.6	0
11	950.7	100	2.514	221.1	0
12	1407	100	3.359	311	0
13	2724	100	5.614	311	1

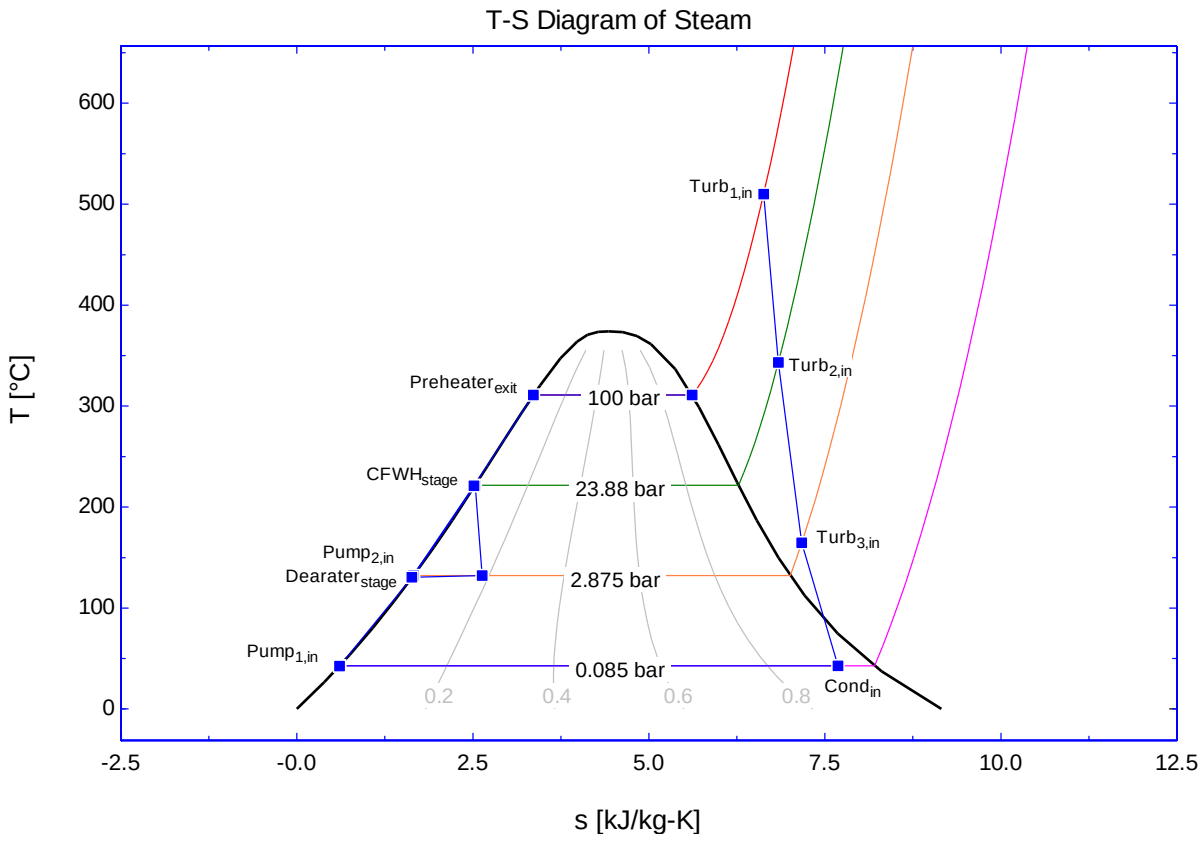

Figure 3-4: T-S Diagram for the Analyzed Rankine Power Cycle

Table 3-2: Output Parameters/Inputs from the Power Cycle Analyzed

Parameter/Input	Value	Description
UA_{econ}	120.5 kW/K	Economizer conductance
UA_{boil}	189.9 kW/K	Boiler conductance
UA_{esh}	99.66 kW/K	Superheater conductance
$\dot{m}_{htf}$	71.11 kg/s	Reference HTF mass flow rate
$\dot{m}_{steam}$	12.14 kg/s	Reference steam mass flow rate
$\dot{W}_{cycle}$	10MW	Net cycle power

η_{cycle}	33.65%	Cycle efficiency
$T_{htf,boil,in}$	489.9 ^{0}C	HTF temperature at boiler inlet
$T_{htf,econ,in}$	341.8 ^{0}C	HTF temperature at economizer inlet
$\dot{m}_{cw}$	428.6 [kg/s]	Reference cooling water mass flow rate

CHAPTER FOUR

MODELLING OF THE POWERPLANT USING TRNSYS

4.1 Introduction

A detailed performance model of the 10 MWe SEGS Central Receiver power plant was created in the TRNSYS simulation environment using the Solar Thermal Electric Component model library (STEC 3.0). Both solar and power cycle parts of the plant were modeled using the TRNSYS16 simulation environment. The TRNSYS simulation environment was selected for use in modeling solar thermal power systems for a number of reasons, including modularity, flexibility, availability, and ease of use. Commercially available power cycle modeling codes have many standard components, but frequently limit the user's ability to create new components, tend to be quite expensive, and are not capable of modeling annual performance using weather file data as input. The latest update of TRNSYS, Version 16, was used for this work. It has a number of improvements to the graphical user interface that were found to be very useful.

TRNSYS is an acronym for "Transient System Simulation program" which has been under development at the University of Wisconsin-Madison since the 1970's (Klein SA et. al. 1996). TRNSYS is written in ANSII standard Fortran-77 and its component library includes many of the components commonly found in thermal energy systems. This includes a Solar Thermal Electric Component (STEC) library that has been created under the SolarPACES umbrella as well as components that are not ordinary considered part of a system. Such components are utility subroutines that use to handle the weather and insolation data and output simulation results.

TRNSYS relies on a modular structure and system concept, in which a system is defined as a set of components that are interconnected to accomplish the specified task. Each model is the functional relationship between its input and output quantities which are defined using algebraic and first-order differential equations. Thus, system performance simulation can be done by collectively simulating the performance of the interconnected components. The major field of application of TRNSYS is the evaluation of solar systems for heating and cooling purposes and domestic hot water applications. However, the flexibility of the code

results in the fact that a world-wide user group has created component models in many other application fields. The version 14.2 of TRNSYS with the IISiBat 2 (graphical) interface was used for the first release of the STEC library. It was upgraded for TRNSYS version 15 and Iisibat3 and now to TRNSYS16 and the Simulation Studio.

The principle philosophy behind TRNSYS is the implementation of algebraic and first-order ordinary differential equations describing physical components into software subroutines called Types with a standardized interface. This interface consists of so called "input" and "output" quantities. Outputs can be either physical quantities or first order derivatives (with time) of physical quantities. The functional relations between inputs and outputs are defined in each subroutine. To create a system model, the user simply connects the outputs of components with the inputs of other components. The user does not have to worry about how to solve the complex set of equations resulting from the system layout because the TRNSYS kernel performs this function by successive substitution or Powel's Method [STEC].

Once a system model has been established, running TRNSYS causes the program to step through all the system components evaluating output variables at each time step. Thus, weather data (solar radiation, ambient temperature, etc.) and all time dependent variables are determined and calculated every time step through the simulation time period. For a true thermal transient model, the transient equations in the modelled components are solved using either TRNSYS analytical solution or numerical solver features.

A library of Solar Thermal Electric Component (STEC) models for both solar and conventional power cycle elements was created for TRNSYS (Pitz-Paal and Jones, 1998). The component models are linked together to form the desired system, thereby permitting flexibility in modeling different configurations such as standard solar plants or combined fossil-solar (hybrid) designs. The STEC library components are typically detailed steady state models formulated in thermodynamic quantities such as temperature, pressure, and enthalpy. This high level of modeling detail can be valuable in many cases. For example, the ability of a solar steam generation system to handle startup transients could be analyzed.

While annual system performance can be modeled in TRNSYS using these detailed state property components, it is also possible to create less complex component models based on a simple energy balance formulation. This would result in a similar model to SOLERGY

(Stoddard et. al., 1987), but would be more easily adaptable to different configurations such as hybrid plants. SOLERGY is a public-domain software tool frequently used for annual solar plant performance analysis. The ability in TRNSYS to create and share with others new component and system models also helps provide consistency in modeling efforts undertaken by different organizations around the world, and makes their results more comparable.

4.2 Heliostat Field Component

The SolarPACES STEC component library contains heliostat field component (Type 394) constructed by R. Pitz-Paal (DLR, 1997) whose main purpose is to read an input file containing the net field efficiency as a function of solar position, and interpolate the value. Several additional features are included to better model the heliostat field in operation. The number of concentrator units (heliostats) and the power required to track each unit can be entered, allowing the calculation of the total parasitic power required for tracking of the solar position. The ground-level wind velocity is monitored so that in the event that a user-specified maximum wind-speed is reached, the heliostats will defocus and go into a protective "stowed" position. This effectively shuts down the plant in order to protect the heliostat mirror surfaces and the support structure. Additionally, the parasitic power associated with heliostat startup can be modeled.

For receiver models that require the information about the total power from the field to originate from the heliostat component (which is the case for the receiver model produced by this research), the mirror surface area parameter can be used. The surface area (A_{field}) is multiplied by the total field efficiency (η_{field}), the incident horizontal beam radiation (I_{bn}), the mirror reflectivity (ρ_{field}), and the fraction of the field that is tracking and not undergoing maintenance, cleaning, or experiencing control problems (Γ) to provide the total power incident on the receiver surface ($\dot{Q}_{inc}$) as shown in Eq. (4.1). If this power is not required, the area can be set as zero.

$$\dot{Q}_{inc} = A_{field}\rho_{field}\mathrm{I}_{bn}\eta_{field}. \tag{4.1}$$

Certain receiver models require the distribution of reflected flux on the receiver surface in addition to the total incident power available from the heliostat field. Since the heliostat field component serves only as a mechanism for providing the total field efficiency and not the flux distribution on the receiver, central receiver models that require knowledge of an incident flux distribution will conversely have no use for the total reflected power from the field ($\dot{Q}_{inc}$). Receiver components that take the total power from the heliostat field and average the flux over the area of the receiver surface will require the total power from the field.

To specify the total field efficiency, the user provides an input file that indicates the number of azimuth and zenith data points, and this determines the total number of efficiency data points required. For example: four zenith and six azimuth angles would yield 24 data points. The values in this file must be provided in a specific format, and can be determined by a software package such as DELSOL3 or PTGen, or can be entered manually.

The efficiency matrix gives the heliostat field efficiency for a number of pairs of solar azimuth and zenith angle. This file is read in and interpolated by the TRNSYS routine data. The number of solar elevation and azimuth data points must be specified in the parameters of this type. The file has the following format:

- 1st line, list of all solar azimuth data points (e.g. for 3 points -120 0 120) (rising order)
- 2nd line, list of all solar zenith angles (e.g. for 3 points 0 45 90) (rising order) following lines with efficiency data for the solar angle data pairs (-120, 0) ;(-120, 45) ;...;(120, 90) with a maximum of 80 characters per line and minimum of one data point per line.

Table 4.1 provides a summary of the model parameters, inputs, and outputs for the STEC heliostat field component while Figure 4.1 shows the heliostat field connectivity model.

Table 4-1: The Parameters, Inputs, and Outputs for the STEC Heliostat Field Component (Type 394)

Parameters	Inputs	Outputs
Logical Unit No of Field efficiency input data (File)	Direct normal insolation (kJ/h m^2)	Power to the receiver
Number of zenith angle data points	Wind speed	Defocused power(Power which was defocused due to control constraints or wind speed)
Number of azimuth angle data points	Control Parameter (0= Field off, 0.5 = 50% of Field focusing, 1.0 Total field working)	Parasitic tracking power
Number of Heliostats	Solar zenith angle(is delivered by Standard TRNSY Type 16 'Solar radiation Processor')	Concentrator field efficiency
Mirror Surface per heliostat (m2)	Solar azimuth angle(is delivered by Standard TRNSY Type 16 'Solar radiation Processor')	
Reflectivity of heliostat		
Electric work for Startup of one heliostat (kJ)		
Electric power for tracking one heliostat (kJ/h)		
Maximum tolerable wind speed (m/s)		

4.2.1 TRNSYS Model of Heliostat Field Connectivity

The heliostat field receives the solar azimuth and solar zenith angles from the standard TRNSYS radiation processor from which the field efficiency MATRIX is generated. The DNI and wind speed are provided to the field from radiation data reader. Finally the incident power to the receiver is calculated by use of DNI of the area and average heliostat field

efficiency. The field efficiency matrix is a set of data representing the heliostat field efficiency for each solar zenith and solar azimuth angles generated in standard radiation processor. A user specified number of data points are used to evaluate the average field efficiency of the heliostat field. The inputs to the field are obtained from standard weather data (in this case the energy plus weather data for Dire Dawa, Ethiopia) and the reference parameters are obtained through optimization using SAM for reference power plant state values from chapter three.

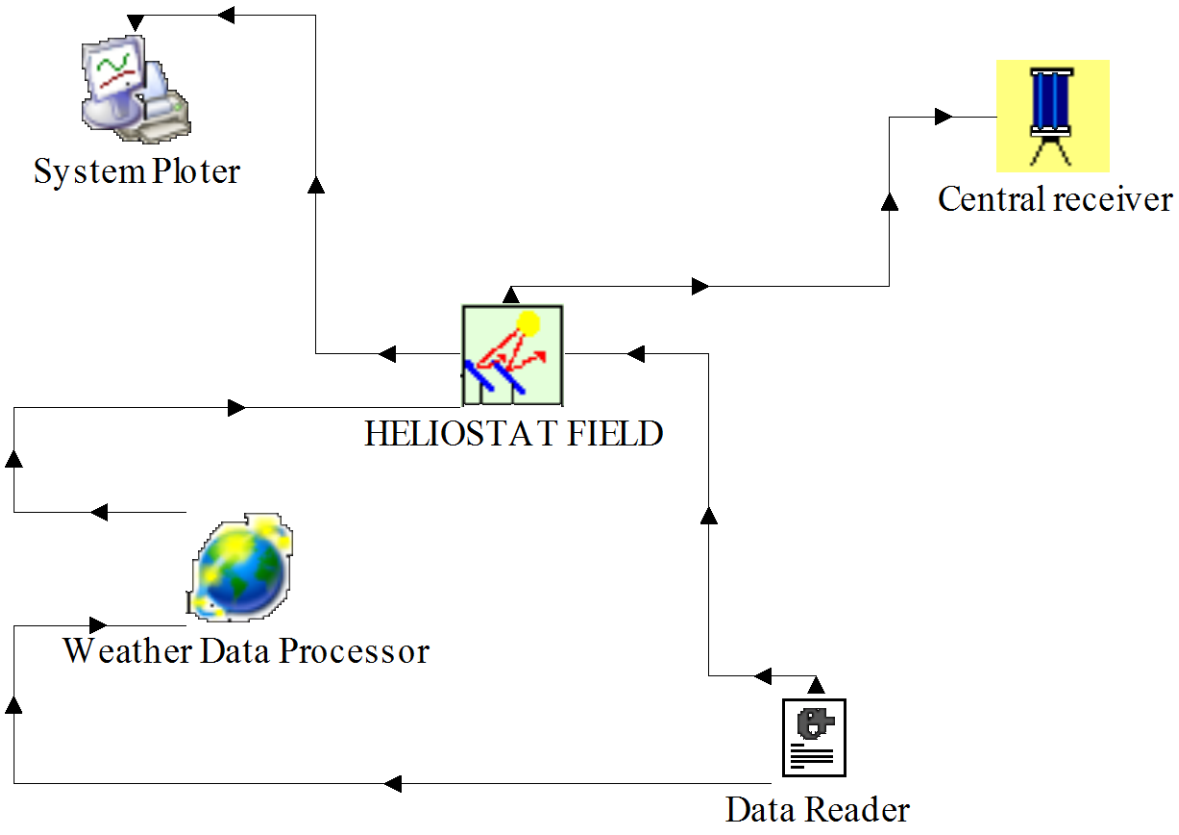

Figure 4-1: TRNSYS Model of the Heliostat Field Connectivity

4.3 Central Receiver Components

The STEC library contains two central receiver models that can accommodate molten salt or another liquid as a heat transfer fluid, and one air-receiver model. The salt/liquid models will be considered in this discussion.

4.3.1 Tower Receiver (Type 395)

The first tower receiver component, which was authored by S.A. Jones of Sandia National Labs (1997), is a simplified model of the central receiver, relying on a receiver thermal efficiency as an input value instead of calculating it directly. This model provides the flow rate required to achieve a temperature set-point as an output. Since the initial heliostat field model, like SOLERGY, is based upon a simple field efficiency table interpolation, only the total power to the receiver is calculated. To find the detailed flux distribution on the receiver, a complex numerical convolution, or ray-trace optical model, must be used. Without detailed flux information, an empirical receiver heat loss model is more appropriate than one based on heat transfer relations at the receiver's surface. In this model, the conductive losses are neglected in the calculation of the net absorbed power as shown in Eq. (4.2).

$$\dot{Q}_{net} = \alpha \dot{Q}_{inc} - \dot{Q}_{conv} - \dot{Q}_{rad} \tag{4.2}$$

where the subscripts *inc*, *conv*, and *rad* stand for the incident power, the power losses to convection, and the power losses to radiation respectively. The losses due to convection and radiation are described by third order polynomials with user-supplied coefficients:

$$\dot{Q}_{conv} = C_0 + C_1 V + C_2 V^2 + C_3 V^3 \tag{4.3}$$

$$\dot{Q}_{rad} = R_0 + R_1 \dot{Q}_{inc} + R_2 \dot{Q}_{inc}^2 + R_3 \dot{Q}_{inc}^3 \tag{4.4}$$

where V is the wind velocity. The user can also specify the turn down ratio- below which the power is discarded. The receiver efficiency ($\eta = \frac{\dot{Q}_{net}}{\dot{Q}_{inc}}$) is also provided as an output.

The model formulation is relatively simple and is contained within a few lines. The required heat transfer fluid mass flow rate is calculated with an energy balance as shown in Eq. (4.5).

$$\dot{m}_{htf,demand} = \frac{\dot{Q}_{inc} \cdot \eta_{rec}}{(C_{htf} \cdot (T_{htf,hot} - T_{htf,cold}))} \tag{4.5}$$

The variables are defined such that:

$\dot{Q}_{inc}$ = incident power on the receiver

η_{rec} = tower thermal efficiency

C_{htf} = heat transfer fluid specific heat

$T_{htf,hot}$ = HTF outlet temperature set point

$T_{htf,cold}$ = HTF inlet temperature

$\dot{m}_{htf,demand}$ = Resulting mass flow rate demand

Alternatively, the outlet fluid temperature is calculated when the heat transfer fluid mass flow rate is specified as:

$$T_{htf,hot} = T_{htf,cold} + \frac{\dot{Q}_{inc} \cdot \eta_{tower}}{C_{htf} \cdot \dot{m}_{htf,demand}} \quad (4.6)$$

The parameters, inputs, and outputs are provided in Table 4.2.

Table 4-2: The Parameters, Inputs, and Outputs for the SolarPACES STEC Tower Receiver Component (Type 395)

Parameters	Inputs	Outputs
Tower efficiency	Incident power [kJ/hr]	Flow rate demand [kg/hr]
	Fluid inlet temperature [^{O}C]	Fluid outlet flow rate [kg/hr]
	Fluid inlet flow rate [kg/hr]	Fluid outlet temperature [^{O}C]
	Fluid outlet pressure [bar]	Fluid inlet pressure [bar]
	Temperature set point [^{O}C]	
	Fluid Specific Heat[kJ/kg K]	

4.3.2 Central Receiver, Variable Efficiency (Type 495)

Type 495 was authored by J.M. Crespo of Ciemat (2000) as an enhancement to the previously described central receiver component (Type 395). This model takes variable tower thermal efficiency into account by scaling it with the ratio of the incident power to the

receiver design thermal power (C_{oc}). This ratio and the ratio of the part-load efficiency to the design efficiency (C_{eff} , set by the user) are correlated using a hyperbolic fit. Two additional parameters (*a* and *b*) are calculated to aid in the process.

$$C_{oc} = \frac{\dot{Q}_{partload}}{\dot{Q}_{design}} \tag{4.7}$$

$$C_{eff} = \frac{\eta_{partload}}{\eta_{design}} \tag{4.8}$$

$$a = \frac{(1-C_{oc}).\eta_{partload}}{C_{eff}-C_{oc}} \tag{4.9}$$

$$b = \left(\frac{a}{\eta_{design}}\right) - 1 \tag{4.10}$$

After calculating the coefficients, the ratio (W_{pl}) of the incident power (converted to the correct units by dividing by 3600 Wh/kJ) to the design incident thermal power is calculated and the overall efficiency is determined.

$$W_{pl} = \left(\frac{\dot{Q}_{inc}}{3600}\right)\frac{1}{\dot{Q}_{design}} \tag{4.11}$$

$$\eta_{tot} = \frac{a.W_{pl}}{a+W_{pl}} \tag{4.12}$$

The parameters, inputs, and outputs for the TRNSYS component are summarized in Table 4.3.

Table 4-3: The Parameters, Inputs, and Outputs for the STEC Central Receiver Model (Type 495)

Parameters	Inputs	Outputs
Mode	Incident power	Outlet mass flow rate
Design power	Inlet temperature	Excess mass flow rate
Receiver efficiency	Inlet flow	Outlet temperature
Part-load power	Inlet pressure	Outlet pressure
Receiver part-load efficiency	Set point temperature	Energy transfer
	Maximum receiver temperature	Excess energy
	Fluid specific heat	Efficiency
	Receiver pressure drop	

4.4 Rankine Cycle Components

The STEC library also contains a collection of components that can be used to assemble a power cycle to match a wide variety of Rankine cycle or Brayton cycle configurations. This paper deals with the Rankine steam cycle components for power cycle part of the power plant system. Models are available for five major equipment categories:

- The condenser and condenser pump for condensing functions
- The deaerator, preheater, and sub-cooler for pre-heating functions
- The economizer/superheater and evaporator for steam generating functions
- A variety of splitters and mixers, a turbine stage, a turbine control, and a throttling valve for turbine functions.

A brief review of selected components is presented below to highlight the premises on which these components are constructed. Each review contains the parameters, inputs, and outputs for the TRNSYS component, the major equations used to develop the model, and a short summary of the component.

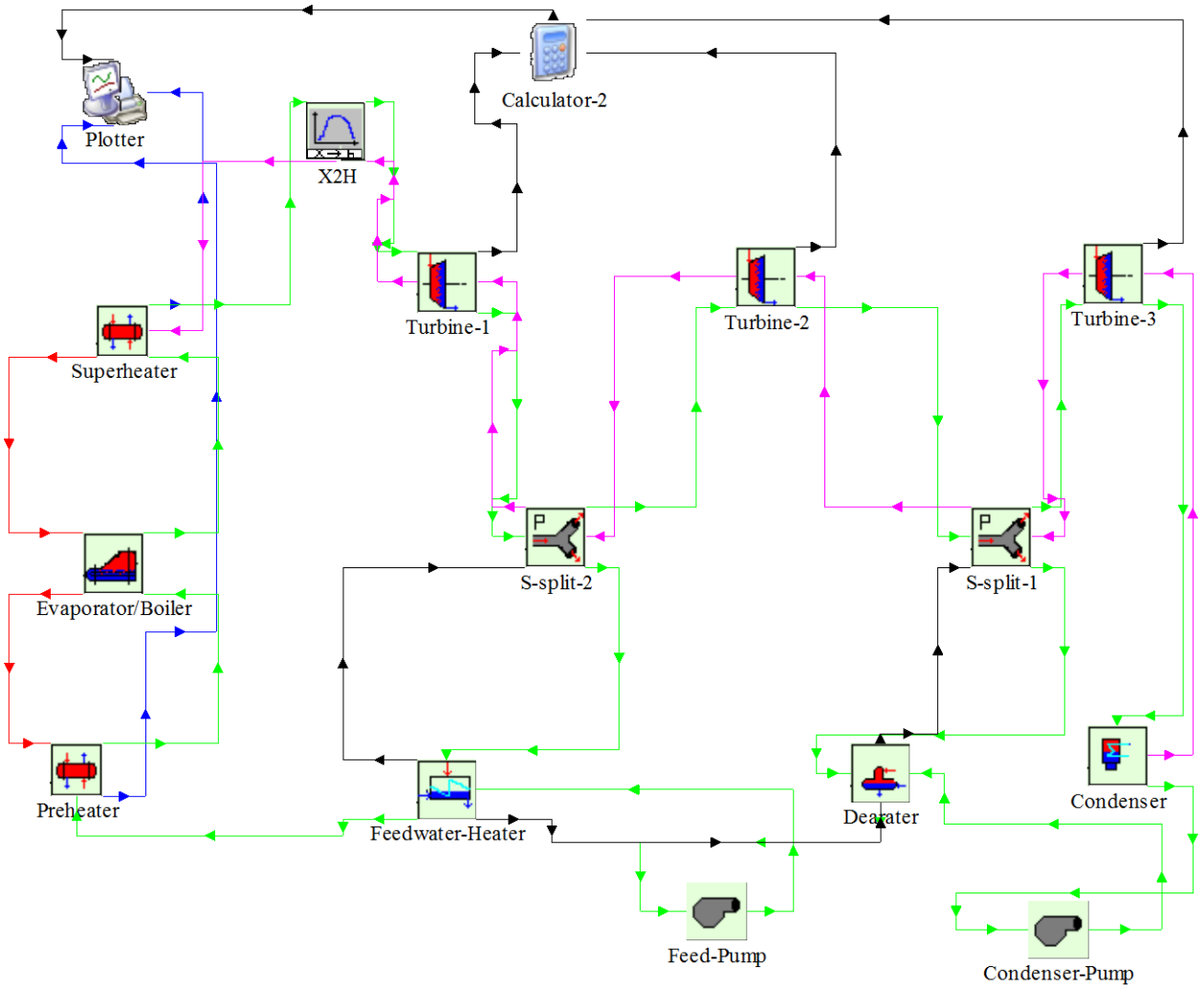

Figure 4-2: TRNSYS Model of the Rankine Cycle showing Components Input- Output Connectivity

The cycle component input-output connectivity is the same as the EES program flow written in chapter three of this document for reference state power plant model.

4.4.1 Economizer, Superheater for Water/Steam Heated by One Phase Fluid (Eco_SH) (Type 315)

A zero capacitance sensible heat exchanger is modeled in counter flow mode. The cold side input is assumed to be water/steam depending on the quality. The respective specific heat of

the cold side fluid is calculated from water/steam property data. The effectiveness η_{ECO} is calculated by using the overall heat transfer coefficient UA.

This component is based on equations commonly used to describe the behavior of counter-flow heat exchangers. First, the derived effectiveness relationship is shown (Schwarzbözl, 2006).

$$\eta_{ECO} = \frac{1-exp\left(-\frac{UA}{\dot{C}_{min}}.(1-\frac{\dot{C}_{min}}{\dot{C}_{max}})\right)}{1-\frac{\dot{C}_{min}}{\dot{C}_{max}}.exp\left(-\frac{UA}{\dot{C}_{min}}.(1-\frac{\dot{C}_{min}}{\dot{C}_{max}})\right)} \quad (4.13)$$

in this equation, $\dot{C}_{min}$ & and $\dot{C}_{max}$ represent the minimum and maximum thermal capacitance rates of the two fluids passing through the heat exchanger.

The relationship for *UA* depends on the ratio of the cold-side fluid mass flow rate to its reference mass flow rate, scaled by an exponent. This exponent was set as 0.8 in this research.

$$UA = UA_{ref}.(\frac{\dot{m}_{cold}}{\dot{m}_{cold,ref}})^{UA\_exp} \quad (4.14)$$

where UA is limited between 0.1 * UA_{ref} and 2* UA_{ref}; A_{ref} ,$\dot{m}_{cold,ref}$, and UA_exp can be specified by the user based on the requirement of net power output and HTF temperature at receiver inlet for specified heat exchanger conductance and hence pressure loss is scaled in a similar way where the user has the freedom to specify a satisfactory exponent.

$$\Delta p = \Delta p_{ref}.(\frac{\dot{m}_{cold}}{\dot{m}_{cold,ref}})^{\Delta p\_exp} \quad (4.15)$$

where Δp is limited to 2*Δp_{ref}. Δp_{ref} , $\dot{m}_{cold,ref}$ and Δp_exp can also be specified by the user. The parameters, inputs, and outputs for super heater is given in table 4.4

Table 4-4: Parameters, Inputs, and Outputs for STEC Library (Type 315)

Parameters	Inputs	Outputs
Mode-2(Counter-flow mode)	Inlet temperature hot side	Outlet temperature hot side
Reference Overall heat-transfer coefficient	Mass flow hot side	Mass flow hot side
Reference pressure loss	Inlet temperature cold side	Outlet temperature cold side
Reference cold side mass flow rate	Mass flow cold side	Mass flow cold side
Power law exponent for UA	Cold side quality	Heat transfer rate
Power law exponent for DP	Cold side outlet pressure	Effectiveness
	Hot side specific heat	Cold side outlet quality
		Cold side inlet pressure

4.4.2 Evaporator/Boiler (Type 316)

In an arrangement similar to Type 315, the evaporator is approached analytically and uses the fluid conductance to determine the effectiveness. The fluid on the cold side of the heat exchanger is assumed to be steam, and the specific heat of the fluid on the hot side is based on the working fluid used for the cycle. An inlet water flow rate is modulated to match the steam evaporation rate within the unit. Conductance is calculated as shown above in Eq. (4.14). The evaporator effectiveness is calculated in Eq. (4.16) and the corresponding heat transfer across the heat exchanger is determined applying Eq. (4.17).

$$\eta_{Evaporator} = 1 - exp\left(\frac{-UA}{\dot{m}_{hot}.C_{p,hot}}\right) \tag{4.16}$$

$$\dot{Q}_{trans} = \eta_{Evaporator}.\dot{m}_{hot}.C_{p,hot}(T_{hot,in} - T_{saturated}) \tag{4.17}$$

Table 4-5: The Parameters, Inputs, and Outputs for the STEC Evaporator (Type 316)

Parameters	Inputs	Outputs
Reference overall heat transfer coefficient	Inlet temperature hot side	Outlet temperature hot side
Blow down fraction	Mass flow hot side	Mass flow hot side
Reference pressure loss	Inlet temperature cold side	Outlet temperature cold side
Reference mass flow rate cold side	Cold side outlet pressure	Cold side inlet pressure
Power law exponent for UA	Cold side inlet quality	Cold side outlet quality
Power law exponent for DP	Hot side specific heat capacity	Cold side flow rate demand
		Mass flow cold side
		Transferred power
		Effectiveness

4.4.3 Turbine Stage (Type 318)

This component models the pressure drop across the turbine using the relationship proposed by Stodola and Lowenstein (1945). The inlet pressure is calculated by considering the relationship between the outlet pressure, the steam mass flow rate, the reference (design) values of inlet and outlet pressure and mass flow rate, as shown in Eq. (4.18).

$$P_{in} = \sqrt{(\frac{\dot{m}_{in}}{\dot{m}_{in}})^2 \left(P_{in,ref}^2 - P_{out,ref}^2\right) + P_{out}^2} \tag{4.18}$$

The behavior of this single-stage turbine is characterized using an isentropic efficiency, which is calculated from a reference value and adjusted based on the mass flow rate of steam through the turbine relative to a reference mass flow rate with the relationship given in Eq. (4.19). The coefficients α, β and γ are set by the user based on equipment performance test

result, but since these are often not known prior without performing simulations or equipment testing, this is a major limitation to the turbine model.

$$\eta_{in,turbine} = \eta_{in,ref} . (1 + \alpha . f + \beta . f^2 + \gamma . f^3) \quad (4.19)$$

(*Limited between 0.2 and 1*)

The ratio of the mass flow rates is given by:

$$f = \frac{\dot{m} - \dot{m}_{ref}}{\dot{m}_{ref}} \quad (4.20)$$

(Limited between ± 0.7)

The turbine can also be combined with a splitter component (Type189) and additional instances of the turbine stage to assemble an extraction turbine.

Table 4-6: The Parameters, Inputs and Outputs for the STEC Turbine Stage (Type 318)

Parameters	Inputs	Outputs
Reference inlet pressure	Turbine outlet pressure	Turbine inlet pressure
Reference outlet pressure	Turbine inlet flow rate	Turbine outlet flow rate
Reference flow rate	Turbine inlet enthalpy	Turbine outlet enthalpy
Reference efficiency	Inlet bypass indicator	Turbine power
Generator efficiency		Outlet bypass indicator
Coefficient for reference efficiency (alpha)		Isentropic efficiency
Coefficient for reference efficiency (beta)		
Coefficient for reference efficiency (gama)		

4.4.4 Water/Steam Attemporator (Type 304)

This model describes the mixing of a steam- and a feed-water flow. For given temperature T_1 and T_2, flow $\dot{m}_1$ and $\dot{m}_2$ and steam quality, the outlet temperature T_{mix} is calculated. For given set point temperature T_{mix} the demanded feed-water flow $\dot{m}_2$ to achieve T_{mix} can be calculated from:

$$\dot{m}_2 = \dot{m}_1 . \frac{c_{p1}(T_1 - T_{mix})}{c_{p2}(T_{mix} - T_2)} \tag{4.21}$$

Table 4-7: The Parameters, Inputs and Outputs for the STEC Water/Steam Attemporator (Type 304)

Parameters	Inputs	Outputs
None	Steam flow rate	Demanded feed-water flow rate
	Steam inlet temperature	Demanded steam flow rate
	Steam quality	Outlet flow rate
	Feed-water inlet flow rate	Outlet temperature
	Feed-water inlet temperature	Outlet quality
	Attemp outlet pressure	Inlet steam pressure
	Set point temperature	

4.4.5 Condenser (Type 383)

Type 383 models a water cooled condenser with a fixed cooling water temperature rise that is supplied by the user as a parameter. The temperature difference between cooling water outlet temperature and condensing temperature is given by an additional parameter. Therefore, this component assumes that the condensing pressure depends on the feed water inlet temperature and is constant when this inlet temperature is constant.

Table 4-8: The Parameters, Inputs and Outputs for the STEC Condenser (Type 383)

Parameters	Inputs	Outputs
dT cool water out + condensing temperature	Cooling water inlet temperature	Condensing Temperature
Temperature increase in cool water	Steam enthalpy inlet	Condensing pressure
	Steam mass flow rate	Transferred power
	Condensate inlet flow rate	Cooling water outlet temperature
	Condensate inlet temperature	Cooling water flow rate
	Condensate inlet quality	Condensate flow rate

The heat transfer across the condenser is calculated by:

$$\dot{Q}_{cond} = h_s.\dot{m}_s + h_c.\dot{m}_c - (\dot{m}_s + \dot{m}_c).h_{sat} \quad (4.22)$$

where:

h_s=main steam inlet enthalpy

$\dot{m}_s$=main steam flow rate

h_c =additional condensate inlet enthalpy

$\dot{m}_c$= additional condensate inlet flow rate

h_{sat}= enthalpy of saturated water at condenser pressure

With the heat flow rate determined, the cooling water flow rate is evaluated.

$$\dot{m}_{cool} = \frac{\dot{Q}_{cond}}{c_{p,w}.\Delta T_{c,w}} \quad (4.23)$$

where:

$\dot{m}_{cool}$= flow rate of cooling water in

$C_{p,w}$= specific heat of water

$\Delta T_{c,w}$= user specified parameter, the temperature increase of the cooling water across the condenser

The condenser pressure is calculated based on the saturation conditions at the condensing temperature. This condensing temperature is determined by evaluating the sum of the temperature increase of the cooling water and the temperature difference between cooling water outlet temperature and condensing temperature. Since all of these values are entered by the user, the temperature is essentially (and thus the pressure) of the hot-side fluid in the condenser are fixed. This component evaluates the required cooling water mass flow from an energy balance.

The overall system model of the central receiver power plant developed using TRNSYS for this research is shown in Figure 4.3. The arrow heads in the model indicate input-output component connectivity.

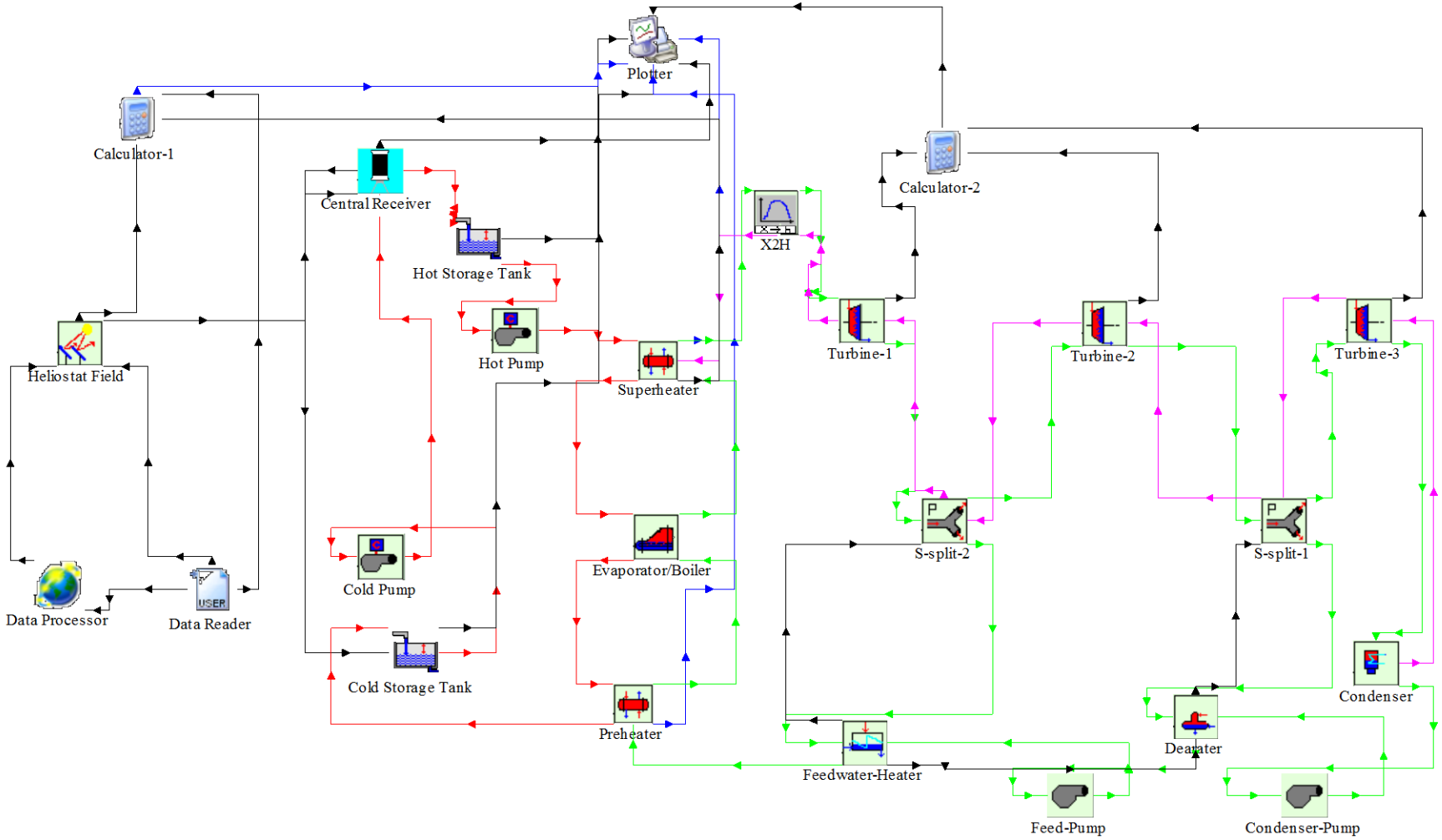

Figure 4-3: TRNSYS Model of the Central Receiver System Power Plant

CHAPTER FIVE

SIMULATION RESULT ANALYSIS

5.1 System Simulation Using TRNSYS

The TRNSYS program is used in order to simulate the CRS power plant modeled in chapter four. The behavior of the central receiver systems depends on the site meteorological conditions such as solar radiation and wind speed. These data are provided to the TRNSYS component (Type 9a) by the meteorological data file and the component is connected to the solar radiation processor (Type16g) that interpolates the solar radiation data at time steps of one hour and at any incident angle. The meteorological site selected for this analysis was Dire Dawa, Ethiopia, because the area has the highest average annual DNI than other eight sites considered as options. The heliostat field gets DNI data from the data reader and the solar azimuth and solar zenith angles from radiation data processor. The output power from heliostat field is used as an input for the central receiver component which is the heating chamber of the HTF. The hot HTF from the central receiver is continuously charged to hot thermal storage tank (Type 39) from which a controlled amount of HTF is sent to the Rankine cycle components called Super-heater, Boiler and Economizer to generate superheated steam which is used by steam turbines for generation of electrical power. The output HTF from Rankine cycle is charged to the cold storage tank (Type 39) that maintains the molten salt temperature at a required condition to protect solidification of the molten salt. The central receiver component of the power plant system completes the HTF cycle by receiving the demanded mass flow rate from cold storage tank. The steam cycle components such as turbines, condenser, pumps, deaerator, closed feed-water heater, economizer, boiler and superheater are connected in a cycle to provide the required power output. Type 65a online system plotter is used for plotting of simulation results

that are used for result analysis. The TRNSYS information flow diagram of this configuration is shown in Fig.5.1.

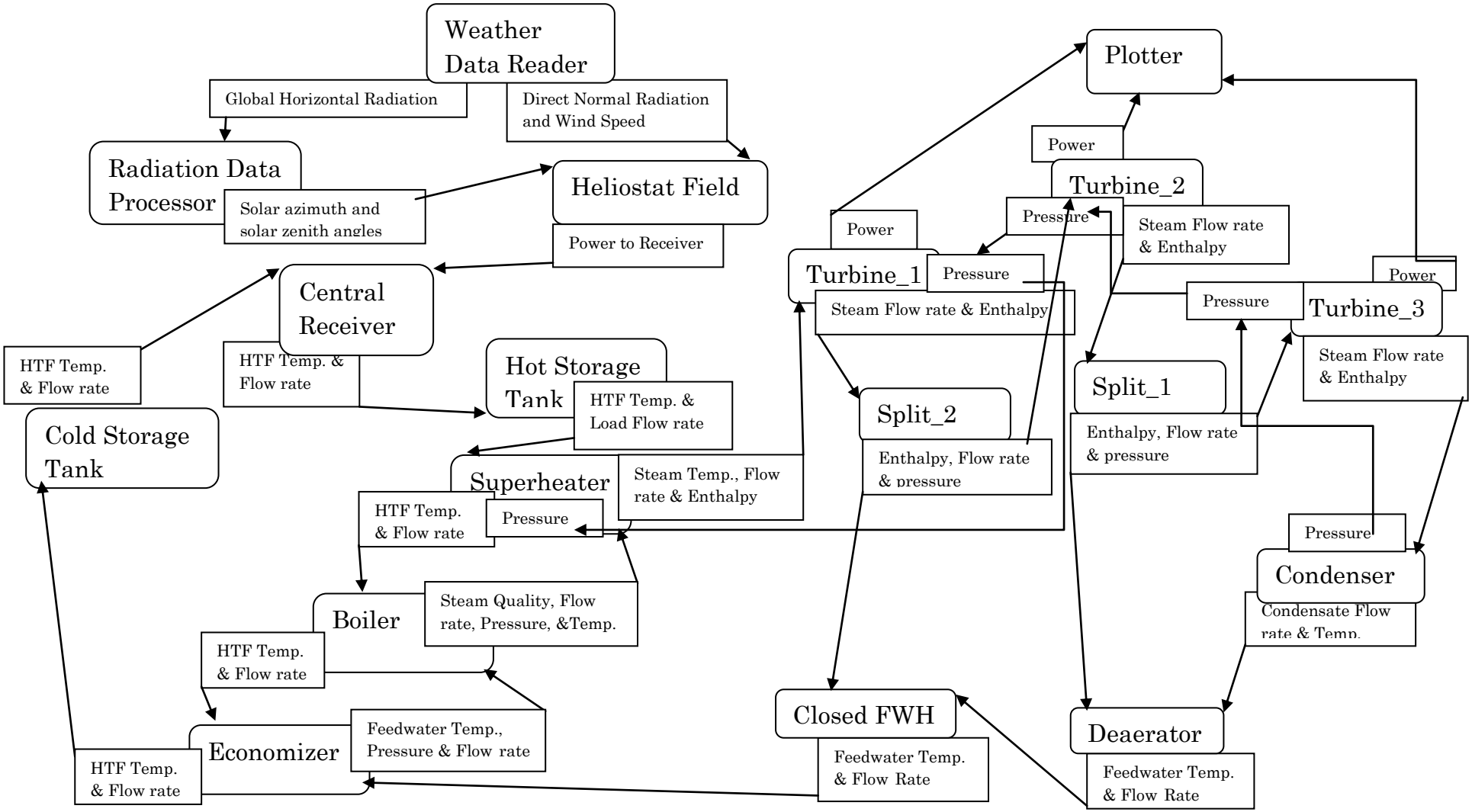

Figure 5-1: TRNSYS Information Flow Diagram

5.2 Results

The goal was to create a detailed model that accurately predicts CRS plant behavior on short time scales (i.e. hours) and through transients. Consequently, the TRNSYS model predictions are plotted on a daily, rather than monthly or annual basis. Results are shown for sunny and cloudy days in 2001 with solar-only operation. Figure 5.2 shows the weather conditions at Dire Dawa for the year 2001.

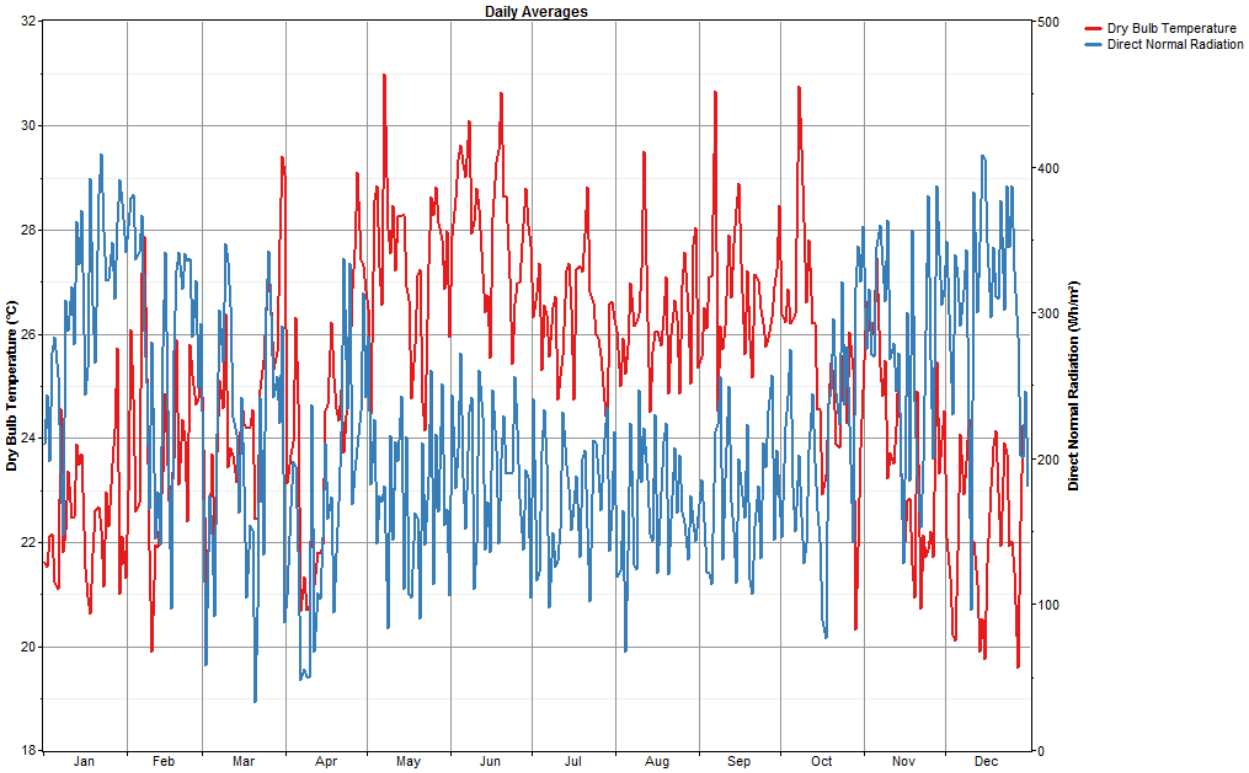

Figure 5-2: Daily Average Weather Conditions at Dire Dawa

The maximum daily average occurs on January 22 and minimum daily average on March 12, Figure 5.2. These days are, therefore, used as clear and cloudy day representatives respectively for system simulation.

5.2.1 Simulation Result for Clear Day

Clear day in this context is a representative day for occurrence of relatively higher daily average DNI from the days of the year considered. In this research, January 21st-23rd is selected for clear day simulation whereas March 11th -13th is selected for cloudy day simulation.

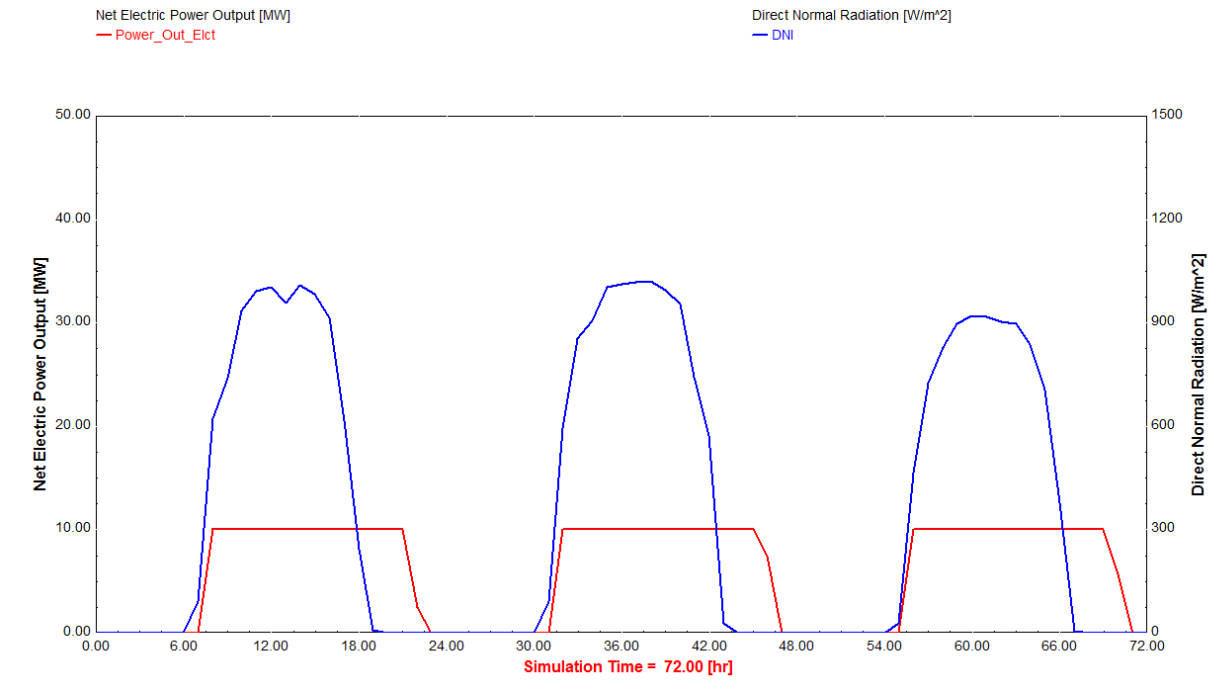

Figure 5-3: Plot of Power Output and DNI for January 21st - 23rd

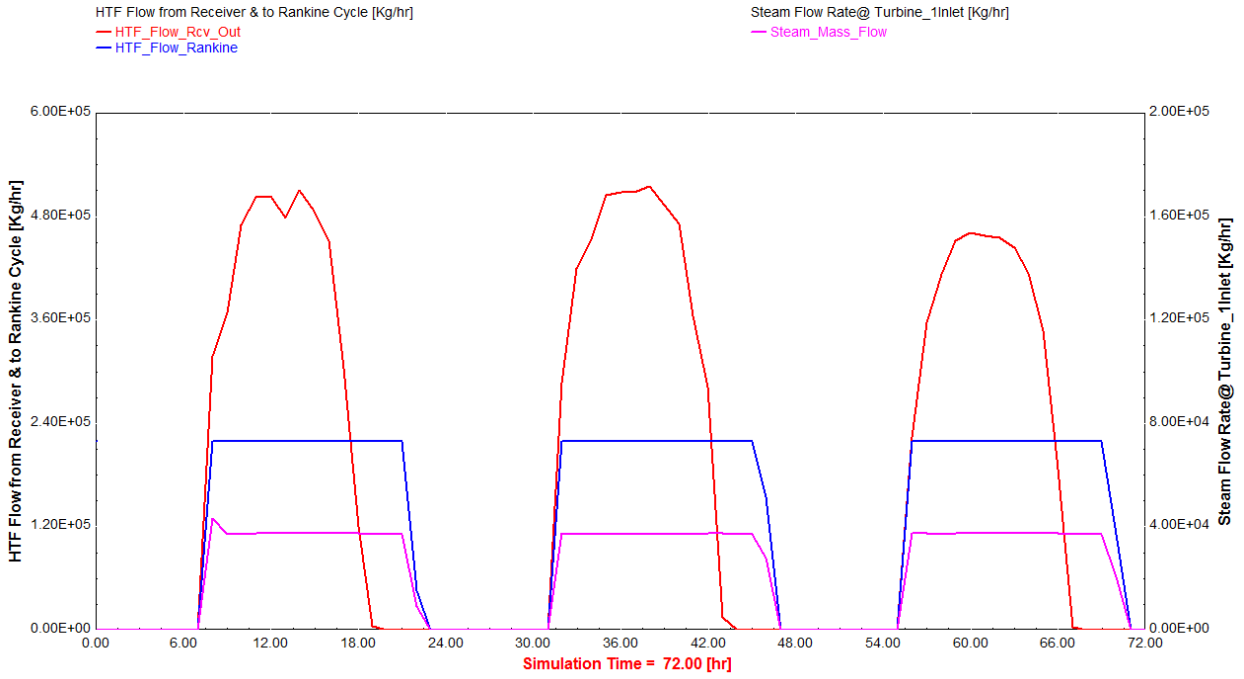

Figure 5-4: The Heat Transfer Fluid Flow Rates to the Power Cycle, from the Receiver and Steam Mass Flow Rate at Turbine_1 Inlet for January 21st - 23rd.

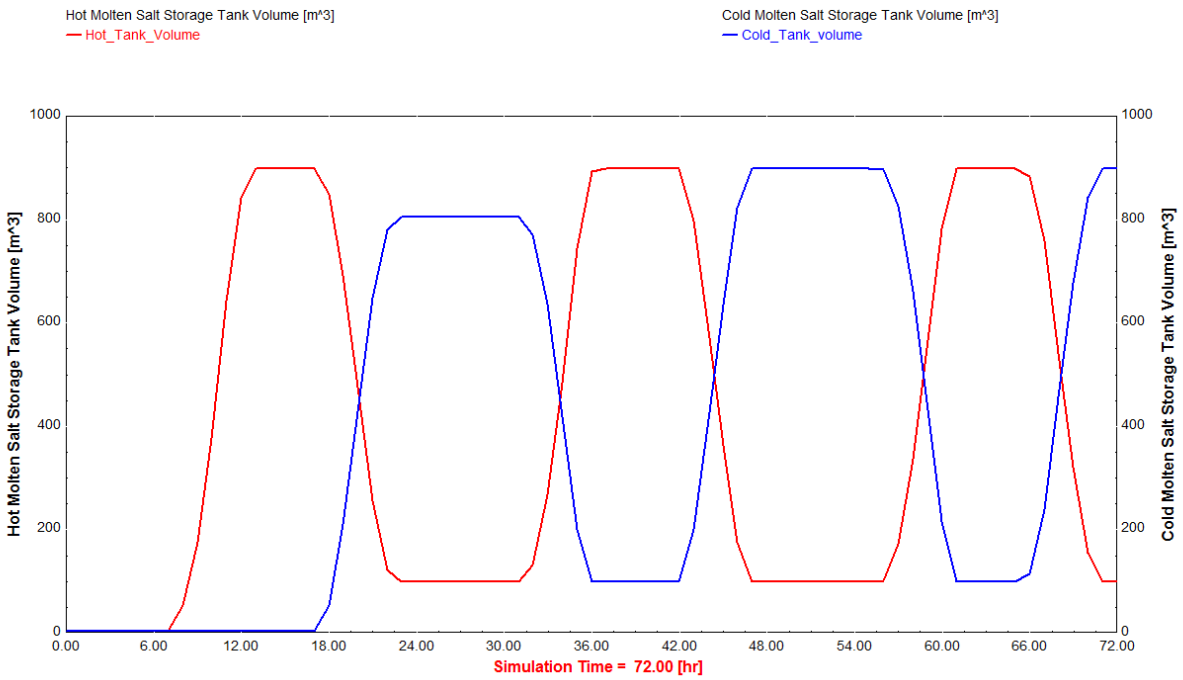

Figure 5-5: Initial Charging of the Hot and Cold Thermal Storage tanks and their Volume levels for January 21st - 23rd.

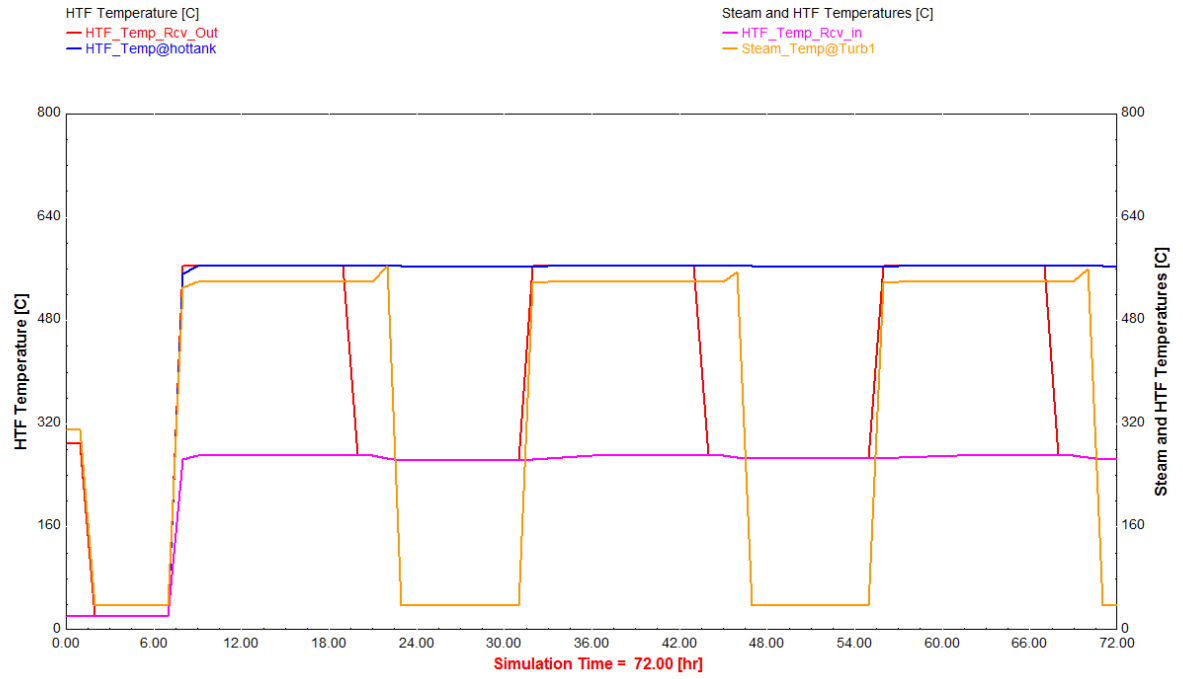

Figure 5-6: HTF Temperatures at Receiver Inlet, Outlet, Hot Tank and Steam Temperature at Turbine_1 Inlet for January 21st - 23rd.

From Figure 5.6 it is observed that during constant power operation, the temperature of steam at Turbine_1 inlet is about 540^0C which is below specified creep limit of 565^0C. The HTF temperature at receiver inlet is about 270^0C, well above the solidification point of nitrate salt of 220^0C.

5.2.2 Simulation Result for Cloudy Day

Cloudy day in this context is a representative day for occurrence of relatively lower daily average DNI from the days of the year considered. In this research, March 11th -13th is selected for cloudy day simulation.

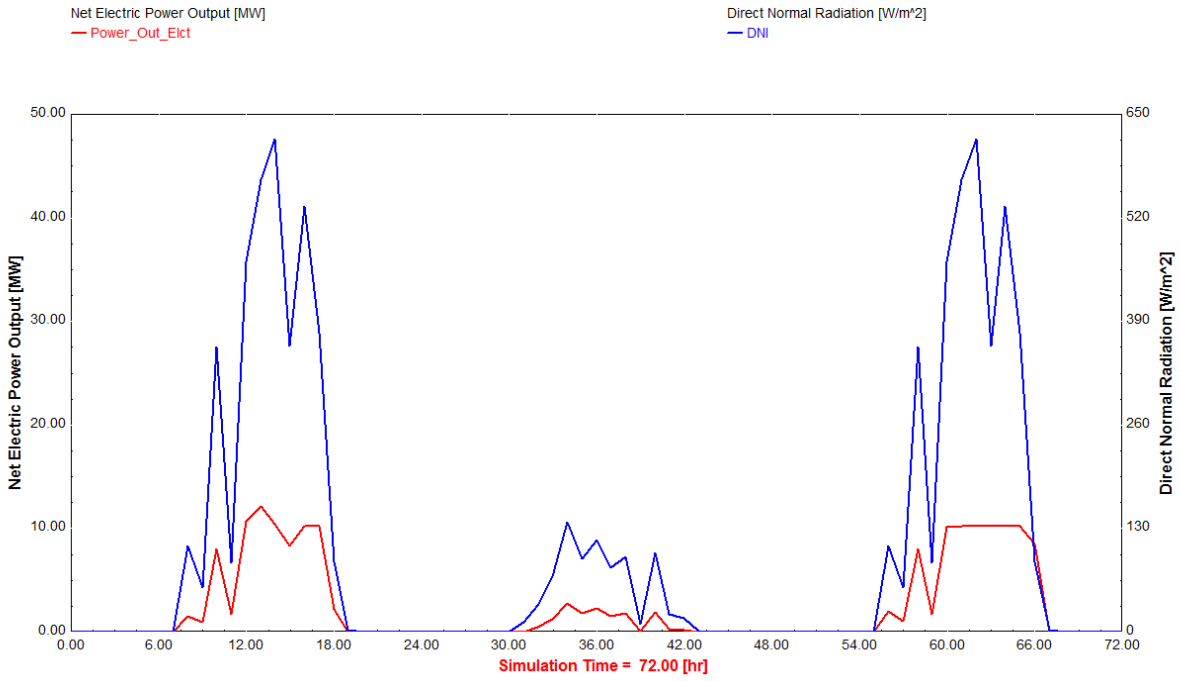

Figure 5-7: Plot of Power Output and DNI for March 11th-13th.

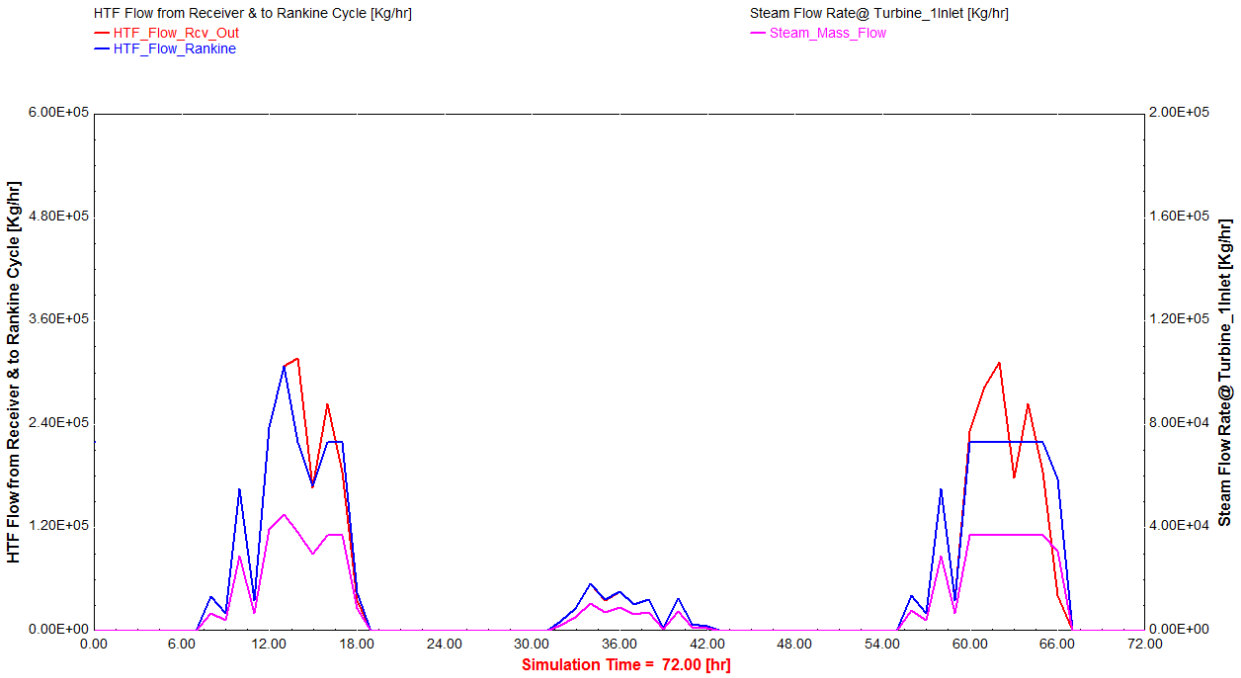

Figure 5-8: The Heat Transfer Fluid Flow Rates to the Power Cycle, from the Receiver and Steam Mass Flow Rate at Turbine_1 Inlet for March 11th-13th.

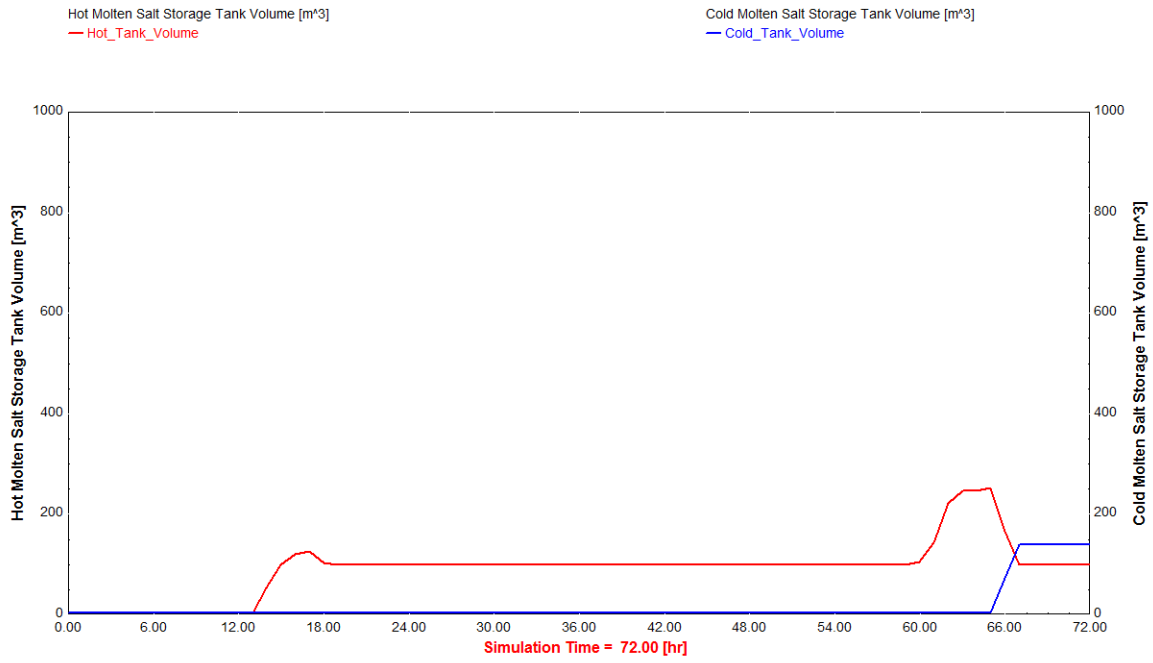

Figure 5-9: Initial Charging of the Hot and Cold Thermal Storage tanks and their Volume levels for March 11th-13th.

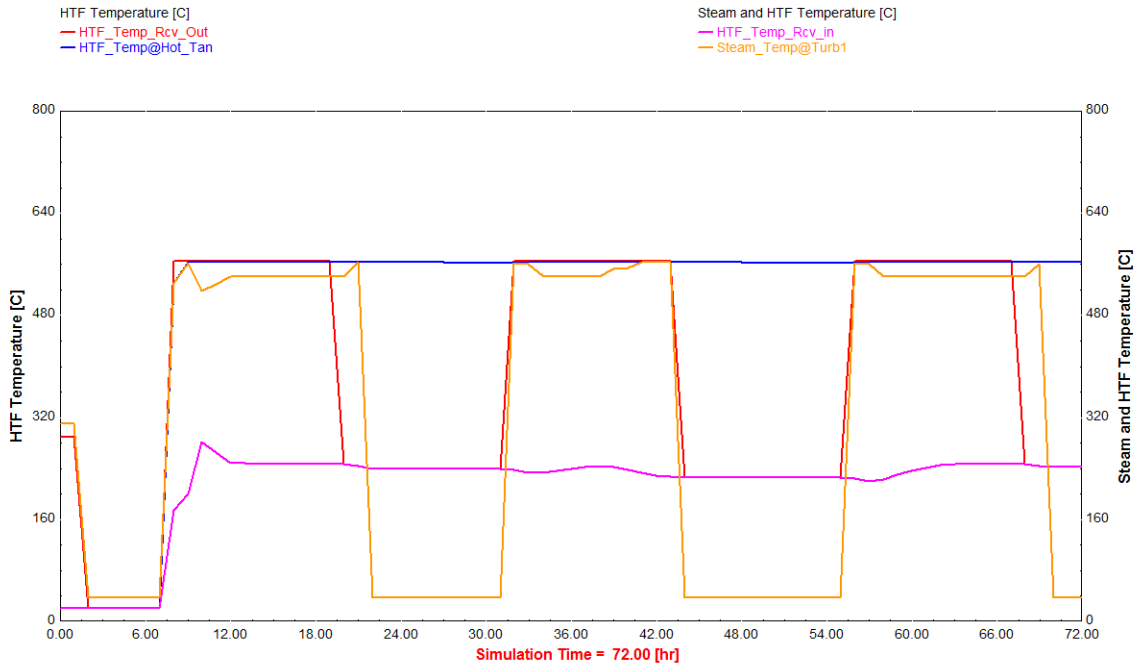

Figure 5-10: HTF Temperatures at Receiver Inlet, Outlet and Hot Tank Plus Steam Temperature at Turbine_1 Inlet for March 11th-13th.

For a clear day simulation, the system operates for 16 hours with 13 hours of constant electric power output of 10.26 MWe. On the other hand, for cloudy day simulation, a maximum of only 2.9 MWe electric power output is achieved out of 12 hours plant operation in transient form, Figure 5.7.

For the cloudy day, the thermal storage has no advantage, Figure 5.9. For such days, therefore, fuel backup or other forms of complementary power generation mechanisms should be implemented to achieve the required power generation capacity.

At times when the heat transfer fluid flow rate to the receiver exceeds the flow rate to the power cycle, the hot storage tank volume increases and the cold storage tank volume decreases. The volume of the fluid in hot storage tank plus the volume of the fluid in the cold storage tank is always equal to a constant, after initial charging of the tanks is completed (in this case, 1000 m^3). Figures 5.3 to 5.10 show power output and DNI, the volumes of the hot and cold fluids in the storage tanks, the power cycle heat transfer fluid (HTF) flow rate, the receiver HTF flow rate,

steam flow rate, and HTF and steam temperatures for a selected period of time in January and March.

The plots in Figure 5.6 and 5.10 show that the steam temperature at the inlet of Turbine_1 remains constant during constant power operation and the temperature of the hot end of the storage didn't drop below the cut off value (which was set at 565 ^{0}C). The temperature of the cold end of the thermal store is also plotted and appears at the bottom of the graph and remains constant. It is also noted that at the beginning(1st day of simulation) of plant operation, the receiver inlet and outlet temperatures of HTF are below set point values showing the requirement of thermal storage at a salt temperature higher than the solidification point of Nitrate Salt (220^{0}C) for the start up of CRS power plant. The year round plant simulation using SAM also reveals that a 26,289,746.8 kWh of annual energy can be harvested from the power plant with a capacity factor of 30%.

CHAPTER SIX

COST AND FINANCIAL ANALYSIS OF THE POWER PLANT

6.1 Overview of Solar Advisor Model

The Solar Advisor Model (SAM) is a performance and economic model based on an hourly simulation engine that interacts with performance, cost, and finance models to calculate energy output, energy costs, and cash flows. The software can also account for the effect of incentives on project cash flows. Solar Advisor's spreadsheet interface allows for exchanging data with external models developed in Microsoft Excel. The model provides options for parametric studies, sensitivity analysis, optimization, and statistical analyses to investigate impacts of variations and uncertainty in performance, cost, and financial parameters on model results [SAM User Guide]. The current version of the Solar Advisor Model has the capacity to model photovoltaic and concentrating solar power technologies for electric applications in several markets.

6.1.1 The Input Page

Solar Advisor's input pages display input variables and options. The navigation menu on the main window provides access to the input pages. The following input pages are available in all Solar Advisor cases:

Table 6-1: SAM Input Page Interface

Input Page	Purpose
System Summary	Displays key characteristics of the system based on input variables on other pages
Climate	Specify a weather file for the system's location
Utility Rate (residential or commercial projects only)	Define the electricity sales price as a flat rate or using a time-of-use schedule

Financing	Define the project's debt structure and rate of return constraints as appropriate for the type of project
Tax Credit Incentives	Define incentives in the form of tax credits that apply to the project
Payment Incentives	Define incentives in the form of cash payments that apply to the project
Annual Performance	Define an annual degradation rate and availability factor to account for expected reductions in system output over time due to equipment aging or due to system down times
Power Tower Systems	Input pages for power tower or central receiver systems

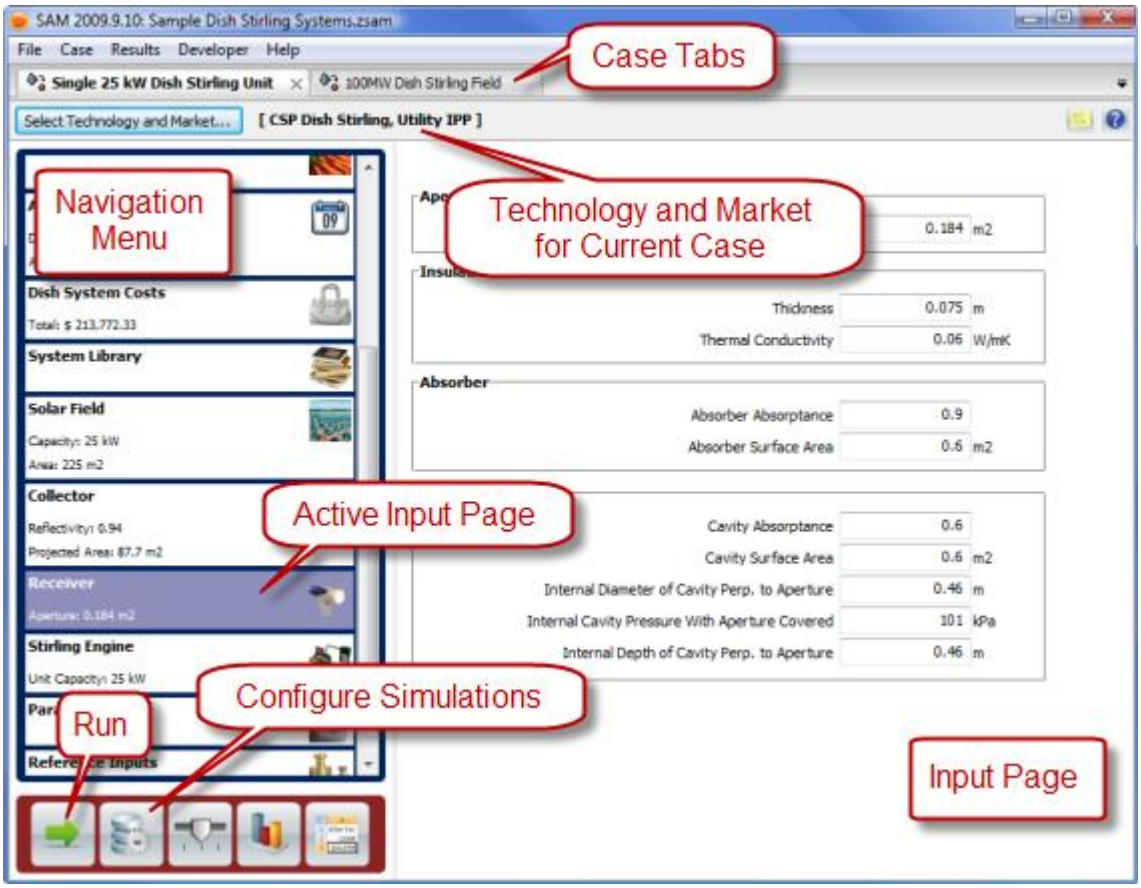

Figure 6-1: SAM Input Page

6.2 Financial and Incentive Models

Solar Advisor's economic model calculates a project's cash flow over a specified analysis period. The cash flow captures installation and operating costs, taxes, incentives, and the cost of debt. Solar Advisor uses the system's hourly output for a single year generated by the performance model, and then calculates a series of annual cash flows for revenues from electricity sales and incentive payments, tax liabilities (accounting for any tax credits for which the project is eligible), and loan principal and interest payments. Solar Advisor reports a set of economic metrics such as the levelized cost of energy that it calculates from the cash flow. Solar Advisor also generates a detailed cash flow table that one can use to evaluate a project's value. The economic model can represent projects in the residential, commercial, and utility markets, and account for a wide range of incentive payments and tax credits, which can be based on investment amounts, capacity ratings, and annual electricity production. Residential and

commercial projects are assumed to be financed through either a loan or cash payment, and to recover investment costs by selling electricity through either a net metering or time-of-use pricing agreement. For these projects, SAM reports a payback period and net present value in addition to the detailed cash flow table. Utility and commercial third-party projects are assumed to sell electricity through a power purchase agreement at a fixed price with optional annual escalation, and to be required to meet a set of financing constraints. For utility projects, SAM calculates an electricity sales price, internal rate of return, and minimum debt service coverage ratio. Projects with commercial and utility financing can be modeled with or without depreciation using MACRS depreciation schedules or customized schedules.

6.2.1 Project Cash Flow

Solar Advisor reports annual data in the cash flow table, including the system's annual electric output in kWh, electricity price in $/kWh, net-metering receipts or sales revenue, project expenses, taxes, and cost streams used to calculate the project payback. The cash flow table only displays data from on the analysis base case, which is the set of results calculated from the input variable values that are visible on the input pages. Solar Advisor calculates the values for the cash flow and other economic metrics after completing the performance simulation calculations. The model uses the first year annual energy output value from the simulation results in the cash flow calculations. It also uses input variable values from the input pages.

6.2.1.1 Energy (kWh)

The energy quantity reported for year one is equal to the Annual Energy value displayed in the Metrics table. The quantities in year two and subsequent years is based on the year one value adjusted for the degradation rate.

6.2.1.2 Energy Price ($/kWh)

For commercial and residential projects, the energy price is the annual average utility rate where as for utility and commercial third party projects, the energy price is the 1st Year PPA price displayed in the Metrics table. For year two and later, the energy price is the first year price adjusted by the PPA escalation rate also displayed on the Metrics table.

6.2.1.3 Energy Value ($)

Residential and commercial projects may receive net-metering offset payments for electricity generated by the project. Commercial projects pay federal and state income tax on these payments. For utility projects, annual revenues are determined in each year by the annual energy output and the electricity sales price for that year.

Energy Value = Energy (kWh) x Energy Price ($/kWh)

6.2.1.4 Operating Expenses

The operating expenses include operation and maintenance costs, and insurance and property tax payments. The value in the Operating Costs row of the cash flow table is calculated as follows:
Operating Costs = Fixed O&M Annual + O&M + Variable O&M + Fuel O&M + Insurance + Property Taxes

The operation and maintenance (O&M) costs are defined on the system costs page and escalated in each year after year one using both the escalation rate for each O&M category and the inflation rate value. The insurance and property tax rates apply to the total installed cost value. CSP trough, CSP tower, and generic fossil systems also include an annual cost of fuel in the total operating expense. When the fossil fill fraction variable on the Thermal Storage page for troughs or towers is greater than zero, the systems consume fuel for backup energy. But For photovoltaic and CSP dish systems, the fuel cost is always zero.

6.2.1.5 Operating Income and Deductible Expenses

For residential and commercial projects, the deductible expenses are project costs that can be deducted from federal and state income taxes.

- For residential projects, the deductible expense amount equals the property tax amount:

Deductible Expenses = - Property Taxes

- For commercial projects, all operating costs are deductible:

Deductible Expenses = - Operating Costs

- For utility projects, the operating income is the difference between revenues and operating costs:

Operating Income = Revenues - Operating Costs

6.2.1.6 Income, Taxes and Incentives

All projects pay state and federal taxes on the total taxable income for each year when the state and federal annual tax rates are non-zero. Federal and state tax cash flows are displayed in two separate sections of the cash flow spreadsheet, under the rows labeled Tax Effect on Equity (State) and Tax Effect on Equity (Federal). The tax amount for each year appears in the Tax Savings row under each section.

6.2.1.7 Depreciation

For utility and commercial third party ownership projects with a depreciation option defined on the Financials page, Solar Advisor displays the depreciation amount in the State Depreciation and Federal Depreciation rows of the cash flow table. The depreciation amounts and applicable years are determined by the options on the Financials page.

6.2.1.8 After Tax Cash and Cost Flow

Year zero of the cash flow represents project capital cost. The capital cost is equal to the total installed cost displayed on the system costs page minus the loan principal amount. Year one is the first year that the project generates electricity. The cash flow for year one and subsequent years account for project expenses, income from electricity sales, taxes, and incentive payments. For Utility power producer, the after tax cash flow for year one and subsequent year is given by:
After Tax Cash flow = After Tax Cost + Revenues

6.3 SAM Output Variables

6.3.1 Levelized Cost of Energy (LCOE)

The levelized cost of energy (LCOE) in cents per kilowatt-hour accounts for a project's installation, financing, tax, and operating costs and the quantity of electricity it produces over its life. The LCOE makes it possible to compare alternatives with different project lifetimes and performance characteristics. Analysts can use the LCOE to compare the option of installing a residential or commercial project to purchasing electricity from an electric service provider, or to

compare utility and third-party ownership projects with investments in energy efficiency, other renewable energy projects, or conventional fossil fuel projects. The LCOE captures the trade-off between typically higher-capital-cost, lower-operating-cost renewable energy projects, and lower-capital-cost, higher-operating-cost fossil fuel-based projects. Solar Advisor calculates the LCOE for residential and commercial projects differently than it does for utility and commercial third-party ownership projects as described below. One can specify the project's financing type (residential, commercial, commercial third-party, and utility) in the Technology and Market window. For all projects, Solar Advisor calculates both a real and nominal LCOE value. The real LCOE accounts for the effect of inflation over the life of the project. The nominal LCOE excludes inflation from the calculation.

6.3.1.1 LCOE for Residential and Commercial Projects

For a project using one of the Residential Market or Commercial Market (except Third-Party Ownership) financing options, the LCOE is the cost of installing and operating a system per unit of electricity it produces over the project's life. Solar Advisor assumes that projects with residential or commercial financing are distributed energy projects installed on a residential or commercial property, and that power generation equipment operates on the retail customer side of the electric meter. For these projects, it is possible to compare a project's LCOE to the electricity rate that the residence or commercial entity would pay to an electric service provider if the project were not installed.

Solar Advisor uses the inflation rate to calculate Year 2 and later costs in the cash flow based on the cost input values specified. The inflation rate accounts for expected price increases over the project life for future operating costs. For the real LCOE, the real discount rate appears in the denominator's total energy output term as:

$$\text{real LCOE} = \frac{\sum_{n=0}^{N} \frac{C_n}{(1+d_{nominal})^n}}{\sum_{n=1}^{N} \frac{Q_n}{(1+d_{real})^n}} \quad (6.1)$$

Similarly, for the nominal LCOE, the nominal discount rate appears in the denominator's total energy output term:

$$\text{nominal LCOE} = \sum_{n=0}^{N} \frac{C_n}{(1+d_{nominal})^n} \sum_{n=1}^{N} \frac{Q_n}{(1+d_{nominal})^n} \quad (6.2)$$

The summation in the numerator term starts at n = 0 to include project's capital costs incurred in year zero of the cash flow and shown as the Total Installed Cost on the system costs pages. The summation in the denominator term begins at n = 1, which is the first year that the project produces energy.

6.3.1.2 LCOE for Utility IPP and Commercial Third Party Projects

For a project using either the Utility and IPP or Commercial Market - Third-Party Ownership financing option, the LCOE is the amount that the project must receive for each unit of electricity it sells to meet financial returns targets. This makes the LCOE for these projects very sensitive to the values specified for the minimum IRR, minimum DSCR, and positive cash flow.

Solar Advisor assumes that utility IPP (independent power producer) and commercial third-party ownership projects are power generation projects installed on the utility side of consumer power meters. These projects recover capital, operating, and financing costs through electricity sales to a utility customer or other off-taker through a power purchase agreement with a fixed annual electricity sales price and optional annual escalation rate.

For these projects, the LCOE is effectively a levelized price of electricity because it is based on the present worth of the project's revenue stream. The electricity sales price reported in the cash flow for year one is equivalent to the first year power purchase price, which Solar Advisor reports as 1st Year PPA Price in the metrics table. Solar Advisor uses the real discount rate and inflation rate to calculate the present worth of future costs. The discount rate accounts for the time value of money and the relative degree of risk for alternative investments.

Solar Advisor uses the inflation rate to calculate Year 2 and later costs in the cash flow based on the cost input values specified on the system costs page. The inflation rate accounts for expected price increases over the project life for future operating costs. For the real LCOE, the real discount rate appears in the denominator's total energy output term:

$$\text{real LCOE} = \sum_{n=0}^{N} \frac{R_n}{(1+d_{nominal})^n} \sum_{n=1}^{N} \frac{Q_n}{(1+d_{real})^n} \quad (6.3)$$

Similarly, for the nominal LCOE, the nominal discount rate appears in the total energy output term:

$$\text{nominal LCOE} = \sum_{n=0}^{N} \frac{R_n}{(1+d_{nominal})^n} \sum_{n=1}^{N} \frac{Q_n}{(1+d_{nominal})^n} \quad (6.4)$$

6.3.4 Real and Nominal LCOE

Solar Advisor reports both a real LCOE and a nominal LCOE value. The form of the discount rate used in the denominator's total energy output term of the equations described above determines the form of the LCOE.

The real LCOE is a constant dollar value that is adjusted for inflation. Because the nominal discount rate used to compute the nominal LCOE includes inflation, inflation is effectively factored out of the nominal LCOE. The nominal LCOE is a current dollar value. If the inflation rate is set to zero, the real and nominal LCOE will be equal. The choice of real or nominal LCOE depends on the analysis. Most long-term analyses are conducted in real (constant) dollars to account for many years of inflation over the project life, whereas most short term analyses use nominal (current) dollars. The nominal discount rate can be calculated based on the values of the real discount rate and the inflation rate:

$$\text{dnominald}_{nominal} = (1 + d_{real})(1 + e) - 1 \quad (6.5)$$

6.3.5 1st Year Power Purchase Agreement (PPA) Price

The first year PPA price is the electricity sales price for projects with Utility and IPP or Commercial - Third- Party Ownership financing. Solar Advisor assumes that such projects sell electricity through a power purchase agreement (PPA) at a fixed price over the life of the project with an optional annual escalation rate. The first year PPA Price and annual escalation rate (PPA

Escalation rate on the Financing page) determine the project's annual revenues. Solar Advisor calculates the annual revenues to meet the minimum requirements of the internal rate of return (IRR), debt service coverage ratio (DSCR), and positive cash flow, which are defined as constraining assumptions. Because of the way the first year PPA price, IRR, and minimum DSCR interact, Solar Advisor uses an iterative algorithm to determine the values of these variables. For projects with Utility and IPP financing, the constraining assumptions defined are the Minimum Required IRR and the Minimum Required DSCR, and a positive cash flow requirement. But for projects with Third-Party Ownership financing, there is a single constraining assumption defined on the Financing page which is the Minimum Required IRR.

The following equations show the calculations used in the iterative algorithm to determine the IRR and minimum DSCR, which are both reported as results. The internal rate of return is the discount rate, IRR in the equation below, that corresponds to a project net present value, NPV, of zero where as the minimum DSCR is the minimum debt-service coverage ratio that Solar Advisor calculates for projects with Utility and IPP or Commercial - Third-Party Ownership financing. The debt-service coverage ratio in each year n is the ratio of operating income to expenses in that year. Solar Advisor calculates the minimum debt-service coverage ratio to be greater than or equal to the minimum required DSCR target defined.

$$\mathrm{NPV} = \sum_{n=1}^{N} \frac{R_n - C_{\mathrm{AfterTax},n}}{(1+\mathrm{IRR})^n} + C_{\mathrm{AfterTax},0} = 0 \tag{6.6}$$

$$\mathrm{DSCR}_n = \frac{R_n - C_{\mathrm{Operating},n}}{C_{\mathrm{Intererest},n} + C_{\mathrm{Principal},n}} \tag{6.7}$$

6.3.6 Annual Energy

The annual energy quantity reported in the Metric table is the total electric generation in kWh for the first year that the project operates, equivalent to Year one in the project cash flow. The output in subsequent years may be lower than in the first year depending on the value of the degradation rate.

6.3.7 Capacity Factor

The capacity factor is the ratio of the system's predicted electrical output in the first year of operation to the output had the system operated at its nameplate capacity:

$$CF = \frac{E_{OutputYear1}}{P_{SystemCapacity.8760}} \tag{6.8}$$

6.3.8 Debt Fraction and PPA Escalation

The debt fraction is the percentage of the project total installed cost that is financed through a loan and the PPA escalation rate is an annual escalation rate that Solar Advisor uses to calculate future electricity sales prices based on the first year PPA price, The values are reported as a results only for projects with Utility and IPP or Commercial - Third-Party Ownership financing. For these types of projects, depending on the financial optimization option, the debt fraction and PPA are either a user defined input on the Financing page, or a value that Solar Advisor calculates. When the Automatically minimize LCOE with respect to Debt Fraction and PPA Escalation Rate option are checked, Solar Advisor finds the debt fraction and PPA Escalation Rate that results in the lowest levelized cost of energy. Solar Advisor uses the debt fraction to calculate the principal and interest payments, and used in the iterative search algorithm described in 1st Year PPA Price.

6.3.9 Net Present Value

The net present value is the present value of the after-tax cash flow discounted to year one using the nominal discount rate, plus the after-tax cash flow in year zero:

$$NPV = \sum_{n=1}^{N} \frac{R_n - C_{AfterTax,n}}{(1+d_{nominal})^n} + C_{AfterTax,0} \tag{6.9}$$

6.3.10 Payback

The simple payback is the time in years starting in year one of the project that it takes for the cumulative cash flow (expenses included) to switch from negative to positive.

6.4 Results of SAM Analysis

The Solar Advisor Model is a performance and economic model based on an hourly simulation engine that interacts with performance, cost, and finance models to calculate energy output, energy costs, and cash flows. The weather data format used here is EPW from SWERA website. The results of SAM analysis were presented in this section.

6.4.1 Financial Page

The Financing page displays the variables that Solar Advisor uses to calculate the project cash flow and other related financial metrics. The variables that appear on the Financing page depend on the financing option specified. In this case CSP Power Tower technology for Utility IPP market is analyzed. In the financials page the analysis period, inflation period, loan amount, taxes and insurance, power purchase agreements and other inputs are found. Figure 6.2 shows the financial page with its different inputs

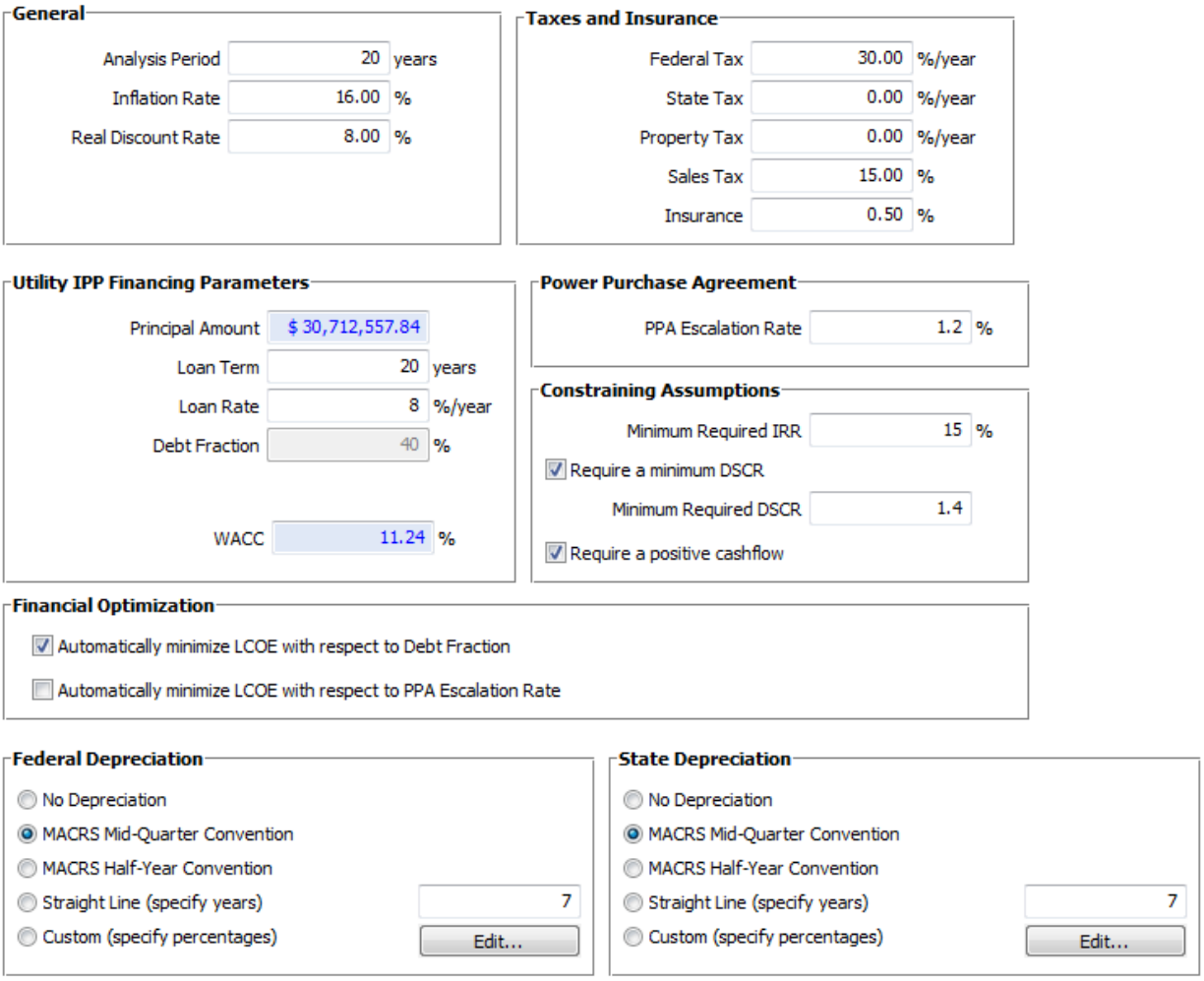

Figure 6-2: Financial Page

6.4.2 Costs

In the costs page, SAM calculates the different estimates for direct, indirect, and operation and maintenance cost components for the project. This page is used to determine the total installed cost that can be used as input for the financial page. The direct capital costs include site improvements, heliostat field, and balance of plant, power block, storage system, tower receiver and contingency estimate for the project. According to this analysis a total direct capital cost is $58,836,317.71. Engineering procurement, sales tax, land and project management costs are considered as indirect capital costs which in this case estimated to be $17,945,076.90. The total installed capital cost is the sum of direct and indirect capital costs which is $76,781,394.61 as shown in Figure 6.3. Inclusion of thermal storage in the system has a significant increase in total

installed capital cost from $58,072,837.73 to $76,781,394.61. This is due to increased number of heliostats for collection of execs energy and cost of the thermal storage itself. The tower system page for system without storage case is shown in Appendix part.

Direct Capital Costs

Site Improvements	116982.0	m2		5 $/m2	$ 584,910.00
Heliostat Field	116982.0	m2		165 $/m2	$ 19,302,030.00
Balance of Plant	11	MWe, Gross		345 $/kWe	$ 3,795,000.00
Power Block	11	MWe, Gross		575 $/kWe	$ 6,325,000.00
Storage System	194.118	MWht		30 $/kWht	$ 5,823,529.41
				Fixed Solar Field Cost	$ 0.00
Fixed Tower Cost	$ 901,500.00				
Tower Cost Scaling Exponent	0.01298			Total Tower Cost	$ 2,356,280.61
Receiver Reference Cost	$ 59,148,900.00				
Receiver Reference Area	1110	m2	Area 160.85	m2	
Receiver Cost Scaling Exponent	0.7			Total Receiver Cost	$ 15,300,811.53
				Contingency 10 %	$ 5,348,756.16
				Total Direct Cost	$ 58,836,317.71

Indirect Capital Costs

	% of Direct Cost	Non-fixed Cost	Fixed Cost	Total
Engineer,Procure,Construct	15 %	$ 8,825,447.66	$ 0.00	$ 8,825,447.66
Project,Land,Management	3.5 %	$ 2,059,271.12	$ 0.00	$ 2,059,271.12
Sales Tax of	15 %	applies to	80 %	of Direct Cost	$ 7,060,358.12
			Total Indirect Cost	$ 17,945,076.90

Total Installed Costs

Total Installed Cost	$ 76,781,394.61
Estimated Total Installed Cost per Net Capacity ($/kW)	$ 7,678.06

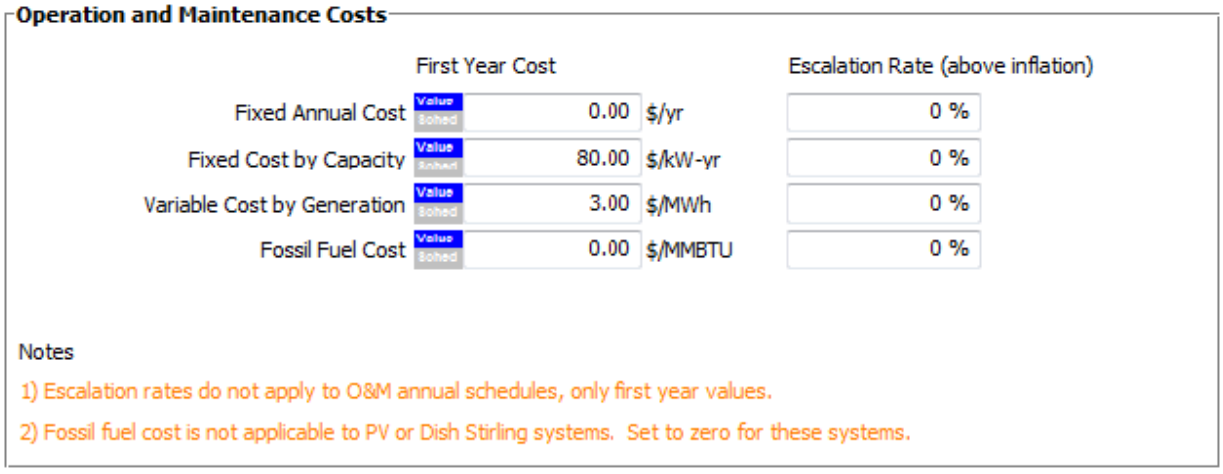

Figure 6-3: Tower System Page

6.4.3 Heliostat Field Page

The Heliostat Field page displays the variables that specify the position of the heliostats in the solar field along with the heliostat geometry and optical properties. Unlike parabolic trough and dish system designs, which can be based on modular designs of individual components, power tower system designs typically require optimization of the tower height, receiver geometry, and distribution of heliostats around the receiver as a complete system. The heliostat properties define the area of a single heliostat mirrored surface, shape of the heliostat, and the boundaries of the solar field area. Solar Advisor assumes that each heliostat employs a two-axis drive system with a pivot at the center of the mirrored surface.

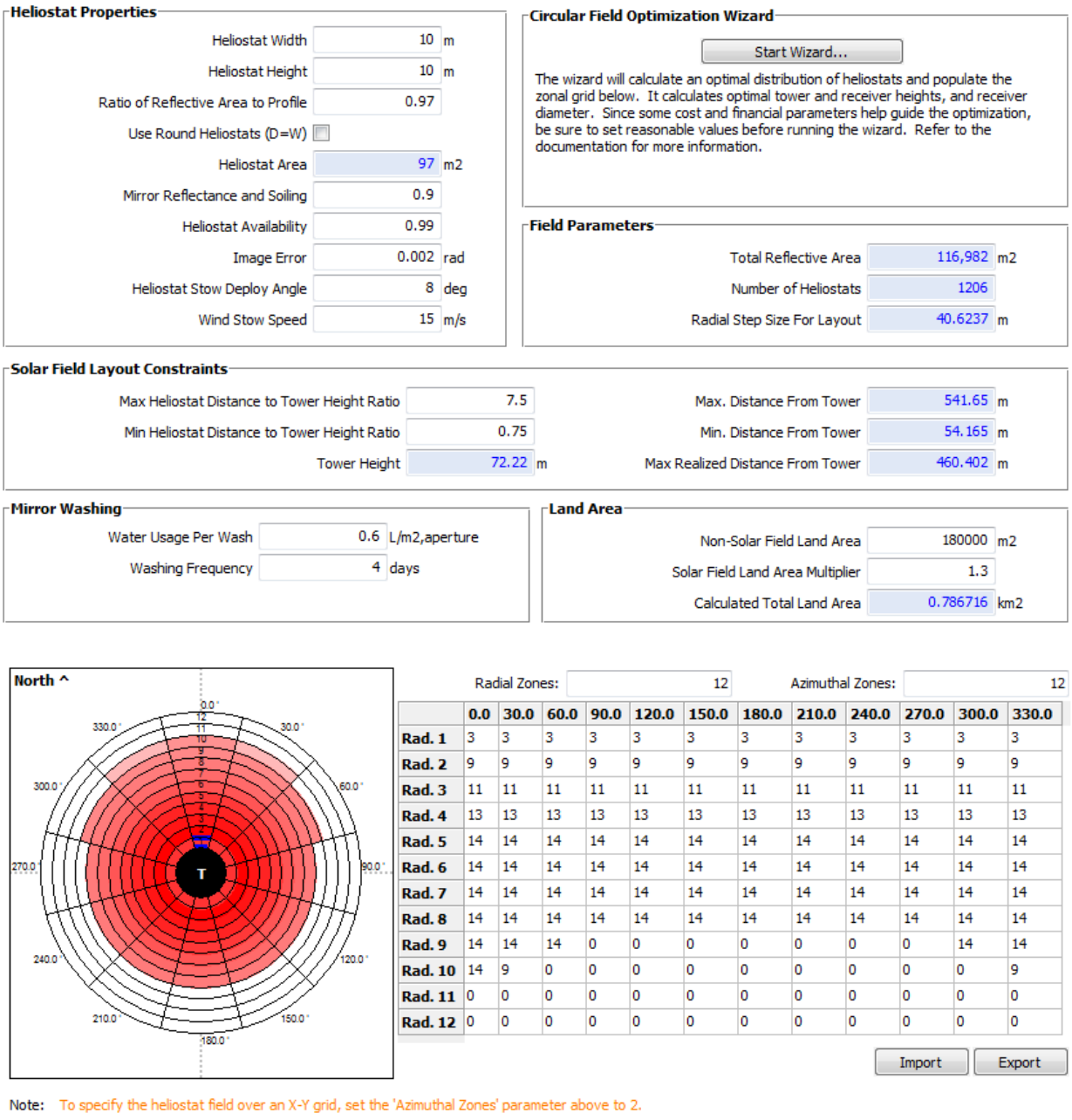

	0.0	30.0	60.0	90.0	120.0	150.0	180.0	210.0	240.0	270.0	300.0	330.0
Rad. 1	3	3	3	3	3	3	3	3	3	3	3	3
Rad. 2	9	9	9	9	9	9	9	9	9	9	9	9
Rad. 3	11	11	11	11	11	11	11	11	11	11	11	11
Rad. 4	13	13	13	13	13	13	13	13	13	13	13	13
Rad. 5	14	14	14	14	14	14	14	14	14	14	14	14
Rad. 6	14	14	14	14	14	14	14	14	14	14	14	14
Rad. 7	14	14	14	14	14	14	14	14	14	14	14	14
Rad. 8	14	14	14	14	14	14	14	14	14	14	14	14
Rad. 9	14	14	14	0	0	0	0	0	0	0	14	14
Rad. 10	14	9	0	0	0	0	0	0	0	0	0	9
Rad. 11	0	0	0	0	0	0	0	0	0	0	0	0
Rad. 12	0	0	0	0	0	0	0	0	0	0	0	0

Figure 6-4: Heliostat Field Page

6.4.4 Tower and Receiver Page

The Tower and Receiver page displays variables that specify the geometry of the heat collection system. The receiver model uses semi-empirical heat transfer and thermodynamic relationships to determine the thermal performance of the receiver. This allows the model to represent a wide array of geometries without deviating from a hypothetical reference system.

The model makes several assumptions about the system geometry:

- The receiver consists of a discrete number of panels.
- Each panel in the receiver consists of a set of parallel tubes in thermal contact that shares a common heat transfer fluid (HTF) header.
- The panel tubing is vertical and the heat transfer fluid flows through each sequential panel in a serpentine pattern (up one panel and down the adjacent panel).
- The number of tubes per panel is a function of the Number of Panels, Receiver Diameter, and Tube Outer Diameter variables.

The model varies the heat transfer fluid mass flow rate through the receiver to maintain the required outlet heat transfer fluid temperature. The model includes several practical safeguards to ensure realistic behavior in the receiver. For example, the mass flow rate through the receiver is limited to the value of the Max Flow Rate to Receiver variable, and the maximum receiver heat transfer fluid inlet temperature is kept at a value below the value of the Max Temp to Receiver variable.

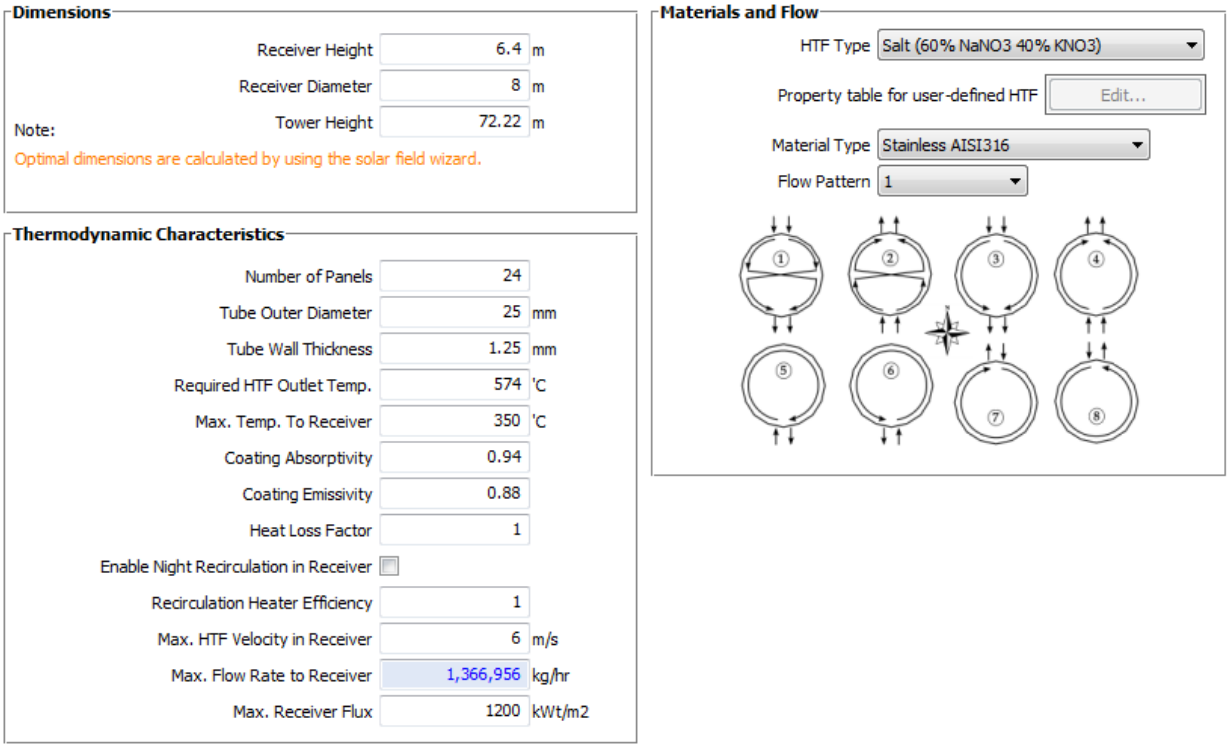

Figure 6-5: Tower and Receiver Page

6.4.5 Power Block

The Power block parameters describe the equipment in the system that converts thermal energy from the solar filed or thermal energy storage system into electricity. The power block is based on a steam turbine that runs on a conventional Rankine power cycle and may or may not include fossil fuel backup. Power block components include a turbine, heat exchangers or transfer heat from the solar field or thermal energy storage to the turbine, and a cooling system to dissipate waste heat.

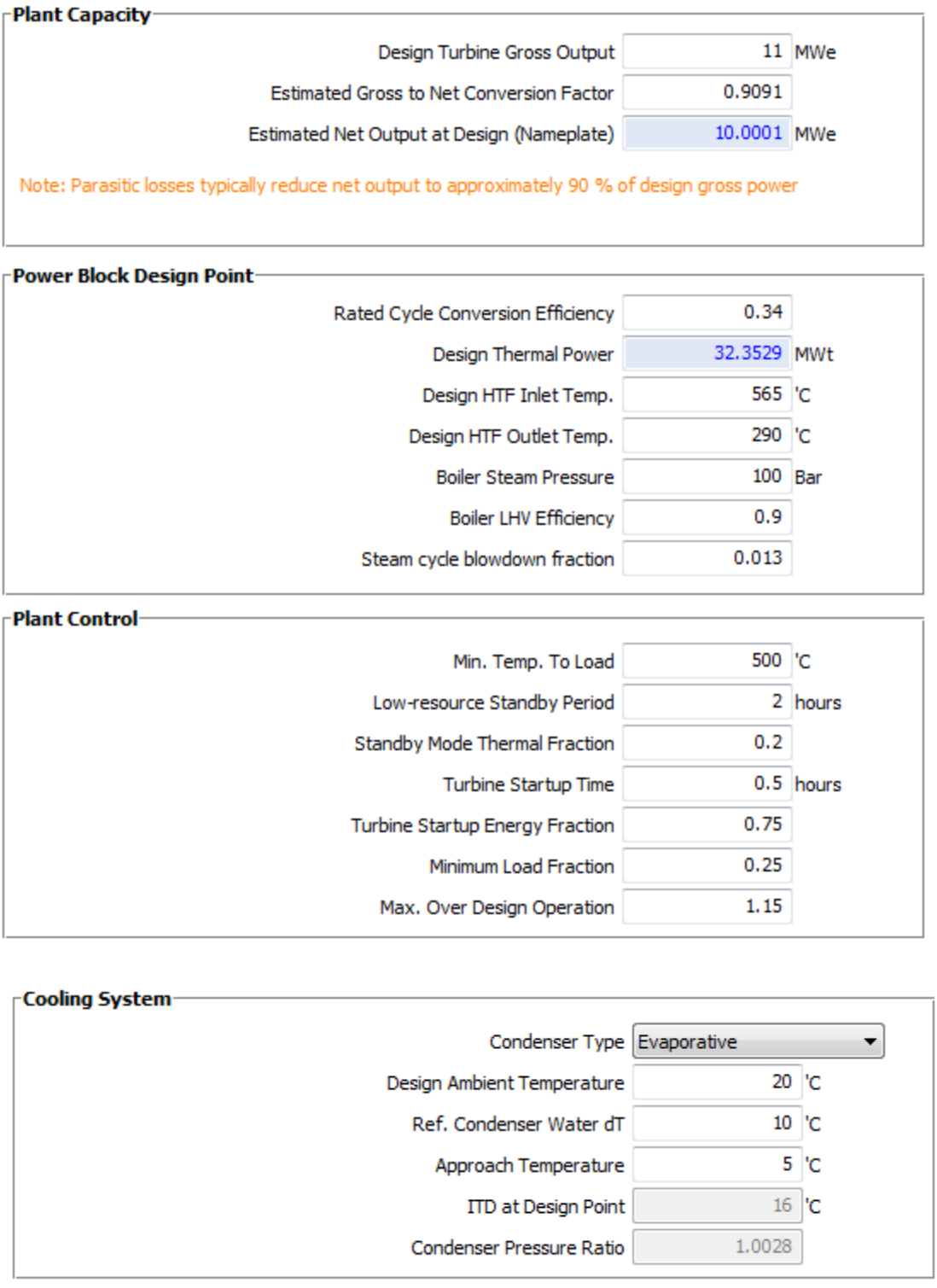

Figure 6-6: Power block page

6.4.6 Thermal Storage page

The parameters on the Thermal Storage page describe the properties thermal energy storage system and the storage dispatch controls. The power tower storage model uses storage tank geometry, which requires that the heat transfer fluid volume, tank loss coefficients, and tank temperatures be specified. Solar Advisor calculates the storage tank geometry to ensure that the storage system can supply energy to the power block at its design thermal input capacity for the number of hours specified by the Full Load TS Hours variable. Solar Advisor models only two-tank storage systems for power towers. A two-tank system consists of separate hot and cold storage tanks.

The storage capacity expressed in hours at full load is the number of hours that the storage system can supply energy at the power block design turbine input capacity.
Solar Advisor calculates the total heat transfer fluid volume in storage based on the storage hours at full load and the power block design turbine thermal input capacity. The total heat transfer fluid volume is divided among the total number of tanks so that all hot tanks contain the same volume of fluid, and all cold tanks contain the same volume of fluid.

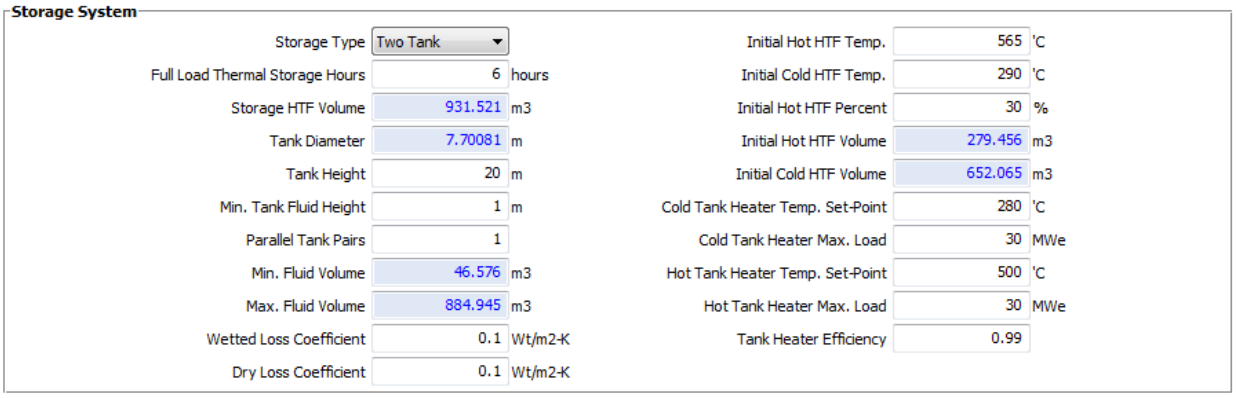

Figure 6-7: Thermal Storage page

6.4.7 After Tax Cash Flow

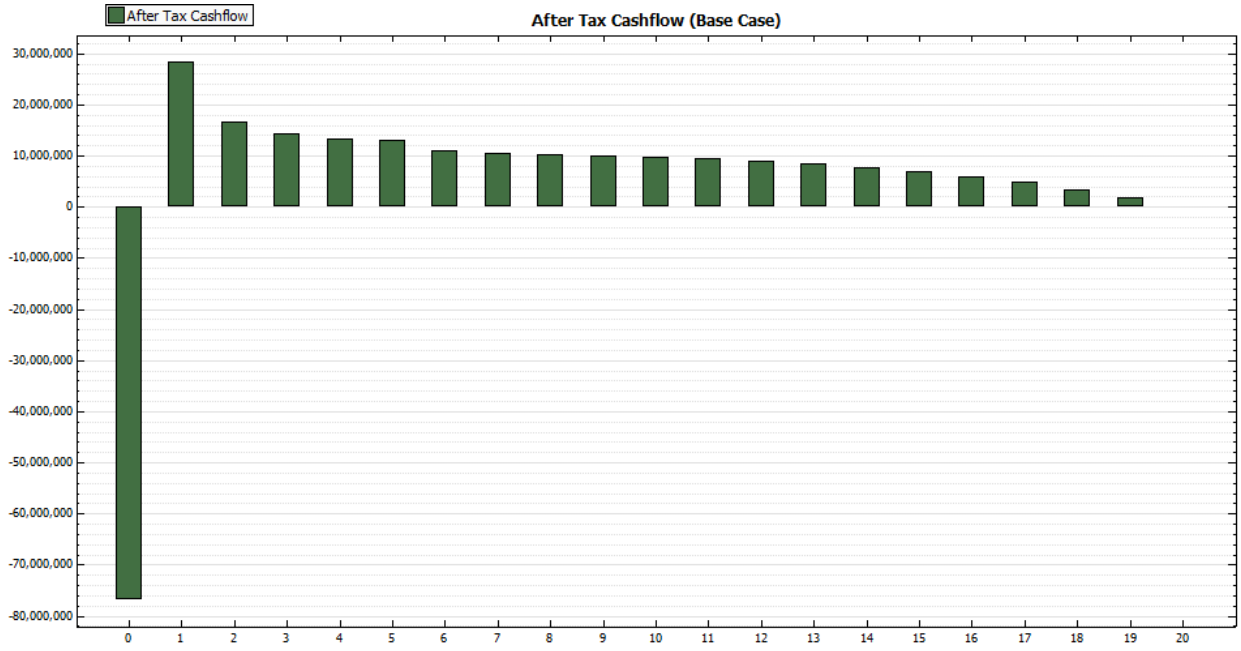

Figure 6-8: Project Cash Flow

Table 6-2: Project Cash Flow

Year	After Tax Cash Flow ($)	Year	After Tax Cash Flow ($)
0	-76,781,400	10	9,800,490
1	28,393,500	11	9,420,580
2	16,628,300	12	8,956,500
3	14,332,000	13	8,394,510
4	13,282,500	14	7,718,670
5	13,208,800	15	6,910,470
6	10,994,200	16	5,948,430
7	10,545,800	17	4,807,650

8	10,353,600	18	3,459,240
9	10,108,100	19	1,869,680
10	9,800,490	20	61,770

Based on the above cash flow, the payback period is calculated as:

Year	0	1	2	3
Yearly cash flow	-76,781,400	28,393,500	16,628,300	14,332,000
Commutative cash flow	-	-48,383,900	-31,759,600	-17,427,600
Year	4	5	6	
Yearly cash flow	13,282,500	13,208,800	10,994,200	
Commutative cash flow	-4,145,100	9,063,700	20,057,900	

Payback period= 4years + 4,145,100/13,208,800 year = 4.314 years or 4 years and four months

6.4.8 Monthly Energy Flow

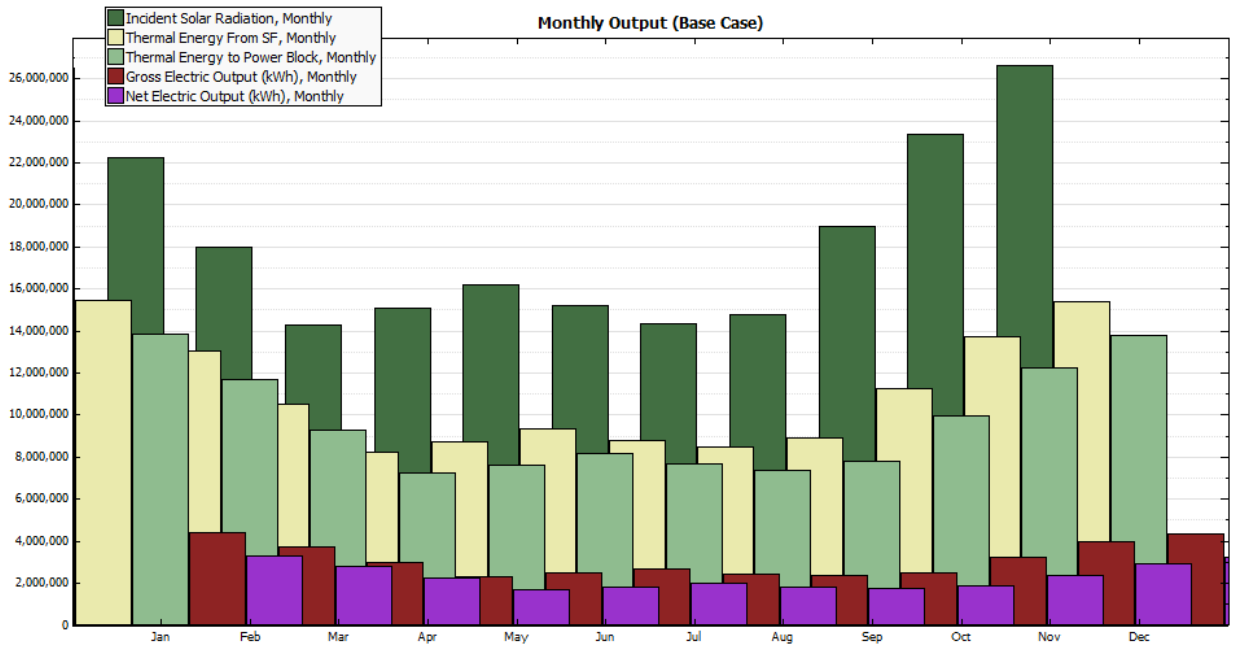

Figure 6-9: Monthly Energy Flow

Table 6-3: Monthly Energy Flow in kWh

Month	Incident Solar Radiation	Thermal Energy from SF	Thermal Energy to Power Block	Gross Electric Output	Net Electric Output
1	2.65E+07	1.55E+07	1.38E+07	4.42E+06	3.30E+06
2	2.23E+07	1.31E+07	1.17E+07	3.75E+06	2.80E+06
3	1.80E+07	1.05E+07	9.28E+06	2.99E+06	2.23E+06
4	1.43E+07	8.27E+06	7.22E+06	2.31E+06	1.72E+06
5	1.51E+07	8.73E+06	7.62E+06	2.48E+06	1.85E+06
6	1.62E+07	9.34E+06	8.20E+06	2.66E+06	1.99E+06
7	1.52E+07	8.79E+06	7.65E+06	2.45E+06	1.83E+06
8	1.44E+07	8.49E+06	7.38E+06	2.39E+06	1.78E+06

9	1.48E+07	8.89E+06	7.78E+06	2.52E+06	1.89E+06
10	1.90E+07	1.13E+07	9.95E+06	3.21E+06	2.40E+06
11	2.34E+07	1.37E+07	1.23E+07	3.96E+06	2.95E+06
12	2.66E+07	1.54E+07	1.38E+07	4.35E+06	3.24E+06

6.4.9 Cost Stacked Bar

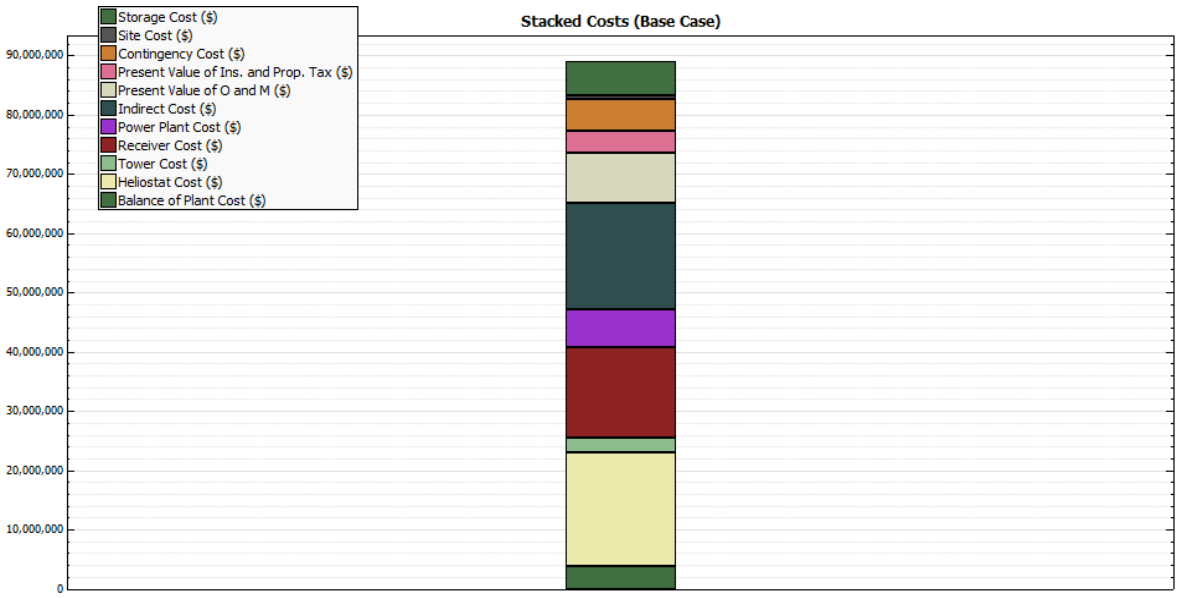

Figure 6-10: Cost Stacked Bar

Table 6-4: Cost stacked bar values

Type of Cost	Amount
Site Cost ($)	584,910
Storage Cost ($)	5,820,000
Balance of Plant Cost($)	3,795,000
Heliostat Cost ($)	19,302,000
Tower Cost ($)	2,356,280

Receiver Cost ($)	15,300,800
Power Plant Cost ($)	6,325,000
Contingency Cost($)	5,350,000
Indirect Cost($)	17,945,100
Present Value of O & M	8,530,000
Present Value of Ins. and Prop. Tax ($)	3,725,810

Table 6-5: Summary of Results

Metric	Base
Annual Energy [kWh]	26,289,746.8
1st Year PPA Price	64.24 cents/kWh
LCOE(nom)	67.24 cents/kWh
LCOE(real)	26.79 cents/kWh
IRR	18.33%
Minimum DSCR	1.73
PPA Escalation	1.20%
Dedt Fraction	0.00%
Capacity Factor	30.0%
Gross to Net Conversion Factor	0.75

Table 6-5, shows that the real levelized cost of energy is 26.79cents/kWh with IRR of 18.33% for the power plant analysed in this research. The cost of energy is relatively very high when compared with hydroelectric electricity cost of Ethiopia but it is in line with the cost of the first commercial molten salt power tower plant ($24 U.S cents/kWh), called Solar Tres, that was planned for deployment in southern Spain [James E. PACHECO, etl...]. This is due to inherent

characteristics of high per kilo watt cost of CSP technologies, lower generation capacity of the analyzed power plant (i.e. 10MWe). Therefore; major cost reduction mechanisms like increasing mass production of heliostats at local level to minimize cost of heliostat, scaling up the plant to larger power capacity and detail techno economic analysis of the plant are forwarded as recommendations for solar electricity cost minimization strategies.

CHAPTER SEVEN

CONCLUSIONS AND RECOMMENDATIONS

7.1 Conclusions

The power plant analyzed in this paper has a capacity of generating 10MW electric power. The power cycle was modeled using EES program to obtain the reference inputs and parameters used during simulation by TRNSYS. The EES program is used only to model full load operation of the power plant at steady state condition. The TRNSYS model of the power plant is used to model both the solar field and the power block. The CRS was modeled in TRNSYS simulation studio using existing TRNSYS 16.0 components most of which are from STEC library release 3.0 packages. The CRS cost as well as different system component size and number were optimized using SAM.

The plant model was simulated to predict the performance for representative clear and cloudy days at Dire Dawa weather condition which have relatively higher annual average DNI among other Ethiopian regions. Simulation results have shown that the power output and mass flow rate from central receiver are directly proportional, which is in line with theoretical expectations. A 6 hour capacity two tank thermal storage is incorporated with the power plant in order to avoid power transient during low or high DNI, to have power when there is no sunlight, to increase the capacity factor and to minimize the levelized cost of electricity. The addition of a thermal storage extends the power plant operation to 16 hours with 13 hours of constant 10MWe net electrical power output for a clear sunny day of higher DNI.

Without the incorporation of thermal storage, as optimized in SAM software, 788 heliostats with $97m^2$ area satisfies the power demand specified for this research which is 10MWe but the addition of thermal storage increases the number of heliostats to 1200 with significant increase in initial system cost and decrease in levelized energy cost. The financial and economic analysis of the power plant was performed in SAM software at climatic condition of Dire Dawa. The analysis reveals that the addition of thermal storage in the system significantly increase the

investment cost from $58,072,837.73 to $76,781,394.61with minimizing effect of LCOE from 33.02 to 26.79 cents/kWh and increasing capacity factor from 17.3 to 30.0%

7.2 Recommendations

Through the course of this research, several items have emerged as likely candidates for future work. These include work that were initiated as part of this research work such the cavity receiver model, stratified thermal storage tank model, and fuel backup incorporation for overnight operation.

The receiver model used in this research is a simplified model of the central receiver, relying on a receiver thermal efficiency as an input value instead of calculating it directly. This model provides the flow rate required to achieve a temperature set-point as an output. The solar flux concentration on the surface of the receiver should be evenly distributed over the absorber surface to avoid thermal failure. Moreover; the flux concentration varies with solar radiation availability, cloud transients, solar position, and plant configuration. Therefore; thermal analysis of the central receiver model that is capable of calculating transient receiver thermal efficiency could be other candidate for further work.

It is possible to lengthen the plant operation time by solar only mode either through decreasing the net power output of the plant or increasing number of heliostats and thermal storage size. The first option has the positive effect of decreasing total installation cost, and increasing the capacity factor. But the levelised cost of energy increases at the same time. For the second case, total installation cost and capacity factor increases while the levelised cost of energy decreases. Therefore; the first option should be used when there is financial constraint.

Finally, latest modeling and simulation software should be available at Addis Ababa University since this was the major limitation during this research work.

APPENDIX

Appendix A

The EES program written during this research for power cycle of the power plant

```
{"muaz bedru thesis, power cycle model using EES"}

PROCEDURE turbine(h_in,P_in,P_out,Eff :h_out,W_t)
        s_in = entropy('Steam',h=h_in, P=P_in)
{s_in:=entropy(STEAM,h=h_in,P=P_in)}
    h_out_s:=enthalpy(STEAM,s=s_in,P=P_out)
    W_t:=(h_in-h_out_s)*Eff
    h_out:=h_in-W_t
END

PROCEDURE pump(P_in,P_out,Eff :h_in,h_out,W_p)
    h_in:=ENTHALPY(STEAM,P=P_in,x=0);
    v:=volume(STEAM,P=P_in,x=0)
    W_p:=v*(P_in-P_out)/Eff
    h_out:=h_in-W_p
END


eta_turb=0.70           "Isentropic turbine efficiency;  same for all turbines"
eta_pump=0.695          "Isentropic pump efficiency;  same for all pumps"
"Define the state points"
turb_in = 1 "High-pressure turbine inlet"
turb_split2 = 2 "The higher pressure splitter stage"
turb_split1 = 3 "The lower pressure splitter stage"
cond_in = 4 "The condenser inlet"
pump1_in = 5 "The condenser outlet, pump inlet"
dartr_in = 6 "Low pressure feedwater heater inlet"
pump2_in = 7 "Intermediate stage pump inlet"
{subcol_in = 8 "feedwater inlet for sucooler"}
cfwh_in = 10 "closed feedwater heater inlet"
econ_in = 11 "Preheater HX inlet"
boil_in = 12 "Boiler inlet"
sh_in = 13 "Superheater HX inlet"
throtl_in=8 "steam inlet to throtle valve"
throtl_out=9"outlet of throtle valve"

"Salt conditions:"
T_htf_hot = 565 [C] "The known salt hot inlet temperature"
T_htf_cold = 290 [C] "The known salt temperature leaving the heat exchangers"
w_dot_cycle = 10e3 [KW] "Desired power"
```

```
"Heat transfer fluid"
HTF$='Salt (60% NaNO3, 40% KNO3)'
"Start at the turbine 1 (highest pressure turbine) inlet"
"!Turbine 1"
CALL Turbine(h[1],P[1],P[2],eta_turb:h[2],W_t1)

T[1] = 510 [C]
P[1] = 100 [bar]

P[4] = 0.085 [bar]        "pressure at condenser inlet"
 h[1] = enthalpy('Steam',T=T[1], P=P[1])
s[1] = entropy('Steam',h=h[1], P=P[1])
TsatHI = T_sat('Steam',P=P[1])
TsatLO = T_sat('Steam',P=P[4])
"The turbine 1 outlet: turb_split2 pressure is"
P[2]=P_sat('Steam',T=TsatHI-(TsatHI-TsatLO)/3)   "Pressure at the splitter stage"

"!Turbine 2"
CALL Turbine(h[2],P[2],P[3],eta_turb:h[3],W_t2)
s[2] = entropy('Steam',h=h[2], P=P[2])

"!Turbine 2 outlet: turb_split1"
P[3]=P_sat('Steam',T=TsatHI-(TsatHI-TsatLO)*2/3) "Pressure at the splitter stage"

"!Turbine 3"
CALL Turbine(h[3],P[3],P[4],eta_turb:h[4],W_t3)
s[3] = entropy('Steam',h=h[3], P=P[3])
s[4] = entropy('Steam',h=h[4], P=P[4])
W_dot_t1 = W_t1*m_dot_steam "Power from the first turbine"
W_dot_t2 = W_t2*m_dot_steam*(1-m) "Calculate the power"
W_dot_t3 = W_t3*m_dot_steam*(1-m)*(1-k)
"--"
W_dot_tot = (W_dot_t1+W_dot_t2+W_dot_t3)*convert(kW,MW)
"!Pump 1"
P[5]=P[4]
P[6]=P[3]
x[5] = 0 [-]
CALL Pump(P[5],P[6],eta_pump:h[5],h[6],W_p1)
s[5] = entropy('Steam',h=h[5], P=P[5])
x[6] = 0 [-]
v=volume(STEAM,P=P[6],x=x[6])
"!Pump 2"
P[7]=P[3]
P[10]=P[1]
CALL Pump(P[7],P[10],eta_pump:h[7],h[10],W_p2)
x[10] = 0 [-]
```

```
"Condenser outlet: pump1_in"
"Calculate condenser properties ----------"
q_cond = h[4] - h[5] "Heat per unit mass"
q_dot_cond = q_cond*m_dot_steam*(1-m)*(1-k) "Heat rate"
"!Dearater"
h[7] = (1-m)*k*h[3] + m*h[9]+(1-m)*(1-k)*h[6]  "Enthalpy balance"
s[6] = entropy('Steam',h=h[6], P=P[6]) "Entropy at inlet"
s[7] = entropy('Steam',h=h[7], P=P[7]) "Entropy at inlet"

"!Feedwater Heater "
"Calculate the feed-water inlet/outlet temps (El-Wakil, M.M., Powerplant Technology, 1984) "
x[8]=0
h[8]=enthalpy('Steam',P=P[2],x=x[8]) "Get enthalpy"
T[11]=temperature(STEAM,h=h[11],P=P[11])
x[11]=0

h[11]=h[8]
T[8]=temperature(STEAM,h=h[8],P=P[2])

P[11]=P[1]
P[8]=P[2]
"!Feedwater Heater "
h[10]-h[11] = m*(h[8]-h[2])  "Energy balance for HP FWH"
s[10] = entropy('Steam',h=h[10], P=P[10]) "Entropy at inlet"
s[11] = entropy('Steam',h=h[11], P=P[11]) "Entropy at inlet"

"!Calculate the fwh size"
q_fwh = h[11] - h[10]       "Preheater heat flow"
q_dot_fwh = q_fwh*m_dot_steam "Heat flow rate"
"--"
c_w_fw = specheat('Steam',T=((T[11]+T[10])/2),P=P[11]) "PH water/steam spec.heat"
c_dot_w_fw = c_w_fw*m_dot_steam          "PH steam/steam capacitance rate"

"The ef fectiveness-NTU relationship for countercurrent HX implemented"

  epsilon_fwh=q_dot_fwh/(C_dot_w_fw*(T[2] - T[10]))  "The preheater heat flow"
NTU_fwh = -ln(1-epsilon_fwh) "The transfer units for this heat exchanger"
UA_fwh = NTU_fwh*m_dot_steam*c_w_fw "Conductance"


"Pump 1 outlet: fw1_in"
W_dot_p1 = W_p1*m_dot_steam*(1-m)*(1-k) "Power consumed by the pump"

W_dot_p2 = W_p2*m_dot_steam "Pump power"
```

```
s[8] = entropy('Steam',h=h[8], P=P[8]) "Entropy"

"!Throtle valve "

T[2]=temperature(STEAM,h=h[2],P=P[2])
h[9]=h[8]
P[9]=P[3]
T[9]=temperature(STEAM,h=h[9],P=P[9])
s[9] = entropy('Steam',h=h[9], P=P[9]) "Entropy"
x[9]=0

"economizer outlet: boil_in"
x[12] = 0 [-] "Fixed quality at boiler inlet"
P[12] = P[1] "No pressure drop"
{T[boil_in] = temperature('Steam',P=P[boil_in],x=x[boil_in]) "Get temperature"}
h[12] = enthalpy('Steam',P=P[12],x=x[12]) "Get enthalpy"
s[12] = entropy('Steam',h=h[12], P=P[12]) "Entropy"
T[12]=temperature(STEAM,h=h[12],P=P[12])
"Calculate the economizer size"
q_econ = h[12] - h[11]       "Preheater heat flow"
q_dot_econ = q_econ*m_dot_steam "Heat flow rate"
"--"
c_w_econ = specheat('Steam',T=((T[11]+T[12])/2),P=P[12]) "PH water/steam spec.heat"
c_dot_w_econ = c_w_econ*m_dot_steam          "PH steam/steam capacitance rate"
"---Calculate the HTF flow rate before proceeding"
m_dot_htf = (h[1]-h[11])*m_dot_steam/(c_(HTF$,(T_htf_hot +T_htf_cold)/2)*(T_htf_hot-
T_htf_cold))
"---"
c_htf_econ = c_(HTF$,((T_htf_cold+T_htf_econ_in)/2))      "PH HTF spec.heat"
c_dot_htf_econ = c_htf_econ*m_dot_htf        "PH HTF cap rate"

"Now use the ef fectiveness-NTU relationship to calculate the heat exchanger size"
c_dot_min_econ = MIN(c_dot_w_econ, c_dot_htf_econ)
c_dot_max_econ = MAX(c_dot_w_econ, c_dot_htf_econ)
C_R_econ = C_dot_min_econ/C_dot_max_econ "The capacitance ratio"

"The energy balance on the hot side of the HX"
T_htf_econ_in = T_htf_cold + q_dot_econ/c_dot_htf_econ "Calculate the inlet htf temperature,
NOTE: negates previous guess temp"
"The ef fectiveness-NTU relationship for countercurrent HX implemented"
  epsilon_econ=q_dot_econ/(C_dot_min_econ*(T_htf_econ_in - T[11]))  "The preheater heat
flow"
{call muaz(epsilon_econ, epsilon_sh, C_R_econ, C_R_SH : NTU_econ, NTU_sh ) }
NTU_econ=ln(((epsilon_econ-1)/(epsilon_econ*C_R_econ-1)))/(C_R_econ-1)
UA_econ = NTU_econ*C_dot_min_econ "The corresponding UA"
```

```
"boiler outlet: sh_in"
x[13] = 1 [-]
P[13] = P[12]
{T[sh_in] = temperature('Steam', P=P[sh_in],x=x[sh_in])}
h[13] = enthalpy('Steam',P=P[13], x=x[13])
s[13] = entropy('Steam',T=T[13], P=P[13]) "Entropy"

"Calculate the boiler size"
q_boil = h[13] - h[12]
q_dot_boil = q_boil*m_dot_steam
"--"
c_htf_boil = c_(HTF$, (T_htf_boil_in + T_htf_econ_in)/2)
c_dot_htf_boil = c_htf_boil*m_dot_htf
q_dot_boil = epsilon_boil*c_dot_htf_boil*(T_htf_boil_in - T[12])
NTU_boil = -ln(1-epsilon_boil) "The boiler NTU"
UA_boil = NTU_boil*m_dot_htf*c_htf_boil "The corresponding UA"

"Calculate htf boiler inlet temp, replaces guess value"
T_htf_boil_in = T_htf_econ_in + q_dot_boil/c_dot_htf_boil
"Calculations for the superheater"

q_sh = h[1]-h[13] "Heat flow in the superheater"
q_dot_sh = q_sh*m_dot_steam "Heat flow rate"
c_w_sh = specheat('Steam',T=((T[13]+T[1])/2), P=P[1]) "Spec.heat steam"
c_dot_w_sh = c_w_sh*m_dot_steam "Cap rate steam"
c_htf_sh = c_(HTF$, (T_htf_hot + T_htf_boil_in)/2) "Spec heat HTF"
c_dot_htf_sh = c_htf_sh*m_dot_htf "Cap rate HTF"
c_dot_min_sh = MIN(c_dot_w_sh, c_dot_htf_sh) "Minimum cap rate"
c_dot_max_sh = MAX(c_dot_w_sh, c_dot_htf_sh) "Maximum cap rate"
C_R_sh = c_dot_min_sh/c_dot_max_sh "Cap ratio"
epsilon_sh = q_dot_sh/(c_dot_min_sh*(T_htf_hot-T[sh_in])) "ef fectiveness"
NTU_sh=ln(((epsilon_sh-1)/(epsilon_sh*C_R_sh-1)))/(C_R_sh-1)
UA_sh = NTU_sh*c_dot_min_sh "Conductance"

"The condenser is modeled as a HX with 1 side of infinite cap. rate"
"Calculate the cooling water inlet/outlet temps (El-Wakil, M.M., Powerplant Technology, 1984)
"
dT_in = 15 [C] "Dif ference between sat. temp of steam  and inlet temp of cooling water"
T_cw_in = T_sat('Steam',P=P[4]) - dT_in "The cooling water inlet temp."
dT_out= 4 [C] "Dif ference between sat. temp and outlet temp"
T_cw_out = T_sat('Steam',P=P[cond_in]) - dT_out "The cooling water outlet temp."
T_cwinF = converttemp(C,F,T_cw_in) "Temp in F"
T_cwoutF = converttemp(C,F,T_cw_out) "Temp in F"
c_p_cw = specheat('Water',T=T_cw_in,P=1.01000[bar]) "The specific heat of the cooling water"
m_dot_cw = q_dot_cond/(c_p_cw*(T_cw_out - T_cw_in)) "Calculate the cooling water flow
rate"
```

```
q_dot_cond = -epsilon_cond*m_dot_cw*c_p_cw*(T[4]-T_cw_in) "Ef fectiveness"
NTU_cond = -ln(1-epsilon_cond) "The transfer units for this heat exchanger"
UA_cond = NTU_cond*m_dot_cw*c_p_cw "Conductance"
"Total heat addition"
q_dot_hot_tot = q_dot_econ+q_dot_boil+q_dot_sh
"Calculate the total work from the cycle"
W_dot_cycle = W_dot_t1 + W_dot_t2 + W_dot_t3 + W_dot_p1 + W_dot_p2
"Calculate the total thermal ef ficiency of the cycle"
eta_cycle = W_dot_cycle/q_dot_hot_tot

T[3]=temperature(STEAM,h=h[3],P=P[3])
T[4]=temperature(STEAM,h=h[4],P=P[4])
T[5]=temperature(STEAM,h=h[5],P=P[5])
T[6]=temperature(STEAM,h=h[6],P=P[6])
T[7]=temperature(STEAM,h=h[7],P=P[7])
T[10]=temperature(STEAM,h=h[10],P=P[10])
T[13]=temperature(STEAM,h=h[13],P=P[13])
```

Appendix B

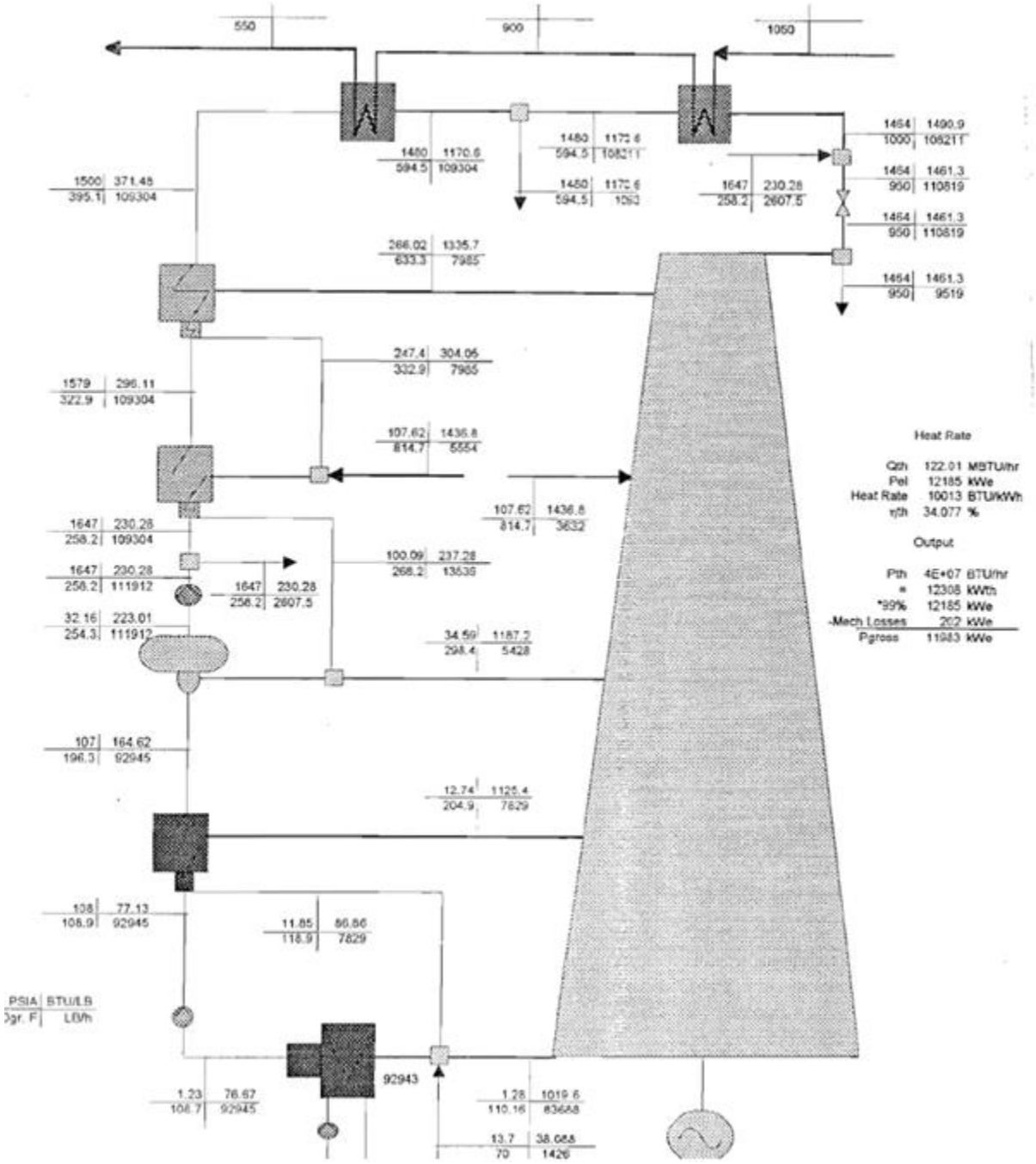

Figure B-1: The designed Rankine cycle for Solar II. This cycle was used as a resource in developing the Rankine cycle model for this thesis.

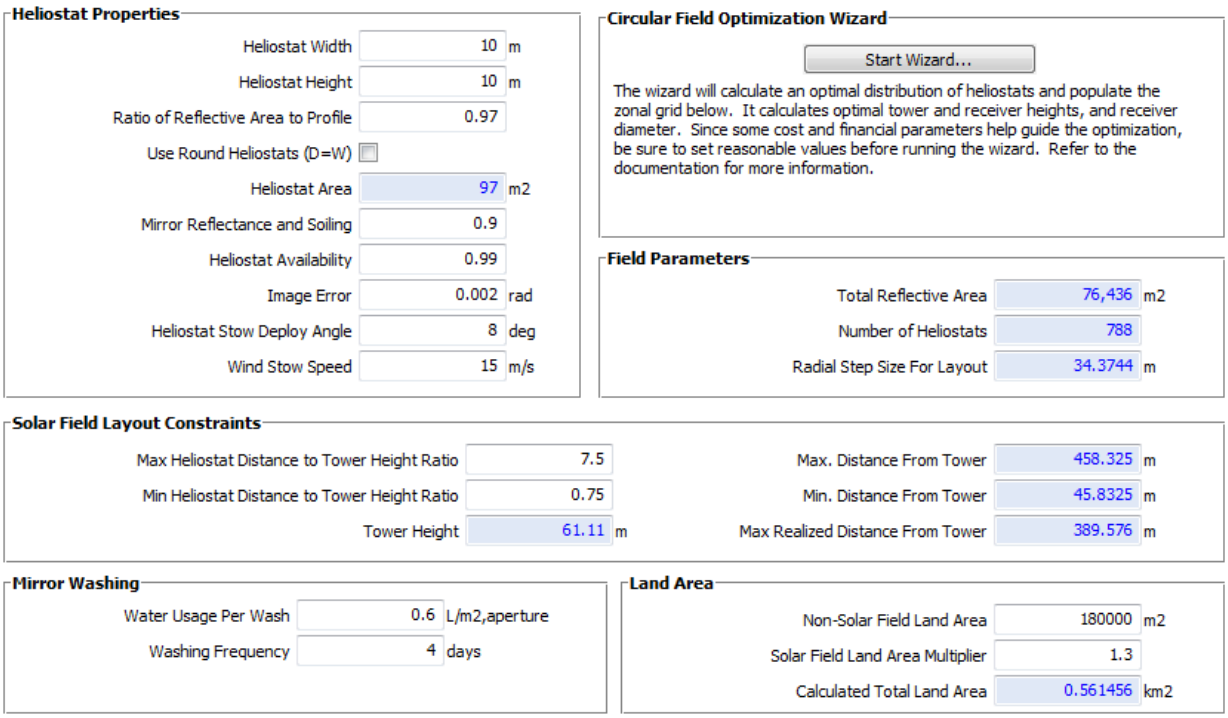

Figure B-2: Heliostat Field Page for the Power Plant Model without Thermal Storage

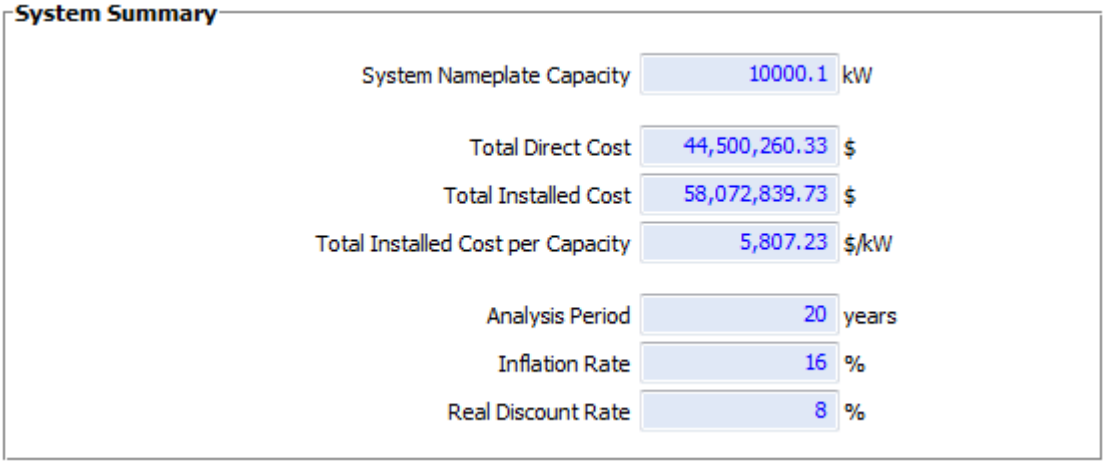

Figure B-3: System Cost Summary for the Power Plant Model without Thermal Storage

Table B-1: Summary of Results for Power Plant without Thermal Storage

Metric	Base
Annual Energy [kWh]	15.173,895
1st Year PPA Price	73.69 cents/kWh
LCOE(nom)	82.87 cents/kWh
LCOE(real)	33.02 cents/kWh
IRR	15.00%
Minimum DSCR	1.51
PPA Escalation	3.00%
Dedt Fraction	6.17%
Capacity Factor	17.3%
Gross to Net Conversion Factor	0.71

REFERENCES

Battleson, K.W.(1981), *Solar Power Tower Design Guide: Solar Thermal Central Receiver Power Systems, A Source of Electricity and/or Process Heat,* Sandia National Labs Report SAND81-8005, April.

Biggs,F. and C.M.Vittitoe,(1979), *The HELIOS Model for the Optical Behavior of Reflecting Solar Concentrators,* Sandia National Labs Report SAND76-0347, March.

Clausing, A.M.(1981), *An Analysis of Convective Losses from Cavity Solar Central Receivers,* Solar Energy **27** (4), 295.

Çengel, Yunus A., and Boles, Michel A. *Thermodynamics an Engineering Approach.* 5th Edition, 2005

ConSolar (1999): http://magnet.consortia.org.il/ConSolar/consolar.html, latest update 1999.

Dellin,T.A., M.J. Fish, and C. L. Yang (1981), *A User's Manual for DELSOL2: A Computer Code for Calculating the Optical Performance and Optimal System Design for Solar Thermal Central Receiver Plants,* Sandia National Labs Report SAND81-8237, August.

DOE IV (1997): *US Department of Energy - Concentrating Solar Power programme, Solar Power Tower*, www.eren.doe.gov/csp/resources.html.

Duffie, John A., and Beckman, William A. *Solar Engineering of Thermal Processes*. 2nd edition, New York: John Wiley and Sons, Inc., 1991.

EEPCO (Website). *EEPCo in Brief*. Available at: http://www.eepco.gov.et. Last accessed: May 20, 2010

Eisenbeiß G. (1996): *Solar Thermal Power Stations - solar thermal power is the bigger brother of photovoltaics*, EUROSUN '96.

El-Wakil, M. M. *Power plant Technology*. New York: McGraw-Hill, Inc., 1984.

Engineering Equation Solver (EES**)**. Middleton, WI: F-Chart Software, 2005, Available at http://www.fchart.com.

Grasse W. (1992): *Solar Power and Chemical Energy Systems*: Report on Activities and Results 1989 1991. Deutsche Forschungsanstalt fur Luft- und Raumfahrt Report, Almería, May 1992.

Heliotech (2000): available at http://www.heliotech.dk/industrial/stpp-info/stpp-info-index.htm.

Holl R.J.(1989): *Status of Solar-Thermal Electric Technology*. Electricity Power Research Institute, report EPRI GS-6573, December 1989.

Holl, R.J. (1978), *Definition of Two Small Central Receiver Systems,* Sandia National Labs Report SAND78-7001, April.

James E. PACHECO, Hugh E. REILLY, Gregory J. KOLB and Craig E. TYNER, *SUMMARY OF THE SOLAR TWO TEST AND EVALUATION PROGRAM* ,Sandia National Laboratories

Jiménez M.D. (1995): *Pataforma Solar de Almería*: Annual Technical Report. PSA-TR03/95-MS, Almería June 1995.

Lata, J. M., Rodriguez, M., & Lara, M. A. (2006). *High Flux Central Receivers of Molten Salts for the New Generation of Commercial Standalone Solar Power Plants*. SolarPACES.

Léon J., et al (1994): *Design and First tests of an Advanced Salt Receiver Based on the Internal Film Concept.* Presented at the 7th symposium on 'solar concentrating technologies', Moscow, 26-30 September 1994.

Lipps, F.W., and L.L.Vant-Hull (1978), *A Cellwise Method for the Optimization of Large Central Receiver Systems,* Solar Energy **30**(6), 505.

Lippke, F. (1995). *Solar II Overall Efficiency at Reduced Receiver Outlet Temperatures*. Sandia National Labs., Albuquerque, NM.

Nellis, G.F., Klein, S.A. (2009) *Heat Transfer*. Cambridge University Press. Manuscript submitted for publication.

Pitz-Paal, R., and Jones, S.A., 1998, *A TRNSYS Model Library for Solar Thermal Electric Components (STEC),* A Reference Manual, Release 1.0, IEASolar Power and Chemical Energy Systems, Task III: Solar Technologies and Applications.

Power from the Sun. Available at: http://www.powerfromthesun.net/book.htm. Last accessed: April 18, 2010.

Romero, M., Buck, R., Pacheco, J. (2002). *An Update on Solar Central Receiver Systems, Projects, and Technologies*. Journal of Solar Energy Engineering, 124(2), 98-108.

Sam User Guide, SAM Software, Available at: https://www.nrel.gov/analysis/sam.

Sargent & Lundy LLC Consulting Group. (2003). *Assessment of Parabolic Trough and Power Tower Solar Technology Cost and Performance Forecasts*. NREL.

Schwarzbozl, P. (2006). *A TRNSYS Model Library for Solar Thermal Electric Components (STEC) (Reference Manual, Release No. 3.0).* Deutsches Zentrum für Luft und Raumfahrt e.V. (DLR). D-51170 Köln, Germany.

Siebers, D.L., and J.S. Kraabel (1984), *Estimating Convective Energy Losses from Solar Central Receivers,* Sandia National Labs Report SAND84-8717, April.

Sterns Roger Engineering Company (1979), *Tower Cost Data for Central Receiver Studies,* Sandia National Labs Report SAND78 -8185, June.

Stoddard, M.C., et. al., SOLERGY - *A Computer Code for Calculating the Annual Energy from Central Receiver Power Plants*, Sandia National Laboratories, Livermore, CA: May 1987. Report SAND86-8060.

Stodola, A., and Loewenstein, Louis C. (1945). *Steam and Gas Turbines*. Volume I. New York: McGraw-Hill Book Company.

Weather Data, Available at: http://swera.unep.net. Last accessed: April 18, 2010

Websites:

http://www.nrel.gov/csp/troughnet/pdfs/kelly_two_tank_indirect_tes.pdf

http://www.ep.liu.se/ecp/043/080/ecp09430048.pdf

http://www.nrel.gov/csp/troughnet/pdfs/27925.pdf

http://www.energy.wsu.edu/documents/engineering/Thermal.pdf thermal store222

http://www.solarmillennium.de/upload/Download/Technologie/eng/Andasol1- 3engl.pdf

http://www.solarpaces.org/Tasks/Task1/ps10.htm

http://www.solarpaces.org/CSP_Technology/docs/solar_trough.pdf

http://www.cogeneration.net/direct_solar_steam.htm

http://www.nrel.gov/csp/troughnet/power_plant_systems.html

http://www.gepower.com/prod_serv/products/tech_docs/en/downloads/ger4201.pdf

http://en.wikipedia.org/wiki/File:Rankine_cycle_layout.png